PhD thesis

SUPPORT TOOLS FOR GROUNDWATER MANAGEMENT IN THE PROXIMITY OF A MINE SITE

Laura Scheiber Pagès

Advisors

Carlos Ayora Ibáñez

Enric Vázquez Suñé

Institute of Environmental Assessment and Water Research (IDAEA, CSIC)

Department of Geotechnical Engineering and Geosciences, Universitat Politècnica de Catalunya (UPC)

Associated Unit: Hydrogeology Group (UPC-CSIC)

MAY, 2017

SUMMARY

The natural environment in which we live, is subjected, to a greater or lesser extent, to the pressure of human activity, with water being one of the most sensitive elements. For this reason, aware of this situation, from all the forums (Administration, Companies and stakeholders) is imposing the practice new standards unthinkable during the decades of industrial development, aimed at making the environment and industry compatible. A new model of mining seeks to achieve a balance between good environmental practices and efficiency, so that production is linked to environmental respect.

The Niebla-Posadas aquifer (NP) constitutes one of the water resources within the Guadalquivir Basin, which supports traditional agriculture in the area and is the source of drinking water for many populations. In recent decades, competition for this resource has increased due to the expansion of irrigated agriculture and in turn affected by the development of mining activity with the opening of the Cobre Las Cruces mine (CLC). The CLC is one of Europe's largest open pit copper mine which has implemented pioneering

water management methodologies in the mining industry. One of the highlights of this methodology is the Drainage and Reinjection system (DRS) for groundwater near the mining activity. The DRS allows the drainage of the groundwater before it can appear in the open pit, through a set of wells surrounding it. Moreover, once treated to meet environmental requirements, this water is reinjected into the aquifer through another set of wells surrounding the extraction wells. In addition, groundwater in the vicinity of the CLC presents poor natural quality, so they are unsuitable for direct use without previous treatment. High natural concentrations of some components, initially alerted the public opinion. Nevertheless, today it has been demonstrated that this is not due to mining activity but to natural processes.

The general goal of this thesis is to provide a series of tools to improve the methodology of groundwater management in a mining environment. Development of a methodological framework is of great interest and may constitute a support tool for sustainable management and protection of groundwater resources affected by mining activities.

This methodological framework includes hydrogeochemistry, isotopic and statistics studies related to groundwater and water-rock interaction and flow and reactive transport modelling.

The combination of hydrogeochemical and radioactive isotopes using both stable and radioactive techniques allowed the following:

Identification of two principal groundwater facies: 1) Niebla-Posadas aquifer (NP): groundwater with a low degree of mineralization and calcium-bicarbonate water composition. This water is used for agricultural and human consumption and is strictly regulated by the water authority. 2) Paleozoic mass water: water from the Paleozoic rocks is older, shows a high degree of mineralization and has a sodium chloride water composition. Due to the quality of these waters, they are not used directly for any use of water. In addition, this work detected an evolution in aquifer hydrochemistry due to the existence of

mixtures between both waters and reactions such as cation exchange, calcite dissolution, and oxidation of organic matter.

Determination of the renewability rate of groundwater resources. The residence time of the groundwater of the NP aquifer was estimated using ^{3}H, ^{14}C and ^{36}Cl. The dating of these waters allowed the study area to be zoned into a recharge zone (<0.06 ky), an intermediate zone (0.06-20 ky), deep zone 1 (20-30 ky) and deep zone 2 (> 30 ky).

Identification of the origin of certain compounds present in groundwater (ammonium, arsenic and boron) and definition between natural and anthropogenic sources. The increase in NH_4 and B is interpreted as the result of degradation of marine organic matter by sulfate dissolved in the recharge water. The high concentrations of arsenic in groundwater result from reductive dissolution of Paleozoic iron oxide mineralizations (gossan) rich in As due to organic matter oxidation. Therefore, these high concentrations were originally attributed to geogenic processes.

However, the water that accumulates at the bottom of the open pit (in contact with the deposit) requires a different management since it is not authorized neither its discharge nor reinjection to the aquifer, serving as the main supply of the hydrometallurgical process. However, the Administration obliges to compensate the part of water that appears in the open pit and comes from the NP aquifer. The use of multivariate statistical methods has allowed us to calculate the monthly mixing ratios of the different water sources. This approach allowed definition of the volume of water extracted from the NP aquifer that must be compensated, annually, in accordance with conditions established by the administration.

Finally, the singularity of the mineralogical composition of some rocks in the CLC deposit have aroused special interest and controversy in the scientific community. This complexity is largely due to the interaction between groundwater (hydrochemistry, hydrodynamics, etc.) and the CLC deposit. To clarify these issues, 1D reactive transport modelling demonstrated that the unusual siderite accumulation may be due to the interaction of

groundwater similar to that in the present and the original iron oxide mass (gossan) on a time scale of 10^5 years.

All these methodological issues are focused on and applied to the CLC, which has allowed validation of joint use to ascertain and quantify the hydrodynamic aspects of the groundwater at mine sites and definition of the bases for sustainable water resource management in the area.

RESUM

L'entorn natural en què vivim, es veu sotmès, en major o menor mesura, a la pressió de l'activitat humana, sent els recursos hídrics un dels elements més sensibles. Per aquesta raó, conscients d'aquesta situació, des de tots els fòrums (administració, empreses i stakeholders) s'està imposant la pràctica de nous estàndards impensables durant les dècades del desenvolupament industrial, encaminats a aconseguir compatibilitzar el medi ambient i la industria. Un nou model de mineria pretén aconseguir un equilibri entre les bones pràctiques ambientals i eficiència, de manera que la producció està lligada al respecte ambiental.

L'aqüífer Niebla-Posadas (NP) constitueix un dels recursos hídrics, dins de la conca del Guadalquivir, que dóna suport a l'agricultura tradicional de la zona i és la font d'aigua potable per varies poblacions. En les últimes dècades, la competència per aquest recurs s'ha incrementat a causa de l'expansió de l'agricultura de regadiu i afectat alhora pel desenvolupament de l'activitat minera amb l'obertura de la mina Cobre Las Cruces (CLC). CLC és una de les mines de coure a cel obert més moderna i gran d'Europa que ha implementat unes metodologies de gestió d'aigües pioneres dins de la indústria minera. Un

dels punts forts d'aquesta metodologia és el Sistema de Drenatge i Reinjecció (SDR) de les aigües subterrànies a l'entorn de l'activitat minera. El SDR permet drenar les aigües subterrànies abans que puguin aflorar en la "Corta minera", mitjançant una sèrie de pous al seu voltant. Alhora, aquestes aigües, un cop tractades per acomplir els requeriments ambientals exigits, són reinjectades al aqüífer mitjançant un altre conjunt de pous que envolten els pous d'extracció.

A més, les aigües subterrànies a l'entorn de CLC presenten mala qualitat natural, de manera que resulten inapropiades pel seu ús directe sense tractament previ. Les elevades concentracions naturals que alguns components presentaven, van alertar inicialment a la opinió pública. No obstant, avui s'ha pogut demostrar que aquesta no es deu a l'activitat minera sinó a processos naturals.

L'objectiu general d'aquesta tesi és proporcionar una sèrie d'eines que permeten millorar la gestió de les aigües subterrànies en un entorn miner. Desenvolupar aquest marc metodològic és de gran interès i pot constituir una eina de suport per a la gestió sostenible i protecció dels recursos hídrics subterranis en zones afectades per activitats mineres.

Aquest marc metodològic inclou estudis hidrogeoquímics, isotòpics, estadístics relacionats amb les aigües subterrànies i la interacció aigua-roca, i modelació de flux i transport reactiu. La combinació de tècniques hidrogeoquímiques i isotòpiques, tant estables com radioactius, en les aigües subterrànies han permès:

1) Identificar dues agües amb característiques molt diferenciades: 1) Aqüífer Niebla-Posadas (NP): aigua jove amb baix grau de mineralització i composició bicarbonatada càlcica. Aquesta aigua s'utilitza per a fins agrícoles i de consum, i el seu ús està regulat per l'activitat minera; 2) Massa d'aigua Paleozoic: aigua amb major temps de trànsit, amb alt grau de mineralització i composició clorurada sòdica. Degut a la qualitat que presenten aquestes aigües, no es destinen de forma directa a cap ús d'abastament. A més, s'ha observat una evolució en la hidroquímica

de l'aqüífer degut a la mescla entre les dues aigües i de reaccions com ara intercanvi catiònic, dissolució de calcita i oxidació de la matèria orgànica, etc.

2) Conèixer la taxa de renovabilitat dels recursos hídrics subterranis. S'ha estimat el temps de residència de les aigües subterrànies de l'aqüífer utilitzant ^{3}H, ^{14}C i ^{36}Cl. La datació d'aquestes aigües ha permès la zonificació de l'àrea d'estudi en: zona de recàrrega (<0.06 ka), zona intermèdia (0,06-20 ka), zona profunda 1 (20-30 ka) i zona profunda 2 (> 30 ka).

3) Identificar l'origen de certs compostos presents en les aigües subterrànies (amoni, arsènic i bor) i definir el seu origen natural o antropogènic. L'increment de NH_4 i B s'interpreta com el resultat de la degradació de la matèria orgànica pel sulfat dissolt en l'aigua de recàrrega. Les altes concentracions d'arsènic en l'aigua subterrània és el resultat de la dissolució reductiva de mineralitzacions d'òxids de ferro (gossan) paleozoics rics en As deguda a l'oxidació de la matèria orgànica dissolta en l'aigua. Per tant, aquestes elevades concentracions s'atribueixen originalment a processos geogènics.

Per altra banda l'aigua que s'acumula al fons de la "corta minera" (que ha estat en contacte amb el jaciment) requereix un tractament molt diferent ja que no està autoritzada ni el seu abocament ni reinjecció a l'aqüífer, servint com abastament principal del procés hidrometalúrgic. No obstant, l'Administració obliga a compensar la part de l'aigua que aflora al fons de la "corta" y que procedeix de l'aqüífer NP. L'ús de mètodes estadístics multivariants ha permès calcular, mes a mes, les proporcions de mescla de cadascuna de les aigües que composen l'aigua bombejada des del fons de la "corta minera" (aqüífer NP, Paleozoic o escolament). D'aquesta manera s'ha determinat el volum d'aigua extret de l'aqüífer Cenozoic que ha de ser compensat anualment, d'acord amb les condicions establertes per l'Administració.

Finalment, la singularitat de la composició mineralògica d'algunes roques del jaciment de Las Cruces han despertat un especial interès i controvèrsia en la comunitat científica. Aquesta complexitat es en gran part deguda al resultat de la interacció entre les aigües subterrànies (hidroquímica, hidrodinámica, etc.) i el propi jaciment. Per aclarir alguns d'aquests aspectes s'ha realitzat un model de transport reactiu 1D amb el qual s'ha calculat que la acumulació inusual de siderita, present a una part del jaciment, s'ha pogut formar degut a la interacció de l'aigua subterrània similar a l'actual amb una massa d'òxids de ferro (gossan) original en una escala de temps d'uns 10^5 anys.

La combinació de tots aquests aspectes metodològics s'han focalitzat i aplicat a CLC, el que ha permès: validar-ne l'ús conjunt per tal de conèixer i quantificar els aspectes bàsics de la hidrodinàmica subterrània en un entorn miner complex i definir les bases per una gestió sostenible dels recursos hídrics de la zona.

RESUMEN

El entorno natural en el que vivimos, se ve sometido, en mayor o menor medida, a la presión de la actividad humana, siendo el agua uno de los elementos más sensibles. Por esta razón, conscientes de esta situación, desde todos los foros (Administración, Empresas y stakeholders) se está imponiendo la práctica nuevos estándares impensables durante las décadas del desarrollo industrial, encaminados a lograr compatibilizar el medio ambiente y la Industrial (en especial, en esta tesis, la actividad minera). Un nuevo modelo de minería pretende lograr un equilibrio entre buenas prácticas ambientales y eficiencia, de forma que la producción está ligada al respeto ambiental.

El acuífero Niebla-Posadas (NP) constituye uno de los recursos hídricos, dentro de la cuenca del Guadalquivir, que da apoyo a la agricultura tradicional de la zona y es la fuente de agua potable para varias poblaciones. En las últimas décadas, la competencia por este recurso se ha incrementado debido a la expansión de la agricultura de regadío y afectado a su vez por el desarrollo de la actividad minera con la apertura de la mina Cobre Las Cruces (CLC).

CLC es una de las minas de cobre a cielo abierto más moderna e importante de Europa, donde se ha implementado unas metodologías de gestión de aguas pioneras dentro de la

industria minera. Uno de los puntos fuertes de esta metodología es el Sistema de Drenaje y Reinyección (SDR) de las aguas subterráneas en el entorno de la actividad minera. El SDR permite drenar las aguas subterráneas antes de que puedan aflorar en la corta minera, mediante una serie de pozos construidos formando un anillo a su alrededor. Asimismo, estas aguas, una vez tratadas para cumplir los requerimientos ambientales exigidos, son reinyectadas al acuífero mediante otro conjunto de pozos que rodean los pozos de extracción.

Las aguas subterráneas en las inmediaciones del CLC presentan mala calidad natural, de forma que resultan inapropiadas para su uso directo sin previo tratamiento. Las elevadas concentraciones naturales que algunos componentes presentaban, alertaron inicialmente a la opinión pública. No obstante, hoy ha podido demostrarse que esta no se debe a la actividad minera sino a procesos naturales.

El objetivo principal de esta tesis es proporcionar una serie de herramientas que permitan mejorar la metodología de gestión de las aguas subterráneas en un entorno minero. Desarrollar este marco metodológico es de gran interés y puede constituir una herramienta de apoyo para la gestión sostenible y protección de los recursos hídricos subterráneos, en zonas afectadas por actividades mineras.

Este marco metodológico incluye estudios hidrogeoquímicos, isotópicos, estadísticos relacionados con las aguas subterráneas y la interacción agua-roca, y modelos de flujo y transporte reactivo.

La combinación de técnicas hidroquímicas e isotópicas, tanto isótopos estables como radiactivos, en las aguas subterráneas han permitido:

1) Identificar dos aguas con características diferentes: 1) Acuífero Niebla-Posadas (NP): agua joven con bajo grado de mineralización y composición bicarbonatada cálcica. Esta agua se utiliza para fines agrícolas y de consumo, y su uso está regulado para la actividad minera; 2) Masa de agua Paleozoico: agua con mayor tiempo de tránsito,

con alto grado de mineralización y composición clorurada sódica. Debido a la calidad que presentan estas aguas, no se destinan de forma directa a ningún uso de abastecimiento. Además, este trabajo ha detectado una evolución en la hidroquímica del acuífero debido a la existencia de mezclas entre ambas aguas y de reacciones como de intercambio de cationes, disolución de calcita, y oxidación de materia orgánica, etc.

2) Conocer la tasa de renovabilidad de los recursos hídricos subterráneos. Se ha estimado el tiempo de residencia de las aguas subterráneas del acuífero NP utilizando ^{3}H, ^{14}C y ^{36}Cl. La datación de dichas aguas ha permitido la zonificación del área de estudio en: zona de recarga (<0.06 ka), zona intermedia (0.06-20 ka), zona profunda 1 (20-30 ka) y zona profunda 2 (> 30 ka).
3) Identificar el origen de ciertos compuestos presentes en las aguas subterráneas (amonio, arsénico y boro) y definir su origen natural o antropogénico. Las concentraciones de NH_4 y B se ha interpretado como el resultado de la degradación de la materia orgánica por el sulfato disuelto en el agua de recarga. Las altas concentraciones de arsénico en el agua subterránea son el resultado de la disolución reductiva de mineralizaciones de óxidos de hierro (gossan) paleozoicos ricos en As debida a la oxidación de la materia orgánica disuelta en el agua. Por lo tanto, estas concentraciones anómalas de NH_4, B y As en el agua subterránea se han atribuido a procesos geogénicos.

Por otra parte, el agua que se acumula en el fondo de la corta minera (que ha estado en contacto con el yacimiento), requiere una gestión muy diferente ya que no está autorizada ni su vertido ni reinyección al acuífero, sirviendo por ello como abastecimiento principal del proceso hidrometalúrgico. No obstante, la Administración obliga a compensar la parte de agua que surge en fondo de corta y procede del acuífero NP. El empleo de métodos estadísticos multivariados ha permitido calcular, mes a mes, las proporciones de mezcla de cada una de las aguas que componen la bombeada desde fondo de la corta minera (acuífero NP, Paleozoicas o de escorrentía). De esta manera se ha determinado el volumen de agua

extraído del acuífero NP que debe ser compensado anualmente, de acuerdo con las condiciones establecidas por la Administración.

Finalmente, la singularidad de la composición mineralógica algunas rocas del yacimiento de Las Cruces han despertado un especial interés y controversia en la comunidad científica. Gran parte de esta complejidad se debe al resultado de la interacción entre las aguas subterráneas (hidroquímica, hidrodinámica, etc) y el propio yacimiento. Para aclarar estos aspectos, se ha realizado un modelo de transporte reactivo 1D que ha permitido calcular que la acumulación inusual de siderita, presente en una parte del yacimiento, se ha podido formar debido a la interacción del agua subterránea semejante a la actual con una masa de óxido de hierro (gossan) original en una escala de tiempo de unos 10^5 años.

La combinación de todos estos aspectos metodológicos se ha centrado y aplicado al caso CLC, lo que ha permitido: validar su uso conjunto con el fin de conocer y cuantificar los aspectos básicos de la hidrodinámica subterránea en un entorno minero complejo y definir las bases para una gestión sostenible de los recursos hídricos de la zona.

AGRADECIMIENTOS

Esta tesis ha sido un reto para mí ya que nunca tuve en mente hacer un doctorado. Por suerte un día surgió esta oportunidad y no la pude rechazar. En estos últimos años se ha cruzado mucha gente en mi camino que de forma directa o indirecta han puesto su granito de arena en esta tesis.

En primer lugar, me gustaría agradecer a dos personas que han sido los pilares de esta tesis, el Dr. Carlos Ayora y el Dr. Enric Vázquez. Os agradezco, la oportunidad que me habéis brindado, el apoyo, ayuda y confianza que me habéis dado día tras día y decir que ha sido un placer contar con personas como vosotros.

Durante mi tesis he tenido la ocasión de realizar una estancia en Australian Nuclear Science and Technology Organisation (ANSTO) la cual fue una experiencia muy positiva. Sin lugar a duda, mil gracias al Dr. Dioni Cendón por su acogida durante mi estancia, por su inestimable ayuda y disponibilidad, y por enseñarme otra manera de trabajar. En esos cuatro meses tuve el placer de conocer a dos personas muy especiales, Clara y Rani, que ayudaron que me sintiera más cerca de casa.

También quiero agradecer a la Dra. Manuela Barbieri, ya que contigo empezó todo. Gracias por los momentos que hemos compartido y por ser mi guía en el inicio de mi doctorado, por tu apoyo y cariño durante este tiempo.

Gracias a Fundación Migres por la financiación de esta tesis. Agradezco también a Cobre Las Cruces, especialmente a Juan Carlos Baquero, por vuestra colaboración y contribución a esta tesis.

Quiero extender un sincero agradecimiento al grupo de Mineralogía aplicada y geoquímica de fluidos de la Universidad de Barcelona, especialmente a Albert Soler, Mercè Olamendi y

Roger Puig, y Mercè Cabañas, Rafael Bartrolí y Oriol Font del IDAEA-CSIC. Gracias a vosotros ha sido posible obtener parte de los resultados de esta tesis.

Muchísimas gracias a todos mis compañeros y amigos del Grupo de Hidrología Subterránea (GHS), especialmente a todos aquellos que me habéis hecho disfrutar cada día de esta aventura. A Katrien y Ana por los buenos momentos que hemos compartido desde el primer día que llegué al grupo. A Sheila, Berta y Miguel Ángel por nuestras charlas locas de despacho y porque poco a poco nos hemos convertido en una familia. A nuestro fabuloso grupito de cafés, cervecitas, algunas excursiones y lo que surja, ya que sin vosotros y esos momentos todo hubiese sido muy aburrido, especialmente a Jordi, Alba, Quim, Bayaraa, Gonzalo, Alessandro, Silvia, Tere, Carles Cayuela, Maria Roig. Gracias a Cristina y Gaby por ser unas grandes compañeras de viaje. A Serranito y a Mar por los momentos que hemos podido disfrutar desde el inicio de la tesis y por vuestra ayuda y paciencia. Quiero agradecer de forma especial a Rotman por ser un gran compañero y amigo, por tus ideas, motivación, ánimos, cafés, cervecitas, y por ser un gran apoyo.

No me quiero olvidar a los amigos que he hecho durante mi formación, a mis mañitos Raúl y Jose, a Xavi, Anna, Isra, Roger y especialmente a Santos por ser quien me ha embarcado en esta aventura (eres un liante!!).

Finalmente, un especial agradecimiento a mis padres y hermano, que sin tener muy claro en que gasto mi tiempo siempre me han apoyado y han estado presentes. Esta tesis se la quiero dedicar a Raúl, mi compañero de todos mis caminos y que gracias a tu apoyo constante y cariño he podido llegar hasta aquí. Tenerte a mi lado me ayuda a superar cualquier obstáculo, gracias.

LIST OF CONTENTS

LIST OF FIGURES

LIST OF TABLES

CHAPTER 1. Introduction

1.1.MOTIVATION AND OBJECTIVES

The natural environment in which we live is being degraded by human activity, and water is one of the main victims of these impacts. Increasingly, governments around the world are putting greater pressure on industries that use large amounts of water, especially water used for mining activities, to be more sustainable. Mining primarily requires water for mineral processing, dust suppression and sludge transport and to meet the needs of employees. Most mining operations obtain water from underground, river and lakes. However, mining activities are often located in areas where water is scarce, and communities and local authorities commonly oppose these activities because they use water requiring maximum protection. While water collection may pose a problem, its extraction is usually also inconvenient. In several cases, mining operations intercept the water level, and groundwater must be pumped, producing problems as the water level decreases and water quality changes, affecting the environment and other users of groundwater in the surroundings. Mined materials support 45% of the world's economic activities, but large scale mining leaves social and environmental scars. Usually, any discussion of mining and the environment conjures environmental disasters related to mining activities. A quick

search of industry news shows many worldwide cases of water affected by mining activities. Most accidents involve bursting of a holding dam. There is a growing awareness of the need to ensure maximum sustainability of water in the mining industry, but there is still a long way to go. In many countries, mining companies are required to follow and comply with strict codes of environmental protection to minimize environmental impacts and avoid problems with adjacent communities. Thank to social pressures and awareness, mining companies have developed what is known as new mining. The new mining model seeks to achieve a balance among good environmental practices, cost reduction and mining productivity (Figure 1.1).

Figure 1.1. Schematic view of concepts in new mining: good environmental practices, cost minimization and mining productivity.

A good example is the Cobre Las Cruces (CLC) mining complex located in southern Spain in the Guadalquivir basin. This basin, with a surface of 60.000 km^2, is a major geological and hydrological area in southern Spain, sustaining an important population. It is a semiarid region where the distribution of water resources between human use and the environment is a challenge (CHG 2012). The Niebla-Posadas (NP) aquifer is a main groundwater resource for the lower Guadalquivir basin. It supports traditional agriculture and is a drinking water

reserve for many localities, including Sevilla. Further competition for water resources in recent years in the area has arisen from the expansion of irrigation agriculture, with an increase of 64% of irrigated crop area in 2000-2011 (SIGEA 2014), gas exploration, and the opening of a major open-pit mine, the CLC. The Niebla-Posadas (NP) aquifer close to the CLC has high ammonium, arsenic and boron concentrations within the confined, deep portion of the aquifer. The concentrations of these three compounds locally exceeds current World Health Organization guidelines for drinking water (WHO 2008) and recommended values from the U.S. Environmental Protection Agency for continuous irrigation (USEPA 2012). The Spanish regulations for drinking water (RD140/2003), according to the European Water Framework Directive (WFD), have values close to the WHO values, which are more restrictive for some compounds. High concentrations of contaminants have attracted public attention, and numerous environmental groups have drawn focus to the main anthropogenic activities in the zone, especially the mining exploitation of Cobre Las Cruces (CLC). This has had an important impact in the media, with evidence in the headlines in national and international newspapers.

This mining complex is an open pit copper mine highlighted in Europe for its large dimensions (up to 200 mbsl) and high-purity (99.999%) copper cathodes. The ore body is located in a Paleozoic basement buried by Cenozoic materials below groundwater level. CLC deposits have also sparked an interest in the scientific community due to the uniqueness of their mineralogical composition. The Las Cruces gossan shows a particular mineralogy, formed primarily by siderite as well as galena, calcite, goethite, hematite and precious metals, differentiating it from other deposits. The genesis of this mineralogical composition presents a number of uncertainties and is discussed in some reports proposing different hypotheses about its origin and evolution.

Another peculiarity of this mining complex is its drainage system. The open pit constitutes a discharge point where water must be pumped to the surface, where it will be treated for proper management, so that mining can proceed under safe conditions. To balance the needs of mine water drainage with maintaining the equilibrium of water in the NP aquifer,

the mining project has implemented a Drainage and Reinjection System (DRS). This system allows advanced drainage of the pit with a peripheral ring of 45 wells intercepting the water flowing through the aquifer and preventing it from falling down the sidewalls of the mine pit. After treatment, the water is redirected to a second ring reinjection system composed of 37 wells 0.7 to 2.5 km from the mine pit. The main objective of this system is to prevent the decrease in the piezometric level in areas outside the mining complex and to maintain groundwater quality.

There are several questions that be must addressed:

- ***Is groundwater renewable or a fossil resource?***
- ***What is the origin of groundwater chemistry?***
- ***Is groundwater suitable for human use without treatment? If not, what are the limitations?***
- ***Is the use of groundwater in mining activities sustainable?***
- ***What is the effect of the groundwater-ore mineralogy interaction?***

Considering the abovementioned factors, the general objective of this thesis is to provide a methodological framework for the management of groundwater in a mining environment. The development of a methodological framework is of great interest and may constitute a support tool for the sustainable management and protection of groundwater resources affected by mining activities. This methodology is based on a combination of hydrochemical, isotopic, multivariate statistical and modelling techniques, allowing evaluation of the influence of mining activities on groundwater, determination of the genesis of water chemistry as a deposit and the assessment and management of groundwater use in mining activity.

1.2.THESIS OUTLINE

This thesis is organized into seven chapters: an introduction chapter (chapter 1), a materials and methods chapter (chapter 2), chapters 3 to 6 are related to articles published in or submitted to international journals, and finally chapter 7 presents the conclusions of this thesis.

Chapter 3 uses hydrogeochemical and dating techniques to identify the part of the aquifer that contains groundwater that can be regarded as a renewable resource and the part that is mostly composed of fossil groundwater. This will enhance our understanding of groundwater system dynamics and become a support for the sustainable management and protection of groundwater resources, which can likely be generalized and influence other similar studies.

Chapter 3 is based on the following paper: Scheiber, L., Ayora, C., Vázquez-Suñé, E., Cendón, D. I., Soler, A., Custodio, E., & Baquero, J. C. (2015). Recent and old groundwater in the Niebla-Posadas regional aquifer (southern Spain): Implications for its management. Journal of Hydrology, 523, 624-635.

Chapter 4 aims to assess a set of tools to differentiate geogenic/anthropogenic sources and processes, with particular attention to processes controlling ammonium, arsenic and boron concentrations. This chapter presents a detailed hydrogeochemical and isotopic study suggesting the natural origin of high ammonium, arsenic and boron concentrations in the deeper sections of the aquifer.

Chapter 4 is based on the following paper: Scheiber, L., Ayora, C., Vázquez-Suñé, E., Cendón, D. I., Soler, A., & Baquero, J. C. (2016). Origin of high ammonium, arsenic and boron concentrations in the proximity of a mine: Natural vs. anthropogenic processes. Science of the Total Environment, 541, 655-666.

Chapter 5 proposes an approach based on multivariate statistical methods for computing the mixing ratios of various waters (end-members) in open pit mining operations, including the identification of different water sources and the evaluation of mixing ratios. This approach will be applied to evaluate the contributions from each water input (run-off, Cenozoic and Paleozoic end-members) that forms the CLC open pit water and to determine the water volume extracted from the Cenozoic aquifer that must be compensated by the company according to the regulation in force, using an approach based on mixing calculations from the CLC mining complex.

Chapter 5 is based on the following paper: Scheiber, L., Ayora, C. and Vázquez-Suñé. Quantification of proportions of different water sources in a mining operation. In process.

Chapter 6 seeks to quantitatively discuss the feasibility of a genetic model for the Las Cruces siderite rock resulting from the interaction of a previous gossan with groundwater similar to the present day composition. To reach this objective, it was necessary to 1) characterize the hydrochemistry and isotopes of present day groundwater, 2) quantify the groundwater flow rate through the gossan by performing a hydrogeological numerical model, and 3) quantify the biogeochemical interaction of groundwater flow through gossan rocks using reactive transport numerical modelling.

Chapter 6 is based on the following paper: Scheiber, L., Ayora, C., Vázquez-Suñé & Soler, A. (2017). Groundwater-Gossan Interaction and the Genesis of the Siderite rock from the Las Cruces Ore Deposit (SW Spain). Ore geology reviews. Accepted.

Chapter 7 consists of a synthesis of the research, with main conclusions and an answer to the questions addressed above. Additionally, it provides general reflection on the conclusions, the scientific contribution of this thesis and recommendations for further research.

1.3.SCIENTIFIC ARTICLES, PROCEEDINGS AND REPORTS

As a result of this thesis, articles and technical reports were written on the subject, and the topic has been included in several proceedings.

SCIENTIFIC ARTICLES

2014	**Laura Scheiber**, Carlos Ayora, Enric Vázquez-Suñé, Albert Soler, Lola Yesares, José Miguel Nieto. Groundwater-Gossan Interaction at the Las Cruces Ore Deposit (SW Spain). Macla 19, Sociedad Española de Mineralogía
2015	**Scheiber, L.,** Ayora, C., Vázquez-Suñé, E., Cendón, D. I., Soler, A., Custodio, E., & Baquero, J. C. Recent and old groundwater in the Niebla-Posadas regional aquifer (southern Spain): Implications for its management. Journal of Hydrology, 523, 624-635. IF: 3.043
2016	**Scheiber, L.,** Ayora, C., Vázquez-Suñé, E., Cendón, D. I., Soler, A., & Baquero, J. C.Origin of high ammonium, arsenic and boron concentrations in the proximity of a mine: Natural vs. anthropogenic processes. Science of the Total Environment, 541, 655-666. IF: 3.976
2016	J. Carlos Baquero, Mª José de los Reyes, Emilio Custodio, **Laura Scheiber** and Enric Vázquez-Suñé. Groundwater Management in Mining. The Drainage and Reinjection System in Cobre Las Cruces. Modern Environmental Science and Engineering, 2333-2581. IF: 0.4
2017	**Laura Scheiber**, Carlos Ayora, Enric Vázquez-Suñé, Albert Soler. Groundwater-Gossan Interaction and the Genesis of the Secondary Siderite rock at Las Cruces Ore Deposit (SW Spain) Ore geology reviews. IF: 3.819

PROCEEDINGS

2014 **Laura Scheiber**, Carlos Ayora, Enric Vázquez-Suñé, Albert Soler, Lola Yesares, José Miguel Nieto. Groundwater-Gossan Interaction at the Las Cruces Ore Deposit (SW Spain). SEM 2014, XXXIV Reunión Científica de la Sociedad Española de Mineralogía. 2-7 July de 2014, Granada. Oral presentation.

2014 **Scheiber, L.,** Ayora, C., Vázquez-Suñé, E., Cendón, D. I., Soler, A. and Baquero, J. C. Importante papel de la geoquímica y de los procesos de mezcla en la datación de las aguas subterráneas del acuífero Niebla-Posadas en el entorno de Gerena, sur de España. II Congreso Ibérico de las aguas subterráneas. 8-10 September 2014, Valencia. Oral presentation.

2015 **Scheiber, L.,** Ayora, C., Vázquez-Suñé. Groundwater management in the proximity of a mine site: Cobre Las Cruces (Spain). 1st Meeting of Young researchers from IDAEA-CSIC. 22 October 2015, Barcelona. Oral presentation.

2015 **Scheiber, L.,** Ayora, C., Vázquez-Suñé, E., Cendón, D. I., Soler, A. and Baquero, J. C. Origen de las altas concentraciones de amonio, arsénico y boro en el acuífero Niebla-Posadas en la proximidad de la actividad minera de Cobre Las Cruces (Gerena-Sevilla). SIAGA, 4-6 November 2015, Málaga. Oral presentation.

2016 **Laura Scheiber**, Carlos Ayora, Enric Vázquez-Suñé and Albert Soler. Groundwater-Gossan interaction and the genesis of the siderite rock at the Las Cruces Ore Deposit. American Geophysical Union (AGU), 12-16 December 2016, San Francisco. Poster presentation.

2016 Dioni I Cendon, Stuart I Hankin, Cath E Hughes, Karina Meredith, Mark Peterson, **Laura Scheiber** and Yuta Shimizu. A Nine-year Record of Groundwater Environmental Tracer Variations in a Weathered Sandstone Plateau Aquifer. American Geophysical Union (AGU), 12-16 December 2016, San Francisco. Oral presentation.

TECHNICAL REPORTS

- Estudio hidrogeológico e hidrogeoquímico del acuífero profundo del entorno minero de Cobre Las Cruces (IDAEA-CSIC, 2013).

- Datación de las aguas subterráneas en el entorno minero de CLC (IDAEA-CSIC, 2013).

- Establecimiento de porcentajes de mezcla entre Mioceno y Paleozoico en las aguas de fondo de corta de la explotación minera de CLC (IDAEA-CSIC, 2013).

- Estudio hidrogeológico e hidrogeoquímico del área minera de CLC y su influencia en el acuífero Niebla-Posadas. Origen del arsénico (IDAEA-CSIC, 2015).

- Establecimiento de porcentajes de mezcla en las aguas de fondo de corta de la explotación minera de CLC de los años hidrológicos 2009-10 A 2013-14 (IDAEA-CSIC, 2015).

- Establecimiento de porcentajes de mezcla en las aguas de fondo de corta de la explotación minera de CLC. Año hidrológico 2014-15. (IDAEA-CSIC, 2016).

- Establecimiento de porcentajes de mezcla en las aguas de fondo de corta de la explotación minera de CLC. Año hidrológico 2015-16. (IDAEA-CSIC, 2017).

CHAPTER 1

CHAPTER 2. Materials and methods

2.1. GEOLOGICAL SETTING

The Las Cruces ore deposit is located at the eastern edge of the Iberian Pyritic Belt (IPB), approximately 20 km North of Seville (South Spain). The IPB is a metallogenic province 250 km long and 30-50 km wide, extending from south of Lisbon (Portugal) to Seville (Spain) (Figure 2.1A). It contains half of the worldwide giant volcanogenic massive sulfide deposits and has been extensively described. The IPB shows a stratigraphic succession formed by upper Paleozoic sedimentary marine materials and volcanic rocks (Schermerhorn, 1971; Moreno and Sáez, 1990; Pascual et al., 1994). These materials were affected by several tectonic phases during the Variscan orogeny that resulted in NW-SE to W-E structures and low-grade metamorphism (Quesada, 1991; Silva et al., 1990). Later, the Alpine orogeny played an important role and reactivated the structures previously formed. The exhumation of the Variscan chain exposed the massive sulfide deposits to the surface and thus promoted oxidation and the formation of gossans. Part of the IPB was covered by Cenozoic marine materials that refilled the Guadalquivir basin because of marine transgression-regression (Abad de los Santos, 2007). The Cenozoic sediments are composed of a monotonous marls unit related to shallow marine environments and bioclastic calcarenites at the base, interpreted as paleochannels.

The study area consisted of a Paleozoic basement composed of black shales and volcanic rock sequences that outcrop to the north of the area coinciding with higher topography. The

Paleozoic basement is overlain by two Cenozoic formations: the Niebla and Gibraleon formations (Fm.).

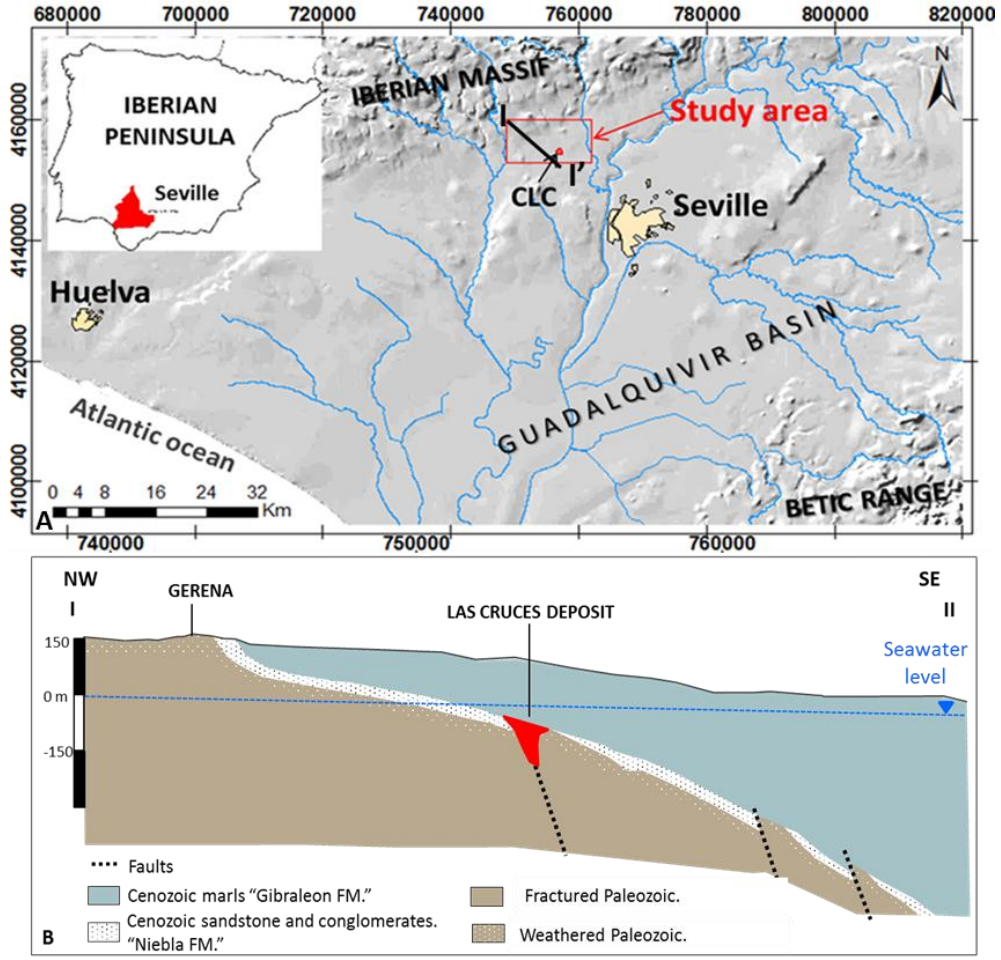

Figure 2.1. A) Location of the study area and the Las Cruces deposit; B) Section showing the main geological trends.

The Niebla Fm. is composed of basal conglomerates (bioclastic calcarenites) and sandstones rich in marine micro/macro fauna. The Gibraleon Fm. is formed by marine bluish marls rich in organic matter (Figure 2.1B). All these materials are affected by Alpine faults with a main SW-NE and a secondary NW-SE orientation (Figure 2.1B). Based on the age of river terraces in the region, it is considered that the geomorphological and hydraulic (and therefore hydrogeological) functioning of the study area have not changed significantly from low-

Pleistocene (1,8 Ma) to recent times (Escudero, 1994; Moral et al., 2013; Salvany et al., 2001).

The Las Cruces ore deposit is located in a sulfide massive body wedged in Paleozoic materials. The deposit was exhumed in Miocene time and the Paleozoic rocks and the massive sulfides were weathered under subaerial conditions. Consequently, a supergene profile was developed in the upper part of the sulfide massive composed of the primary zone, cementation zone and oxidation zone. The secondary deposit of Las Cruces has a peculiarity in its composition where the original gossan formed by goethite and hematite have been replaced by siderite, galena and iron metastable sulfides such as greigite and smythite (Tornos et al., 2014). Ore deposit description details is described in chapter 6.

2.2. HYDROGEOLOGICAL SETTING

The conglomerate and sand strata of the Niebla formation, together with a narrow layer of weathered Paleozoic basement, constitutes an aquifer. The upper part of fractured Paleozoic basement also constitutes a zone of moderate permeability. These aquifers outcrop to the north of the study area, constituting the recharge zone. The Niebla Fm. dips southward and is confined by the overlying marls of the Gibraleon Fm. that reaches a thickness of hundreds of metres (Figure 2.2A). Five zones can be differentiated based on their transmissivity values: (1) corresponds to the marls of the Gibraleon Fm.; (2) the sands and conglomerates of Niebla formation; (3) the weathered part of upper Paleozoic formation; (4) the Paleozoic rocks; and (5) the faults (Figure 2.2A). The approximately 10 to 30 m thick Niebla Fm. has transmissivity values that range between 10 and 500 $m^2 \cdot d^{-1}$, and its storage coefficient values are on the order of 10^{-2} within the unconfined zone and between 10^{-3} and 10^{-5} in the confined areas (CHG, 2012). It is sealed near the recharge zone by the low transmissivity (<5 $m^2 \cdot d^{-1}$) marls of the Gibraleon Fm. (CHG, 2012). No previous values have been measured for the Paleozoic, the weathered Paleozoic and the main faults. Following the groundwater head inventory and prior to mine operations, groundwater regional flow was dominantly from the northwest to the southeast (Figure 2.2B). There was

an abnormal change of gradient in the area around the mine site attributed to an elevation of the basement paleorelief, where the Niebla Fm. disappears and the marl layer rests directly on the Paleozoic (Figure 2.2A and B). The main recharge of the aquifer is by rainwater infiltration in the outcropping zone (NW). The total estimated annual recharge is 32 hm^3 (25 $mm \cdot y^{-1}$) for an area of 1,300 km^2. The discharge was 34 $hm^3 \cdot y^{-1}$ and corresponds to agricultural and consumption extractions (CHG, 2012; Navarro et al., 1993). Note that the Niebla aquifer was artesian south of the outcropping area prior to mining and agricultural extractions (IGME, 1984). Another important fact is the role of the main fault system as a possible discharge zone.

2.3. SAMPLING AND ANALYTICAL PROCEDURES

Groundwater samples were collected from a total of 40 wells and piezometers during two field campaigns carried out in February 2012 and September 2013. The physico-chemical parameters such as temperature (ºC), pH, Specific Conductance (SC, $\mu S \cdot cm^{-1}$), Eh and dissolved oxygen (DO, $mg \cdot L^{-1}$) were measured in situ inside a closed flow cell. Samples were collected for general chemistry (anions, cations and trace), for CH_4 and H_2S gas, Dissolved Organic Carbon (DOC), δ^2H and $\delta^{18}O$, $\delta^{13}C_{DIC}$, $\delta^{34}S$ and $\delta^{18}O$ in sulfate, $\delta^{15}N_{NH4+}$, ^3H, $^{14}C_{DIC}$ and ^{36}Cl analysis.

A total of 16 solid samples from Las Cruces replacement deposit have been analysed by X-ray diffraction (XRD), $\delta^{34}S_{SO4}$ analysis and electron microprobe (EPMA).

More details about sampling and analytical procedures is found in appendix A.

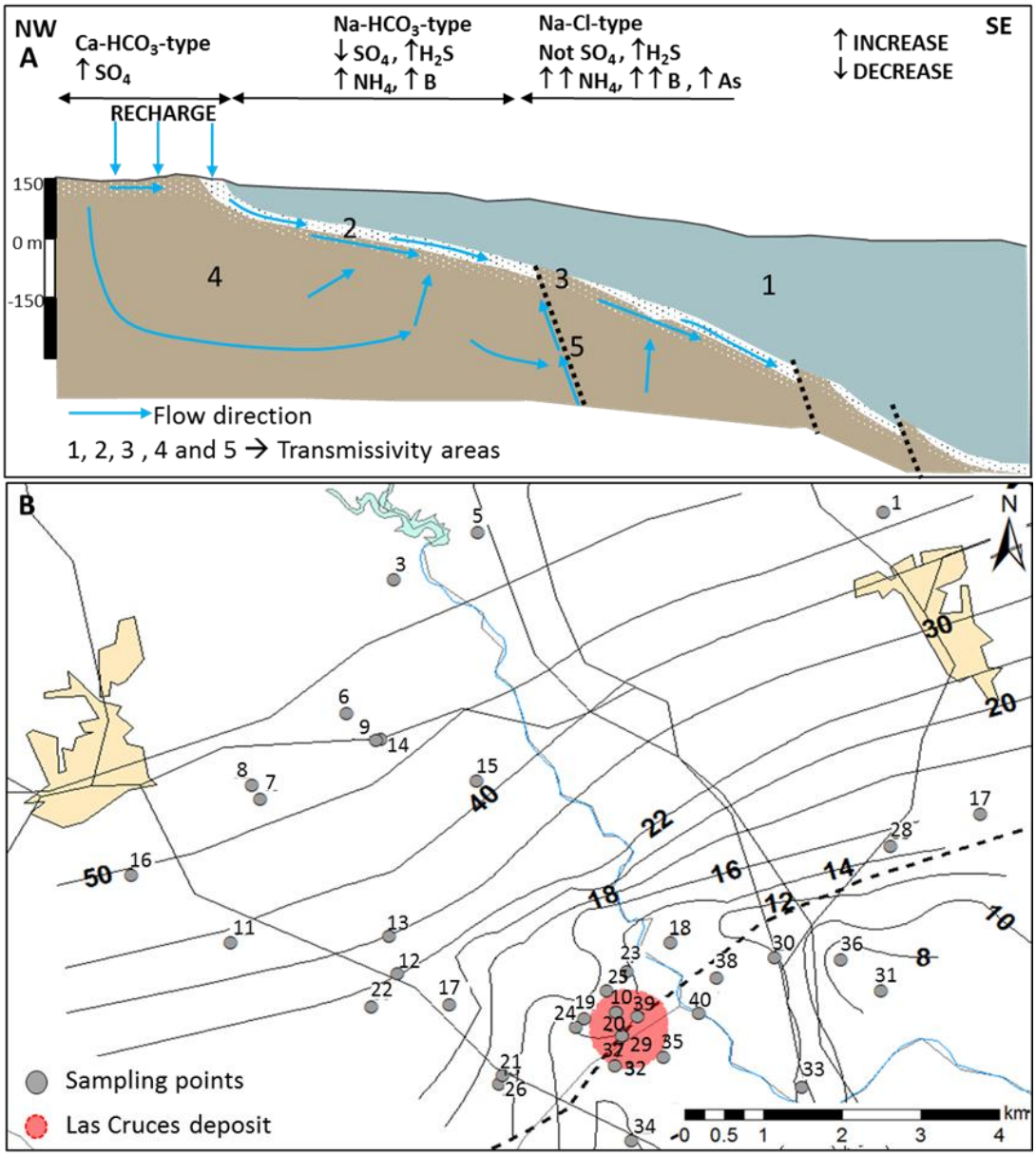

Figure 2.2. A) Simplified hydrogeological cross-section and hydrochemical characteristics of groundwater; B) Piezometric map of study area and sampling points distribution; The lines and bold labels are the interpolated groundwater isopotential lines and heads in masl (meters above sea level).

CHAPTER 2

CHAPTER 3. Recent and old groundwater in the Niebla-Posadas regional aquifer (southern Spain): implications for its management

3.1. INTRODUCTION

With a surface of 60,000 km^2, the Guadalquivir basin is a major geological and hydrological unit in southern Spain, sustaining a population of more than 4 million. It is a semiarid region where the distribution of water resources between human use and the environment is a challenge (CHG 2012). The Niebla-Posadas (NP) aquifer is one of the main groundwater resources of the lower Guadalquivir basin. It supports traditional agriculture and is a drinking water reserve for many localities, including Sevilla. Further competition for water resources in recent years in the area has arisen from the expansion of irrigation agriculture, with an increase of 64% of irrigated crop area in the 2000-2011 period (SIGEA 2014), gas explorations and the opening of two major open-pit mines. The Cobre Las Cruces (CLC) and Aznalcollar

mines (now in the process of reopening after a serious environmental incident about 15 years ago) exploit ore bodies located in contact within the Niebla-Posadas (NP) aquifer. The CLC mining complex is one of the largest open pit mining in Europe. To drain the open pit, a world-class Drainage and Reinjection System (SDR) has been implemented. The SDR is formed by two rings of perimetral wells, one of drainage wells and the other of reinjection wells. The function of this system is to prevent groundwater head drawdown and pollution of the NP aquifer outside the mining project. Farther to the south, the deeper NP sands below the Doñana National Park (>2000 m depth) host gas reserves and the feasibility of temporary CO_2 storage in the sands has been studied.

The hydrogeochemistry of the NP aquifer is complex; groundwater salinity increases with depth following characteristic pattern discussed by Tóth (1999) and common in many aquifers worldwide (e.g.: Frengstad et al. (2001); Wen et al. (2005); Cloutier et al. (2006); Su et al. (2013); and many others). The complex regional geological structure complicates the identification of flow paths and the assessment of tracer travel times. Therefore, groundwater availability and uses in the region are conditioned by the complex hydraulic and hydrogeochemical NP aquifer zonation. This generates groundwater management uncertainties that include key issues such as the definition of uses, water quality, reserves estimation, induced chemical degradation by mixing of different waters due to pumping, pollution risk, etc. In summary, the increasing demand for mining and agriculture and the rising public opinion concerns require a clearer assessment of groundwater.

Despite the described setting, no scientifically based assessment of water reserves is available. To respond to these questions, a hydraulic and hydrogeochemical conceptual model is needed. The objective of the present work is to define a methodology based on a combination of hydrogeochemical and dating techniques to identify which part of the aquifer contains groundwater that can be regarded as a renewable resource and which part is mostly composed of fossil groundwater. This will enhance the understanding of the groundwater system dynamics and become a support for sustainable management and

protection of groundwater resources, which likely can be generalized and influence other similar studies.

To achieve the defined objective, a hydrogeochemical and groundwater dating study has been carried out. The use of hydrochemistry and environmental isotopes is an effective method to differentiate water-rock interactions and define the origin of groundwater, in order to construct a conceptual model of transfer processes between different aquifer waters (Dogramaci et al. (2002); Edmunds et al. (2002); Andre et al. (2005); Edmunds (2009); Cartwright et al. 2010; among many others). Moreover, residence time estimation will be used, employing radioisotopes such as ^{3}H, ^{14}C, ^{36}Cl. This will be crucial to identify the volumes of non-renewable groundwater. A number of studies have used radioisotopes (^{3}H, ^{14}C, ^{36}Cl) to identify ancient and modern recharge and to estimate time scales of groundwater renewal (Bentley et al. (1986); Guendouz et al. (2006); Cartwright et al. (2012); Meredith et al. (2012); Plummer et al. (2012).

Some recent works also combine hydrogeochemical and dating techniques to estimate recharge sources and resident times to assess the sustainability of regional aquifer water resources development (Bouchaou et al. (2008); Mahlknecht et al. (2006); Sukhija et al. (2006); Douglas et al. (2007); Cresswell et al. (2001); Wallin et al. (2005); Currell et al. (2013); Atkinson et al. (2013). The recent proliferation of mining activities foreseeably makes these techniques the most likely immediate application of the methodology and conclusions of the present paper.

3.2. RESULTS AND DISCUSSION

GENERAL HYDROCHEMISTRY

The study area has been divided into 4 zones: recharge, intermediate, and deep (1 and 2) zones. This zonation corresponds to geochemical and isotopic differences and clearly correlates with the main geological features (i.e., the principal faults), as explained below (Figure 3.1).

Field determinations and complete chemical and isotopic data of each water sample are recorded appendix B.

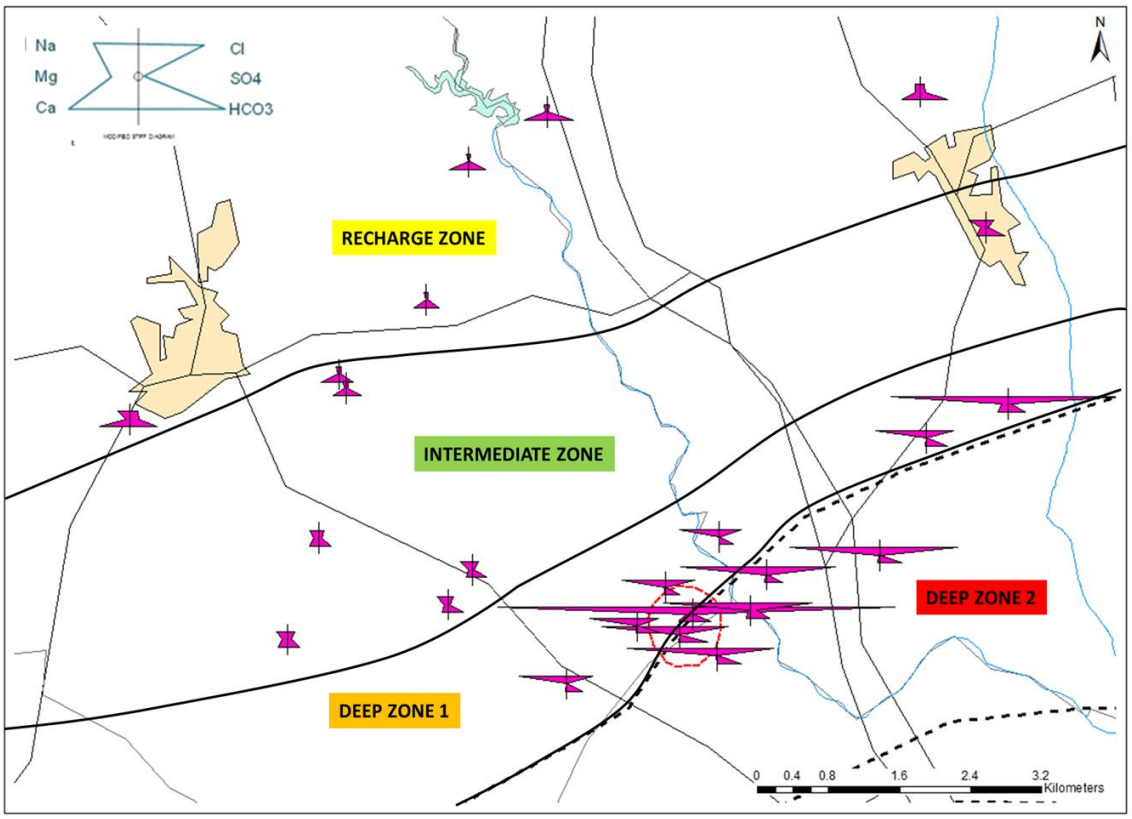

Figure 3.1. Modified Stiff diagram showing the general chemistry of the water samples. Zonification of the study area according to geochemical and isotopic differences.

Groundwater temperatures range between 17.8 and 36.5 °C; the lowest values are for shallow groundwater in the recharge area while higher temperatures correspond to deep samples toward the southeast. A vertical temperature profile obtained along 80 m shows a high geothermal gradient of 12 ˚C/100m, well above the average of the earth crust (3 ˚C/100m). These values are consistent with the thermal anomaly described in this area (IGME 1983) and are associated with the presence of faults with SW-NE orientation, which bring up the deep water contained in the Paleozoic materials.

The pH values measured ranged between 6.9 and 10.1, and the electrical conductivity (EC) ranged between 607 and 2800 µS/cm, in both cases increasing from NW to SE. The alkalinity shows values between 75 and 427 mg/L $CaCO_3$. Water from the recharge zone is characterized by a high content of dissolved oxygen, with values between 5.5 and 8.7 mg/L. As water moves downgradient becomes depleted in oxygen (<1 mg/L). Following the flow direction, the NP aquifer shows a clear evolution of Ca-HCO_3-type water toward Na-Cl-type water, with intermediate compositions (Na-HCO_3) (Figure 3.1).

The Cl/Br molar ratio ($R_{Cl/Br)}$) clearly shows two end points, one corresponding to groundwater of the recharge zone ($R_{Cl/Br}$ = 220-550) and the other ($R_{Cl/Br}$ = 640-680) corresponding to deep wells in the Paleozoic. The Cl/Br and Cl/Na relationship shows a mixture between infiltration water and a more saline end member, probably relict syndepositional water trapped in the pores (Figure 3.2 and Figure 3.3). The Cl-Na molar ratio shows that most of the analyses are shifted to higher Na concentrations, indicating the existence of an extra Na source. This is interpreted as the result of cation exchange with the clayish formations with the consequent replacement of Ca by Na in the groundwater (Appelo 1994). This is a well-known process when pore water in materials deposited in marine environments is slowly replaced by fresh water. The fact that cation exchange is still taking place points to a very slow penetration of continental fresh water into the aquifer.

Saturation indices (SI) were calculated using the PHREEQC code (Appelo et al. 2004) with the WATEQ4F thermodynamic database. Most samples are slightly supersaturated in calcite, with SI values between 0.13 and 0.8, with the exception of the recharge zone. Supersaturation is attributed to CO_2 degasification during sampling. Indeed, this is more evident in samples collected from a high pumping rate (>10 L/s). Gas bubbles appeared when the bottle was opened in the laboratory. By re-equilibrating the analyses with calcite, the final P_{CO2} calculated with PHREEQC varies between $10^{-3.3}$ atm and $10^{-1.2}$ atm, and the new recalculated pH values decreased between 0.3 and 0.7 units.

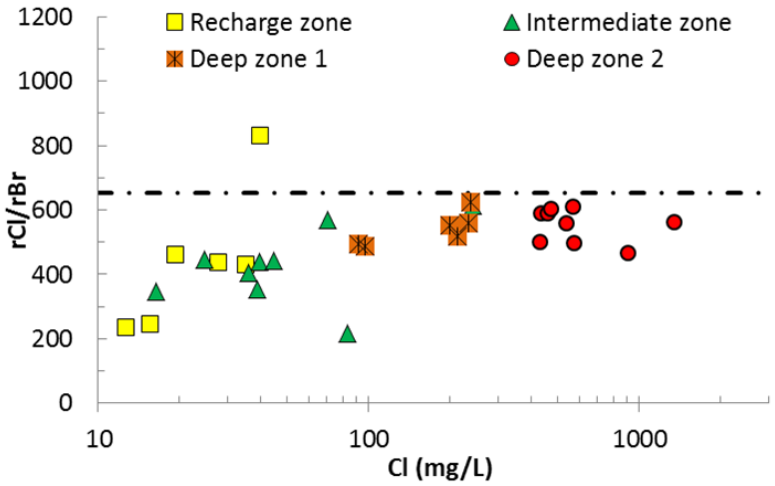

Figure3.2. Br-Cl molar ratios of analyzed groundwaters. Dashed line marks the marine Cl/Br ratio) Most of the analyzed samples plot along a line of continental values evolving toward more marine values as salinity increases (Whittemore, 1988; Davis et al., 1998; Herrera and Custodio, 2000; Alcalá and Custodio, 2008).

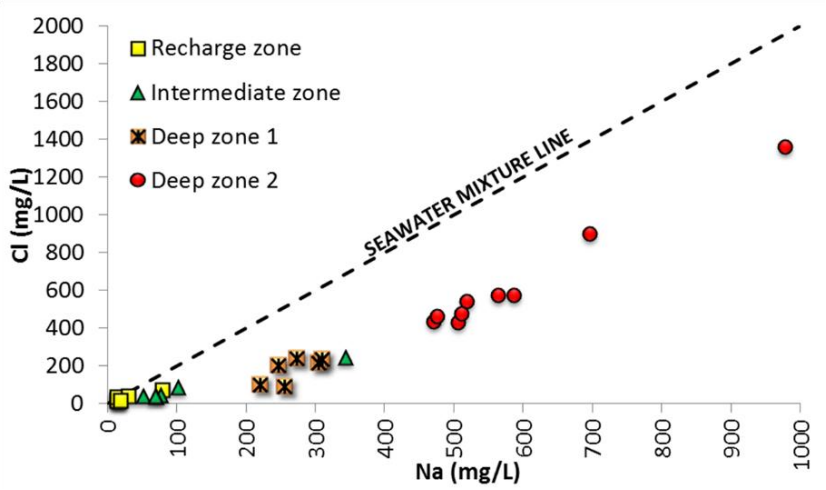

Figure 3.3. Plot of Cl vs. Na in groundwater (values in mg·L^{-1}).

STABLE ISOTOPES

WATER ISOTOPES

Groundwater samples show isotopic contents ranging from -21.5 to -30.0‰ for δ^2H and -2.9 to -5.2‰ for $\delta^{18}O$ (V-SMOW). As shown in Figure 3.4, the values follow the Global Meteoric Water Line (GMWL; Craig (1961)), indicating recharge by rainwater infiltration . The samples that correspond to the recharge area (NW) show heavier $\delta^{18}O$ and δ^2H values when compared to samples taken further south. The coincidence of depleted δ^2H and $\delta^{18}O$ values with longer residence times (see below) suggests that the recharge of these samples could have occurred in colder climates than recent samples. The $\delta^{18}O$ and δ^2H values show a positive correlation with the temperature with a slope of 0.69‰ per ºC for $\delta^{18}O$ and 5.6‰ per ºC for δ^2H (Dansgaard (1964) and Odezulu (2011)).

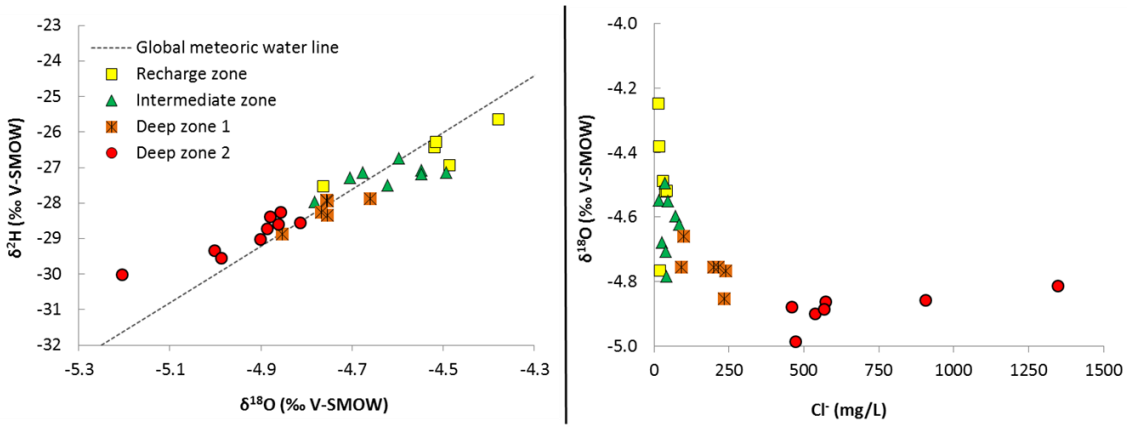

Figure 3.4. $\delta^{18}O$ vs. δ^2H content in groundwater.

From this information, can be calculate the temperature difference between the most recent and the oldest groundwater at the recharge time. It has been estimated that groundwater of the deep zones were recharged for a climate between 1.5 and 3 ° C colder than the current annual average Tª. The excess of deuterium, defined by d = δ^2H-8 $\delta^{18}O$ (Dansgaard 1964), varies between 9.5 and 11.6 ‰. These values are close to 10‰ and suggest an Atlantic origin and are consistent with those registered in Doñana National Park

(d = 10.9±3.1) (Iglesias 1999; Jimenez et al. 2008). There is a trend to lower d (< 10‰) for the fresher waters toward higher d (>10‰) as salinity increases. This may reflect for the more saline water different atmospheric conditions of recharge (colder climate with dryer air) (Figure 3.4).

SULFATE ISOTOPES

The isotope values of the S and O of the sulfate molecule have been determined in 24 samples. The $\delta^{34}S$ range between -17.2 and -20.4‰ (CDT), and the $\delta^{18}O$ values between 0.05 and 16.9‰ (V-SMOW). Sulfate isotope values also show a distinct variation from the recharge to the deep zones. Samples in the recharge area have low $\delta^{18}O$ values and a wide range of $\delta^{34}S$ values (Figure 3.5).

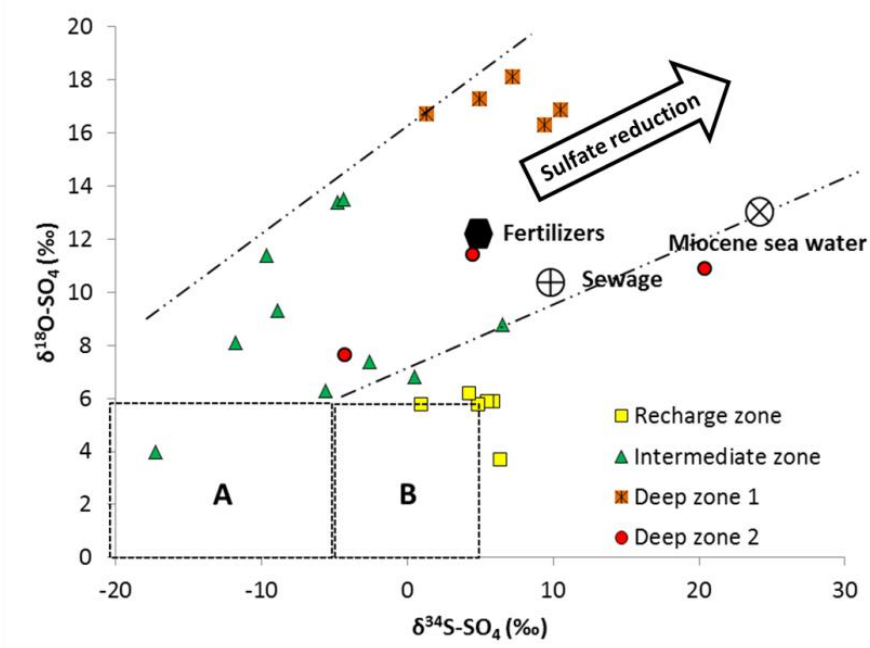

Figure 3.5. Representation of the isotopic content of sulfates in groundwater. A: Sulfate derived from sedimentary sulfide oxidation. B: Sulfate derived from magmatic sulfide oxidation.

This is compatible with oxidation of sulfides either in granites or in massive sulfide deposits, or with its dispersal in sedimentary materials. The range of $\delta^{18}O_{SO4}$ values obtained in the

recharge zone is compatible with $\delta^{18}O_{SO4}$ values of atmospheric sulfates (Mook 2002). Thus, the $\delta^{34}S$ values obtained are consistent with those between -15 and 10‰ reported for the Iberian Pyrite Belt (Sáez et al. 1999). The contribution of other sulfate sources such as those contained in fertilizers or sewage are clearly ruled out.

Samples from the intermediate and especially from the deep zones show a distinct trend toward heavier values of sulfate $\delta^{18}O$ and $\delta^{34}S$ (Figure 3.5), thus indicating a sulfate-reduction processes. Thode et al. (1970) demonstrated that sulfur and sulfides originated by biological sulfate reduction are characterized by heavier isotopic values, following slopes between 0.22 and 0.28 in a plot of $\delta^{18}O$ vs. $\delta^{34}S$. Sulfate-reduction is consistent with clear depletion of sulfate concentration in samples from intermediate and deep zones.

CARBON ISOTOPES

Seventeen samples have been analyzed for $\delta^{13}C$ of dissolved inorganic carbon (DIC). Values increase from -11.5‰ (V-PDB) in the recharge zone to -3.8‰ in the intermediate zone and decrease again to -9.8‰ in the deep zone. This variation is attributed to inorganic C from water-rock reactions that must be quantitatively assessed to correct the ^{14}C values for subsequent dating (Figure 3.6).

Theoretical values are calculated and compared with the analytical value from a hypothetical recharge, considering the water-rock reactions described above, according to Coetsiers et al. (2009):

$$\delta^{13}C_{CALCULATED} = \frac{C_{soil}(-23‰)+C_{calcite}(0‰)+C_{exchange}(0‰)+C_{Fe}(-27‰)+C_{SO4}(-27‰)}{C_{total}} \quad (E1)$$

C_{soil}: C concentration resulting from CO_2 dissolution and bicarbonate speciation.

$C_{calcite}$: C concentration resulting from calcite dissolution.

$C_{exchange}$: C concentration resulting from additional calcite dissolution as a result of cation exchange.

C_{Fe}: C concentration resulting from Fe(III) reduction.

C_{SO4}: C concentration resulting from SO_4 reduction.

C_{total}: the C sum of concentration from all above processes.

It is assumed that soil water initially contains DIC derived from atmospheric CO_2. The photosynthetic activity of C3 type plants generates $\delta^{13}C$ values of approximately -27‰ in vegetal matter (Vogel 1993). When this process overwhelms atmospheric CO_2 diffusion, the respiration of C3 type plants increases the average value of $\delta^{13}C$ in soil CO_2 to -23‰ (Cerling et al. 1991). A theoretical value of the soil carbon (C_{SOIL}) concentration was computed from the chemical composition of the samples located in the recharge zone, eliminating the dissolution of calcite. It accounted for the Ca concentration (inverse modeling). Thus, C_{SOIL} values between 0.0015 and 0.0027 mol·L^{-1} were obtained for the samples of the recharge zone (Table 3.1). Then, C_{SOIL} concentration of 0.0019 mol·L^{-1}, the average value of the range obtained in the recharge zone, was assumed for the intermediate and deep zones.

Following the flow line toward the SE, $\delta^{13}C$ becomes enriched. This fact is related to the strong increase of inorganic carbon from the dissolution of carbonate rocks ($\delta^{13}C \approx 0$ ‰ for marine carbonates). The $C_{calcite}$ value was calculated from the amount of Ca measured in water and is attributed to calcite dissolution according to the stoichiometry of equation 2. This dissolution is enhanced by the Ca-Na cation exchange that occurs in the clay materials, causing high calcium consumption. The calcite dissolution because of cation exchange was calculated from the excess of Na^+ with respect to the theoretical fresh-seawater mixing line (Figure 3.3) and the molal stoichiometry of equations E2 and E3.

$$CaCO_3 + H^+ \rightarrow Ca^{2+} + HCO_3^- \qquad \text{(E2)}$$

$$Ca^{2+}+2X\text{-}Na \rightarrow X_2\text{-}Ca+2Na^{+} \quad \text{(E3)}$$

The oxidation of organic matter provides dissolved inorganic carbon to groundwater that must also be taken into account. Thus, the analysis of dissolved H_2S (0.095-0.113 mg·L^{-1}), the SO_4 depletion and the δS_{SO4} – $\delta^{18}O_{SO4}$ clearly indicate the existence of sulfate reduction process.

$$2CH_2O+SO_4^{-2} \rightarrow H_2S+ 2HCO_3^{-} \quad \text{(E4)}$$

The carbon resulting from SO_4 reduction was computed from the loss of SO_4 concentration with respect to the recharge value and the stoichiometry of reaction (E4). The SO_4 concentration in the recharge water was estimated as the average concentration in the samples from the recharge zone (C_{SO4} = 4·10^{-4} mol·L^{-1}).

$$2CH_2O+4FeOOH+7H^{+} \rightarrow 4Fe^{+2}+ HCO_3^{-}+6H_2O \quad \text{(E5)}$$

Dissolved organic matter (DOC) can also be oxidized by Fe (III) oxides present in the host rocks according to reaction (E5). The inorganic carbon generated (C_{Fe}) could be computed from the Fe(II) dissolved in water. However, the Fe(II) concentration is always below the detection limit (4·10^{-4} mol·L^{-1}). Low Fe(II) concentrations in water could be due to the precipitation of Fe(II) phases such as Fe sulfides and carbonates. Indeed, siderite and small amounts of pyrite are described to replace Fe-oxides extensively. The Cobre Las Cruces ore deposit is a unique mineralization, where initial Fe-oxides of the gossan are replaced by siderite from Miocene to recent times (Yesares et al. 2014). Consistently, the Fe(II) concentration predicted in water in equilibrium with siderite is below the detection level in all samples. Therefore, the HCO_3^- originating from organic matter oxidation by FeOOH reduction is not computed. Consequently, the final $\delta^{13}C$ resulting from calculations will be overestimated.

The production of CH_4 from existing organic matter is another process that can potentially increase the $\delta^{13}C$ values of groundwater dissolved carbon (Coetsiers et al. 2009). However, CH_4 concentrations were below the detection limit (0.58 $mg \cdot L^{-1}$) for all samples. Therefore, methanogenesis has not been incorporated as a process modifying the $\delta^{13}C$ of residual dissolved inorganic carbon.

Applying equation E1, the $\delta^{13}C$ is calculated and incorporates all carbon contribution from each chemical processes identified. Calculated and measured $\delta^{13}C$ are similar in recharge, deep 1 and deep 2 groundwaters. However, some samples located in the intermediate and deep zone 1 calculations result in $\delta^{13}C$ values distinctly more depleted (Table 3.1). Several hypotheses to account for these differences have been considered: 1) Additional calcite dissolution triggered by Ca exchange by Sr and Mg. The unusually high concentrations of Mg^{2+} and Sr^{2+} in this groundwater suggest this process could be viable. Incorporation of this process into the carbon mass balance improves the calculated $\delta^{13}C$ but not enough to explain the observed differences. 2) Dissolution of gypsum intercalations. This would explain the increase of SO_4^{2-} concentrations observed in these samples; however, this would also produce an increase in Ca^{2+} concentration leading to precipitation of $CaCO_3$. This hypothesis can be ruled out, as this would be accompanied by a decrease of HCO_3^- that was not observed. 3) Sample degassing during sampling. This was observed, particularly for those wells extracted with a high flow (10 $L \cdot s^{-1}$) pump. It is believed that the sample could not be equilibrated with atmospheric CO_2 during the sampling and the opening of the bottle in the laboratory produced sample degassing. The CO_2 degassing would cause isotopic fractionation in the $HCO^-_3 - CO_2$ system and, consequently, the sample would be enriched (Wendt 1968). The $\delta^{13}C$ value considering this isotopic fractionation was calculated as:

$$\delta^{13}Ci*Xi = \delta^{13}Cf*Xf + \delta^{13}Cco_2*Xco_2 \quad \text{(E6)}$$

where,

X_i, X_f and Xco_2 are, respectively, the initial, final and CO_2 molar concentration.

$\delta^{13}C_i$ and $\delta^{13}C_f$ are the initial and final $\delta^{13}C$ values of HCO_3.

$\delta^{13}Cco_2$ is the CO_2 isotopic composition. This value depends on the temperature and is calculated from the expression of Mook et al. (1974) for the isotopic fractionation $\varepsilon_{CO2/HCO3}$:

$$^{13}\varepsilon_{CO2/HCO3} = -9483/T + 23.89‰ \quad \text{(E7)}$$

These calculations lead to $\delta^{13}C$ values with a maximum enrichment of 2‰, but not high enough to match the analyses. Therefore, a consistent explanation for the anomalous $\delta^{13}C$ values measured in these samples has not been found.

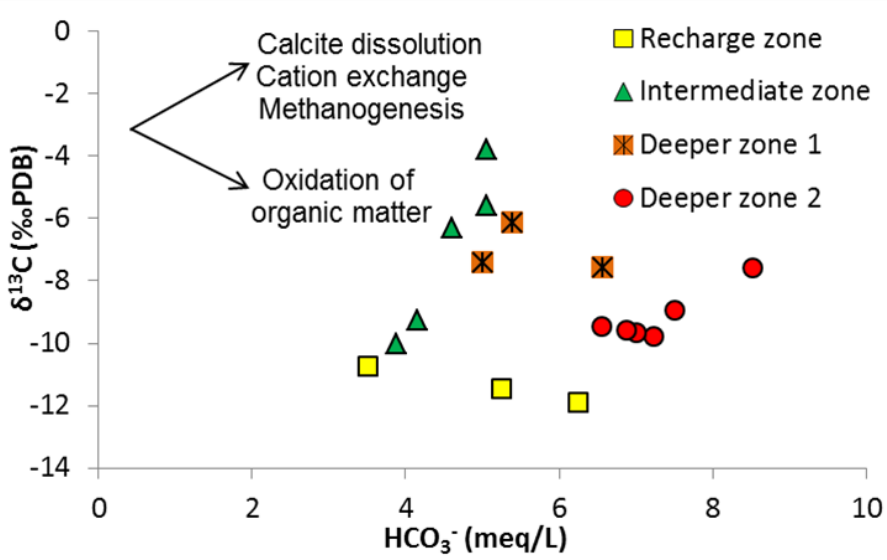

Figure 3.6. $\delta^{13}C$ vs. HCO_3 of the groundwater samples analyzed

	SAMPLE	C_{SOIL}	$C_{CALCITE}$	$C_{EXCHANGE}$	C_{SO4}	C_{Fe}	C_{TOTAL}	$\delta^{13}C$ calculated (‰)	$\delta^{13}C$ measured (‰)
RECHARGE ZONE	1	1.50E-03	1.67E-03	-	-	-	3.17E-03	-10.88	-10.73
	2	2.70E-03	2.74E-03	-	-	-	5.44E-03	-11.41	-11.52
	3	2.00E-03	2.82E-03	-	-	-	4.82E-03	-9.55	-
	4	2.00E-03	3.04E-03	-	-	-	5.04E-03	-9.13	-
	5	1.71E-03	2.54E-03	-	-	-	4.25E-03	-9.25	-
INTERMEDIATE ZONE	6	1.90E-03	2.49E-03	2.32E-05	-	-	4.41E-03	-9.95	-
	7	1.90E-03	1.81E-03	1.88E-04	-	-	3.90E-03	-11.78	-10.02
	8	1.90E-03	1.57E-03	5.66E-04	-	-	4.04E-03	-10.82	-9.26
	9	1.90E-03	1.28E-03	5.20E-04	-	-	3.70E-03	**-11.83**	**-3.80**
	10	1.90E-03	1.73E-03	9.60E-04	-	-	4.59E-03	**-9.51**	**-6.30**
	11	1.90E-03	1.22E-03	1.06E-03	-	-	4.19E-03	**-10.44**	**-5.57**
DEEPER ZONE 1	12	1.90E-03	5.18E-05	2.58E-03	5.18E-04	8.95E-07	5.05E-03	**-11.42**	**-6.16**
	13	1.90E-03	6.55E-05	2.59E-03	4.96E-04	8.95E-07	5.05E-03	**-11.31**	**-7.44**
	14	1.90E-03	2.48E-05	4.27E-03	4.24E-04	8.95E-07	6.62E-03	-8.33	-
	15	1.90E-03	2.43E-05	3.44E-03	4.52E-04	8.95E-07	5.82E-03	-9.61	-7.57
	16	1.90E-03	7.43E-05	3.87E-03	5.97E-04	8.95E-07	6.44E-03	-9.29	-
	17	1.90E-03	3.69E-05	3.64E-03	4.74E-04	8.95E-07	6.05E-03	-9.34	-
	18	1.90E-03	6.06E-05	3.47E-03	6.38E-04	8.95E-07	6.07E-03	-10.04	-
	19	1.90E-03	2.31E-03	2.39E-03	0.00E+00	8.95E-07	6.59E-03	-6.63	-
DEEPER ZONE 2	20	1.90E-03	2.58E-04	4.25E-03	6.38E-04	8.95E-07	7.05E-03	-8.62	-9.65
	21	1.90E-03	2.86E-04	4.71E-03	6.38E-04	8.95E-07	7.54E-03	-8.06	-9.59
	22	1.90E-03	1.74E-03	2.28E-03	6.38E-04	3.98E-06	6.56E-03	-9.18	-9.47
	23	1.90E-03	4.76E-04	3.71E-03	6.38E-04	8.95E-07	6.73E-03	-9.06	-9.79
	24	1.90E-03	9.47E-05	4.48E-03	6.38E-04	8.95E-07	7.12E-03	-8.52	-8.94
	25	1.90E-03	9.20E-05	4.98E-03	6.38E-04	8.95E-07	7.61E-03	-7.97	-7.58

Table 3.1. Theoretical variation of the concentration of DIC (C in mol·L^{-1}) involved in the different geochemical processes. Values of $\delta^{13}C$ calculated and $\delta^{13}C$ measured (‰).

DATING

TRITIUM (^{3}H) IN GROUNDWATER

The evolution of the tritium activity in rainfall in the area over the last 50 years is recorded from the values registered at the Global Network of Isotopes in Precipitation (GNIP) Gibraltar station. Assuming a piston flow model, the activity (A) for every year is calculated and then compared to groundwater activity obtained analytically.

The tritium concentrations in precipitation near the study area in the past 50 years are over 3 TU, with a maximum of 597 TU for 1963, which corresponds to maximum of atmospheric nuclear bomb tests that took place during that time. If these tritium concentrations are corrected for radioactive decay, some of this tritium could be found in the actual concentration in recent groundwater (Custodio and Custodio-Ayala, 2013). Tritium content in current rainfall is close to natural values since a few years ago, with some small influence of the small increase in the ocean and the possible influence of evaporating recent groundwater in irrigated fields.

Tritium was measured in 9 groundwater samples from wells of different depths and screened in both the NP and the Paleozoic. Tritium activity in groundwater ranged from 2 TU in the recharge zone to less than the quantification limit (0.3 TU) in the rest of the studied area. Therefore, the tritium values registered in the recharge zone indicate that most of this water was recharged after 1952. However, the null tritium values of the rest of the study area indicate that the water recharge was produced prior to 1952.

^{14}C ISOTOPE IN GROUNDWATER

A decrease in the ^{14}C activity is observed along the carbonate dissolution and cation exchange line, as well as an increase in the δ^{13}C values (Figure 3.7). There is a line marked by redox processes where the ^{14}C activity is close to 0 and δ^{13}C values tend to decrease. Finally, there is a line that represents the aging groundwater where the ^{14}C activity decreased and the δ^{13}C values remain more or less constant. Following a flow line: 1) the

composition of the samples of the intermediate zone is dominated by the processes of dissolution of carbonate rocks and cation exchange. 2) The deep zones exhibit low ^{14}C activity and $\delta^{13}C$ values are lightest due to the dominance of the redox reactions.

The activity of ^{14}C of 14 groundwater samples decreases downgradient along a NW-SE flow line. Activities range from 93 pMC to <1 pMC (Table 3.2), with three different ranges that broadly correspond to the groundwater zones. These ranges are differentiated as follows: (1) values between 93 and 84 pMC in the recharge zone; (2) values from 82 to 9 pMC in the intermediate zone; and (3) activities lower than 2 pMC found in the deep saline waters to the SE of the study area.

	SAMPLES	ACTIVITY (pmC)	$\delta^{13}C_{MEASURED}$ (‰)	$\delta^{13}C_{CALCULATED}$ (‰)	TAMERS (ky)	PEARSON (ky) from $\delta^{13}C_{MEASURED}$	PEARSON (ky) from $\delta^{13}C_{CALCULATED}$
RECHARGE ZONE	2	84.17	-10.02	-11.78	MODERN (<0.06)	MODERN (<0.06)	MODERN (<0.06)
	1	93.52	-11.52	-11.41	MODERN (<0.06)	MODERN (<0.06)	MODERN (<0.06)
INTERMEDIATE ZONE	7	81.89	-10.73	-10.88	MODERN (<0.06)	MODERN (<0.06)	MODERN (<0.06)
	8	43.98	-9.26	-10.82	2	-	1
	10	21.97	-6.30	-9.51	**8**	**2**	**6**
	9	6.7	-3.80	-11.83	**17**	**8**	**17**
	11	9.2	-5.57	-10.44	**14**	**9**	**14**
DEEP ZONE 1	12	1.95	-6.16	-11.42	**27**	**22**	**27**
	15	0.87	-7.57	-9.61	>30	>30	>30
DEEP ZONE 2	23	0.65	-9.79	-9.06	>30	>30	>30
	22	0.44	-9.47	-9.18	>30	>30	>30
	24	0.34	-8.94	-8.52	>30	>30	>30
	21	0.32	-9.59	-8.06	>30	>30	>30
	25	0.17	-7.58	-7.97	>30	>30	>30

Table 3.2. Dating of groundwater by ^{14}C with Tamers and Pearson correction (ky). The Pearson correction is calculated from $\delta^{13}C$ measured and $\delta^{13}C$ calculated.

Assuming a piston flow, the ^{14}C age is calculated from the following equation (E8):

$$t = \frac{ln\frac{A}{q * A_0}}{-\lambda} \qquad \text{(E8)}$$

where, A is the measured ^{14}C activity, q is the dilution factor, A_0 is the initial ^{14}C concentration and λ is the decay constant ($\lambda = \ln 2/t_{1/2}$), being $t_{1/2}$ is the half-life.

The value of the initial concentration of ^{14}C (A_0) is affected by the processes that modify the C content in the water, as explained in the discussion of ^{13}C. The dominant processes are the dissolution of carbonate rocks and organic matter oxidation. During the transit in the aquifer, these processes modify the initial ^{14}C content in groundwater because the ancient rocks do not contain ^{14}C. Hence, a correction must be applied to better approximate the A_0 value in carbonate rich aquifers. Here, the chemical correction (Tamers 1975) and the isotopic correction (Pearson 1965) in its simpler forms are considered.

The dating of these waters using both corrections (Tamers and Pearson) is in Table 3.2. The measured and calculated $\delta^{13}C$ values have been used for the Pearson correction. In the intermediate zone, significant differences in age are obtained between the two types of corrections. Samples that show these differences are those that have inconsistencies between the $\delta^{13}C_{CALCULATED}$ and the $\delta^{13}C_{MEASURED}$ values, as already mentioned in Carbon Isotopes section. The Pearson correction using the $\delta^{13}C_{CALCULATED}$ values results in ages very close to those from the Tamers correction. Therefore, age data use the Tamers correction because it is independent of the $\delta^{13}C$ values.

Four zones can be distinguished: (1) recent water area (<0.06 ky) where the values calculated of ^{14}C coincide with significant values of tritium and consequently affected by post-nuclear recharge; (2) water of intermediate age area (0.06 to 20 ky); (3) old water (20 to 30 ky); and (4) very old water (>30 ky).

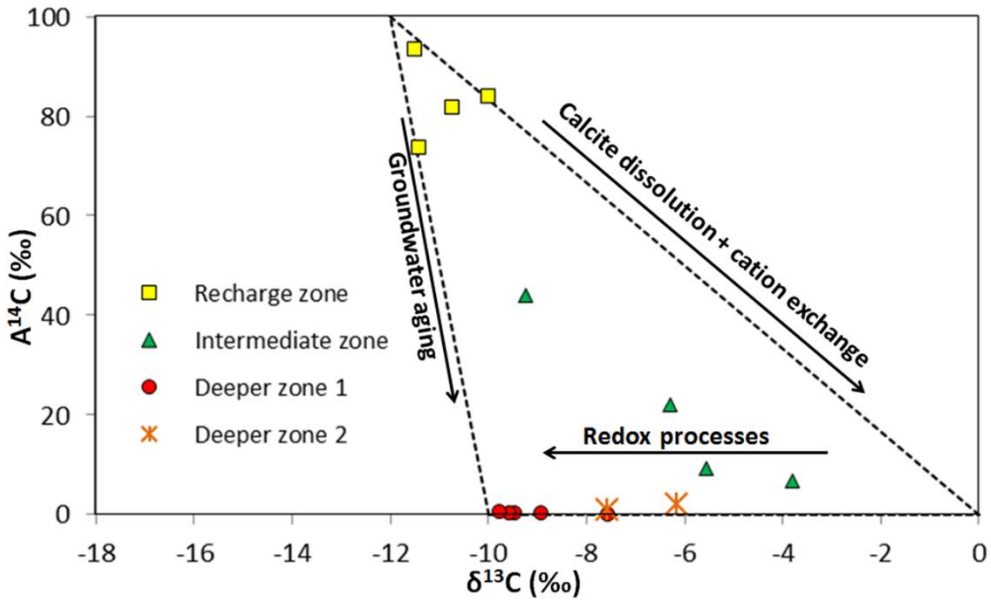

Figure 3.7. $A^{14}C$ vs. $\delta^{13}C$.

^{36}Cl ISOTOPES IN GROUNDWATER

Seven groundwater samples have been analyzed, mostly selected from the deeper zone and expected to have ages beyond ^{14}C dating range. They are subjects for the application of ^{36}Cl. While the ideal range for ^{36}Cl is for samples between 40 ky and 3000 ky (Fabryka Martin et al. 1987), there are important limitations to be considered: (1) variable input of the ^{36}Cl/Cl ratio through time and under prevalent climatic conditions.; (2) in-situ ^{36}Cl production by secular equilibrium with formation rocks; and (3) mixing of waters with different ^{36}Cl (Kulongoski et al. 2008). The local rainfall weighted ^{36}Cl/Cl values in Sevilla, estimated to be 30%, are affected by the arrival of dead (no ^{36}Cl) chloride from the sea (Santos et al. 2004).

Evapotranspiration effects during recharge are expected to modify further the ^{36}Cl/Cl of recharge; however, these cannot be quantified. All of these combined effects make the estimation of the initial ^{36}Cl/Cl of recharge to groundwater problematic, particularly for samples with Cl^- concentration higher than 75-150 mg/kg (Park et al. 2002). However, to estimate ^{36}Cl residence times, a simple piston flow regime is assumed. It is a valid concept if

it is considered that no significant contribution to the NW aquifer comes from the Paleozoic basement. In this case, it has been used in the model of Bentley et al. (1986):

$$t = \frac{-1}{\lambda_{36}} \ln \frac{R - R_{se}}{R_0 - R_{se}} \quad \text{(E9)}$$

where R is the $^{36}Cl/Cl$ ratio measured in the sample, R_0 is the $^{36}Cl/Cl$ initial relationship or meteoric water, and R_{se} is the $^{36}Cl/Cl$ relationship under secular equilibrium with the materials that form in this case the NP aquifer.

A value of 38 ($x10^{-15}$) has been selected as an initial ratio $^{36}Cl/Cl$ (R_0), which is slightly greater than the average value ($32x10^{-15}$). According to Fabryka Martin et al. (1987), the relationship $^{36}Cl/Cl$ under secular equilibrium (R_{se}) with Paleozoic materials is 13 ($x10^{-15}$); in the Cenozoic materials it is 5 ($x10^{-15}$). An intermediate value of 10 ($x10^{-15}$) has been selected for the NP aquifer.

An apparent age of approximately 30 ky has been obtained for the younger waters, consistent with that obtained from ^{14}C, and from 100 to 150 ky for the rest of the deep zone areas (Table 3.3). However, most of the samples have a Cl concentration greater than 150 $mg \cdot L^{-1}$. Therefore, the ages obtained are probably an overestimation.

SAMPLES	^{36}Cl (dpm/L)	Cl (mg/L)	$^{36}Cl/Cl$ ($x10^{-15}$)	Apparent age (ky)
12	7144.1	199	35.9±2.1	41
15	3559.9	97	36.7±2.2	28
23	18777.2	598	31.4±1.9	124
22	41144.5	1349	30.5±1.9	142
24	14490.4	472	30.7±1.9	138
21	14446.3	571	25.3±1.7	269
25	13610.4	428	31.8±2.0	116

Table 3.3. ^{36}Cl values obtained from 7 groundwater samples and estimation of their apparent age.

3.3. CONCLUSIONS

The study area was divided into four zones: recharge, intermediate, and deep (1 and 2) zones. This zonation corresponds to geochemical and isotopic differences and clearly correlates with the primary geological features.

The groundwater from the NP aquifer shows a clear evolution of Ca-HCO^3-type water toward Na-Cl-type water.

The origin of the chloride in the samples collected in the deep areas can be explained by the Na/Cl and Br/Cl ionic relationships. Both relationships suggest a mixture of fresh water with a more saline end member, probably relict syndepositional water trapped in the pores.

Sulfate isotope values indicate the existence of oxidation of sulfides processes in the recharge zone and sulfate-reduction processes in the deep zones.

The ^{13}C isotope values have facilitated identification of hydrogeochemical processes occurring in the NP aquifer: calcite dissolution, Ca-Na cation exchange, SO_4^{-2} and iron oxide reduction. Knowing the processes taking place in each area, enabled to carry out a correction of $\delta^{13}C$ values of each of the sampled points. This correction has improved the results of ^{14}C dating of the groundwater.

Based on the results obtained from isotopic data, ^{3}H, ^{14}C and ^{36}Cl, four age zones can be established in the study area from NW to SE (Figure 3.8). The first zone corresponds to young waters (<0.06 ky); it has been defined using tritium dating and corresponds to the recharge area. The second (0.06 to 20 ky) and third zones (20 to 30 ky) correspond to the intermediate and deep zone 1, respectively; both strips have been defined with ^{14}C values and confirmed by ^{36}Cl dating results. The fourth zone (> 30ky) corresponds to very old water of deep zone 2, with residence times of thousands of years. This was dated using ^{36}Cl, although the high Cl content makes precise dating difficult.

However, relatively high differences in age can be distinguished along the flow. Thus, age gradients appear to be highly conditioned by the local geology. The >30 isochrone coincides with a SW-NE regional fault that constitutes one of the main areas of the Paleozoic aquifer discharge. Discharge zones are very difficult to unravel in such deep aquifers and, therefore, groundwater ages can be an indirect way to infer such deep flow paths.

From the results obtained, particularly with radioactive isotopes, a strip zone with short turnover time (renewable) groundwater and another with almost steady (nonrenewable) groundwater are distinguished (Figure 3.8). Therefore, anyone acting in the area defined as almost steady must consider this aspect to ensure the sustainability of these groundwater resources that are probably nonrenewable due to the slow transfer from the renewable area. Then any extraction of water resources, such as draining operations in a mine, must reset the water pressures by artificial recharge to avoid affecting the area defined as renewable water. Other considerations refer the possible poor water quality, which are not addressed here.

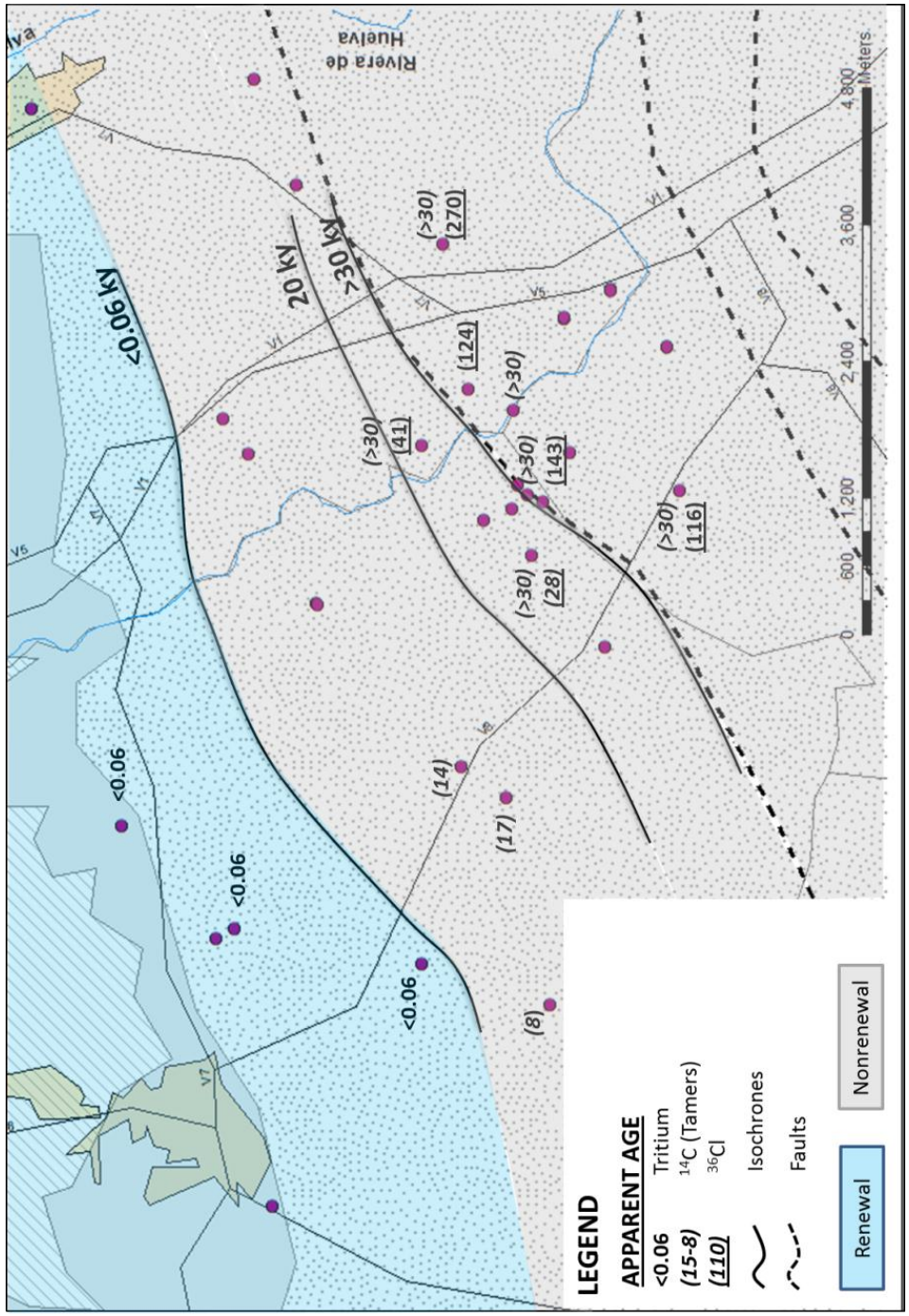

Figure 3.8. Map of groundwater dating (ky) from ^{3}H, ^{14}C (Tamers) and ^{36}Cl. Zoning of renewable and nonrenewable resources.

CHAPTER 4. Origin of high ammonium, arsenic and boron concentrations in the proximity of a mine: natural vs. Anthropogenic processes.

4.1. INTRODUCTION

Increasing demand and conflicting water uses worldwide are leading to groundwater quality changes caused by variations in physical water management (e.g.: Currell et al. 2011 and 2013). The difficulty of managing groundwater lies in its sensitivity to (1) direct anthropogenic pollution (Belkin et al., 2000; Sapek, 2005), (2) indirect pollution due to abstraction induced chemical changes (Cendón et al., 2014; Harvey et al., 2003), and/or (3) geogenic causes related to water interaction with the host aquifer (both rocks and water) or along groundwater flows (Swartz et al., 2004; McArthur et al., 2001). Differentiating natural and anthropogenic sources is therefore crucial to ensure good management of

groundwater. However, it can be very difficult in some instances to ascertain the source and/or processes associated with contamination (Sancha and Castro, 2001; Harms-Ringdahl, 2007; Williams et al., 1998).

Numerous aquifers worldwide have groundwater quality problems related to elevated concentrations of arsenic. High mining-related As concentrations (200-1700 $\mu g \cdot L^{-1}$), often associated to dewatering activities, have been identified in many parts of the world such as Thailand (Williams et al., 1996; Williams, 1997), Greece (Wilson and Hawkins, 1978), Ghana (Smedly, 1996), Alaska (Welch et al., 1988) and Canada (Azcue et al., 1994), among others. However, high arsenic concentrations can also be due to natural processes at many sites around the world. Thus, arsenic can be mobilized by weathering reactions (Manning and Goldberg, 1977b; Nicolli et al., 1989; Welch et al., 2000; Savage et al., 2000; Wang et al., 2006; Mukherjee et al., 2008), geothermal processes (Yokoyama et al., 1993; Robinson et al., 1995; Ellis and Mahon, 1977; Criaud and Fouillac, 1989; Thompson and Demonge, 1996), or reductive dissolution of iron oxides (Nickson et al., 2000, Berg et al., 2001; Smedley and Kinnisburg, 2002; Halim et al., 2010).

Ammonium contamination is often described as being due to agricultural practices such as water irrigation returns and the use of fertilizers and manure (Kohl et al., 1971; Aravena et al., 1993; Chen et al., 2004; Tang et al., 2004, among many others). In some cases, however, ammonium concentrations as high as 390 $mg \cdot L^{-1}$ have also been attributed to geogenic processes. In all cases, ammonium in pore water is related to high concentrations of organic matter in sediments (Ortega-Guerrero, 2003; Hinkle et al., 2007; Mastrocicco et al., 2013). In the Pearl River Delta, China, Jiao et al. (2010) observed concentrations as high as 290 $mg \cdot L^{-1}$ in the aquifer, with a Holocene-Pleistocene aquitard being even richer in ammonium. In all cases, ammonium is attributed to the decomposition of organic matter under reducing geochemical conditions.

Anthropogenic boron contamination in aquifers has been attributed to leaking septic systems (Massmann et al., 2008; Katz et al., 2013) and borate mining in Turkey (Gemici et

al., 2008). Unlike ammonium and arsenic, high boron concentrations of geogenic origin have been more rarely reported in the literature, and most of them are related to geothermal activity (Bernard et al., 2011; Grassi et al., 2014) and Na-Cl brines (Wunsch et al., 2013; Palmucci et al., 2014). High boron concentrations have also been described in deep aquifers in Bangladesh and Michigan (Ravescroft and McArthur, 2003; Halim et al., 2010), and they are associated with chloride and Ca/Na cation exchange and are attributed to the mixing of fresh water with displaced ancient seawater.

The Niebla-Posadas (NP) aquifer (S Spain) is an example where ammonium, arsenic and boron levels are high within the confined, deep portion of the aquifer. This aquifer is part of the Guadalquivir Basin and contributes part of the total resources for supply of drinking water and for agricultural, industrial and mining activities in a highly populated area of southern Spain. Concentrations of these three compounds locally exceed current World Health Organization guidelines for drinking water (WHO 2008) and recommended values by the U.S. Environmental Protection Agency for continuous irrigation (USEPA 2012). The Spanish regulations for drinking water (RD140/2003), according to the European Water Framework Directive (WFD), have values close to the WHO values, which are more restrictive for some compounds. High concentrations of these contaminants have alerted the public opinion and numerous environmental groups have drawn attention to the main anthropogenic activities in the zone, especially the mining exploitation of Cobre Las Cruces (CLC), as well as Aznalcollar past and projected activities.

This chapter presents a detailed hydrogeochemical and isotopic study suggesting the natural origin of high ammonium, arsenic and boron concentrations in the deeper sections of the aquifer. The aim of this research is to provide an assessment of a set of tools to differentiate the geogenic/anthropogenic sources and processes, with particular attention to processes controlling ammonium, arsenic and boron concentrations. To reach this objective, was necessary to: a) characterize the sources of solutes; b) investigate the spatial distributions of solutes in relation to sources, local geology and potential mobilization mechanisms; and

c) identify the geochemical processes that control the presence of these solutes. This approach can be applied to other sites where elevated concentrations of ammonium, arsenic and boron are found and more generally to mine sites where water-rock interactions at a regional level are a concern.

4.2. RESULTS

Groundwater temperatures vary from 14.7 to 37.5 °C, with an average value of 25.5 ºC. Cooler temperatures are found in the recharge zone, and temperatures increase towards the deeper zone. The pH values range between 6.8 and 10.6, with the highest pH values found in the deeper SE zones. Specific conductance (SC) values are between 388 and 5940 $\mu S \cdot cm^{-1}$, also increasing with depth. Eh values, while taken with caution, ranged between 177.7 mV in the recharge zone to -297 mV in the deeper areas (Table 4.1).

Major ion compositions (Figure 4.1) differentiate four main compositional types. Groundwater in the recharge zone is of the Ca-HCO_3-type, and it transitions to Na-(Ca)-HCO_3 in the intermediate zone and to Na-HCO_3 in the Deep zone 1. Samples from the Deep zone 2 are of the Na-Cl-type and represent the most evolved compositions in the study area. In general, Na and Cl show a high correlation of R^2= 0.92 (See appendix B), adapting to a seawater mixture line but with sodium excess.

Nitrate concentrations are only found close to agricultural and farm areas in the recharge zone, with concentrations ranging from 16.4 to 97.2 $mg \cdot L^{-1}$. Samples number 3 and 5 (Figure 2.2B) have nitrate concentrations that exceed or are close to the drinking water guidelines (WHO). Nitrite has not been detected, but high ammonium concentrations ranging from 0.04 to 12.8 $mg \cdot L^{-1}$ are found in 70% of the wells (Table 4.1). Sulfate concentrations are generally low, ranging from 0.1 $mg \cdot L^{-1}$ to 115 $mg \cdot L^{-1}$ (Table 4.1). Concentrations of H_2S are 0.1±0.01 $mg \cdot L^{-1}$ and are only present at samples sites with the lowest sulfate concentrations and where a H_2S-smell was identified in the field. Methane concentrations were mostly

below the detection limit (0.58 mg·L^{-1}), except for one sample with a value of 1.09 mg·L^{-1}, located in the Deep zone 2.

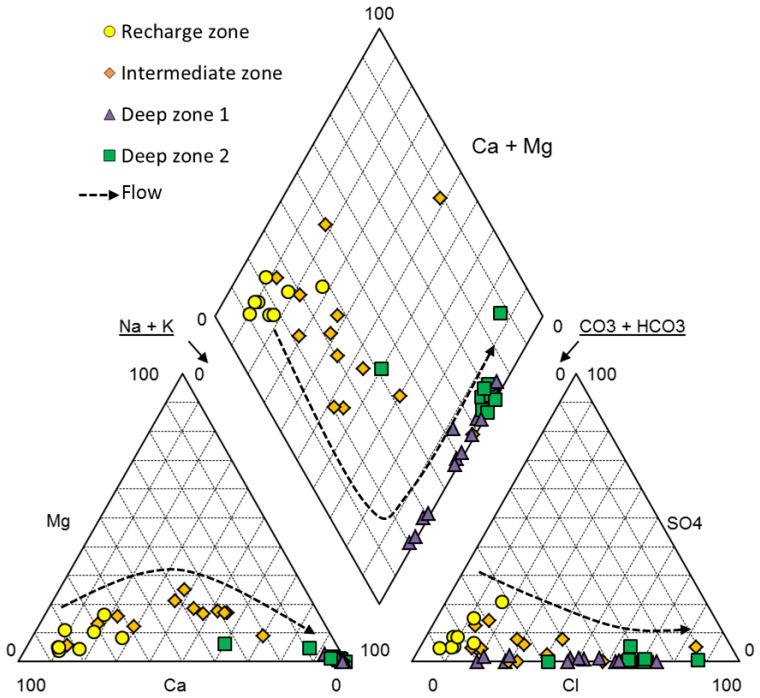

Figure 4.1. Piper diagram showing major ion chemistry of the sampled points. The arrows follow the NW-SE flow direction.

Arsenic generally occurs as As (III), with concentrations ranging from below the limit of detection to 0.18 mg·L^{-1}, with a mean value of 0.006 mg·L^{-1}. Of the 40 points measured, four have As (III) values >0.01 mg·L^{-1} (above the WHO guideline), six points have As (III) concentrations between 5 and 0.01 mg·L^{-1} and the remaining points have concentrations <0.0005 mg·L^{-1}.

Boron concentrations in the study area range between 0.02 and 3.48 mg·L^{-1}, with an average value of 0.94 mg·L^{-1}. Approximately 55% of sampled points have boron concentrations that are above the WHO limit for drinking water, and 50% of the points do not meet the USEPA recommendations for frequent irrigation water (Table 4.1). Similarly, ammonium

concentrations vary between 0.04 and 12.82 mg·L^{-1}, with an average value of 2.61 mg·L^{-1}. This average value is above the guideline value set by the WHO (0.2 mg·L^{-1}) for drinking water, and the standard limit is exceeded in 76% of the sampled points (Table 4.1).

	MIN.	MAX.	AVE	MEDIAN	SD	WHO (2008)	USEPA (2012)
pH	6.8	10.6	7.9	7.7	0.9	6.5-8.5	-
Eh (mV)	-297	177.7	-8.2	44.7	166.6	-	-
SC (uS•cm^{-1})	388.0	5940.0	1611.1	1189.2	1065.8	1500	4000
T (ºC)	14.7	37.5	25.5	25.3	5.2	-	-
DOC	0.2	15.9	3.5	4.2	3.3	-	-
Cl^-	12.6	1581.3	276.4	149.9	315.5	250	-
NO_3^-	<0.1	97.2	11.0	0.1	24.8	50	-
SO_4^{-2}	<0.1	115.3	16.5	9.5	24.2	250	-
HCO_3^-	158.5	570.9	365.6	365.8	100.3	-	-
Ca	0.6	177.0	45.3	24.0	51.0	200	-
Mg	<0.001	50.6	7.2	3.9	9.5	150	-
Na	14.6	1061.8	238.0	218.6	220.0	200	-
NH_4	0.04	12.8	2.6	2.3	2.7	0.2	-
I^-	<0.01	0.67	0.11	0.1	0.13	-	-
Br^-	0.09	5.25	0.90	0.5	1.15	-	-
Fe	<0.002	0.89	0.211	0.09	0.220	0.3	5
B	0.02	3.48	0.94	0.63	0.94	0.5	0.75
As	<0.00003	0.18	0.006	0.002	0.03	0.01	0.1
F	0.15	6.79	2.46	1.64	2.12	1.5	-
$\delta^{18}O$	-5.1	-3.8	-4.7	-4.8	+0.26	-	-
$\delta\,^2H$	-30.3	-20.4	-28.0	-28.4	+1.72	-	-
$\delta\,^{15}N_{NH4}$	-3.9	0.7	-1.4	-1.2	+1.6	-	-

Table 4.1. Groundwater parameters of the studied area (concentrations in mg·L^{-1}). SD (Standard Deviation). Recommended limits for drinking water (WHO 2008) and for frequent irrigation (USEPA 2012).

Water stable isotope data from previous campaigns (Scheiber et al., 2015) have been complemented with new results (see appendix B). Groundwater isotopic ratios range between -20.4 to -30.3‰ for δ^2H and between -3.8 to -5.1‰ for $\delta^{18}O$ (V-SMOW). The deuterium excess, defined as D-excess = δ^2H-8 $\delta^{18}O$ (Dansgaard 1964), has an average of 11.1±1.6 ‰. These values are close to 10‰ and suggest a major Atlantic source for rainfall recharge when compared with the typical deuterium excess values of ~13.7‰ determined for modern western Mediterranean rainfall (Celle-Jeanton et al., 2001). Groundwater

deuterium excess values are also consistent with other regional groundwater values from Doñana National Park (D-excess = 10.9±3.1) (Iglesias, 1999; Jimenez and Custodio, 2008).

A limited number of samples (n=8) have been analysed for $\delta^{15}N$ of dissolved ammonium to assess nitrogen sources. The $\delta^{15}N_{NH4}$ values range between -3.9 and +0.7 ‰, with an average value of -1.4 ‰.

4.3. DISCUSSION

ORIGIN OF MAJOR SOLUTES

The NP aquifer has a well-defined recharge area and an overlying confining layer of increasing thickness as the aquifer dips south along the flow direction. Groundwater salinity increases along the flow direction, with major ion compositions varying from Ca-HCO_3-type in the recharge area to Na-Cl-type in the deeper samples recovered. The increasing salinity could be due to: (1) dissolution of evaporites, (2) evapotranspiration processes in the recharge water or (3) mixing between meteoric water and connate marine water. There is no evidence of the existence of evaporites dispersed within the marls. Moreover, the dissolution of evaporites would lead to Cl/Br ratios much higher than those observed (Cendón et al., 2004). The low chloride concentrations found in wells located within the Palaeozoic recharge zone rule out evapotranspiration in the soil as a significant source of groundwater salinity. Finally, the Cl/Br ratio values approach those of seawater ($R_{Cl/Br}$~ 600) in samples from the deepest zones suggesting mixing with a marine contribution. However, depleted water stable isotopes (Figure 4.2) seem to constrain a significant mixing with seawater. Samples with higher chloride concentrations generally show the most depleted water isotopic values, with all groundwater samples plotting along the modern precipitation weighted least square regression lines PWLSR (Hughes and Crawford, 2012) for Seville and Gibraltar (Figure 4.2). D-excess values in groundwater samples adjusts better with rainfall values derived from Atlantic fronts and are similar to those from Gibraltar. This could be due to the relatively limited rainfall water stable isotope data set available for Seville (six years).

Similar isotopic ratios to those obtained in groundwater have been found in others regional studies, such as in Doñana (Manzano et al., 2001) and the southwest of Portugal (Fernandes and Carreira, 2008).

The depleted $\delta^2H/\delta^{18}O$ values in the deepest groundwater are consistent with palaeo-recharge under different climatic conditions. Palaeoclimatic studies based on nobles gas recharge temperatures (Edmunds et al., 2004) and speleothems (Duran Valsero 2002 and Jimenez de Cisneros et al., 2013) conclude that the Late Pleistocene recorded climatic periods with temperatures up to 5°C colder than the current annual average temperature. This coincides with the findings of Scheiber et al., 2015, where the groundwater travel time from the recharge zone to the deepest zone was >30000 years. These differences in associated groundwater recharge temperatures could explain the depleted $\delta^2H/\delta^{18}O$ values in the deepest zones.

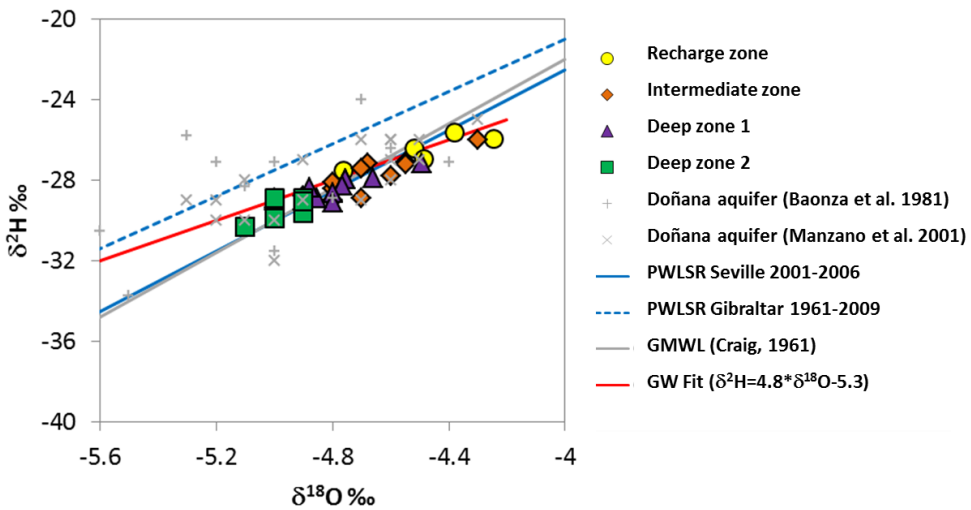

Figure 4.2. $\delta^{18}O$ vs. $\delta^{2}H$ plot for groundwater samples.

Cenozoic marine sediments overly the Palaeozoic substrate, and marine water is expected to have occupied the porosity. Once the marine conditions receded, continental fresh waters progressively pushed and displaced the relict marine waters (Abad de los Santos, 2007). Considering that the salinity originated from mixing between meteoric and relict

marine waters, and based on the Cl/Br ratios, a maximum seawater contribution of up to 8% would explain the salinity of the deepest zones. The small seawater contribution would not produce any significant displacement of water stable isotope ratios based on the $\delta^{18}O$ vs Cl relationship, which is not shown.

A relative increase in Na concentrations with respect to expected seawater ratios is observed from the intermediate zone and towards deeper portions of the aquifer (Figure 4.3). This effect can be explained by a Na-Ca exchange process that takes place within dispersed clay layers in the aquifer or within the overlying formation (blue marls). The exchange of Ca for Na can also be observed in the Piper diagram, where Na increases and Ca decreases while the HCO_3 concentration remains constant (Figure 4.1). This process has been identified in coastal aquifers when continental waters flush marine water (Appelo, 1994; Custodio and Llamas, 1976; Custodio and Bruggeman, 1987).

NO_3 is the only major solute detected that is of anthropogenic origin and it has concentrations reaching up to 102 $mg \cdot L^{-1}$ in localized areas of the recharge zone, with an average concentration of 41.7 $mg \cdot L^{-1}$ (n=6). These local high NO_3 concentrations are due to agricultural practices and may be from sewage/septic tank leaks from the town of Gerena. Nitrate in the intermediate and deep zones is generally below the detection limit (See appendix B). This effect could be due to: (1) nitrate only originating from recent recharge that has not yet affected down-gradient concentrations, or (2) nitrate reduction. However, the absence of ^3H in intermediate groundwater suggests that the nitrate plume has not yet reached the deeper zones.

Sulfate in the recharge zone can be as high as 115 $mg \cdot L^{-1}$, but it decreases below the detection level (0.1 $mg \cdot L^{-1}$) in the intermediate and deep zones, with H_2S concentrations reaching up to 0.1 $mg \cdot L^{-1}$ in some wells. The isotopes of the SO_4 molecule clearly confirm the existence of sulfate reducing processes, with remnant sulfate in groundwater from the intermediate and deep zones showing a distinct trend towards heavier $\delta^{18}O$ and $\delta^{34}S$ values (Scheiber et al., 2015). Although methane has only been detected in one sample, the

possibility of reduction processes progressing up to the methanogenesis stage cannot be ruled out.

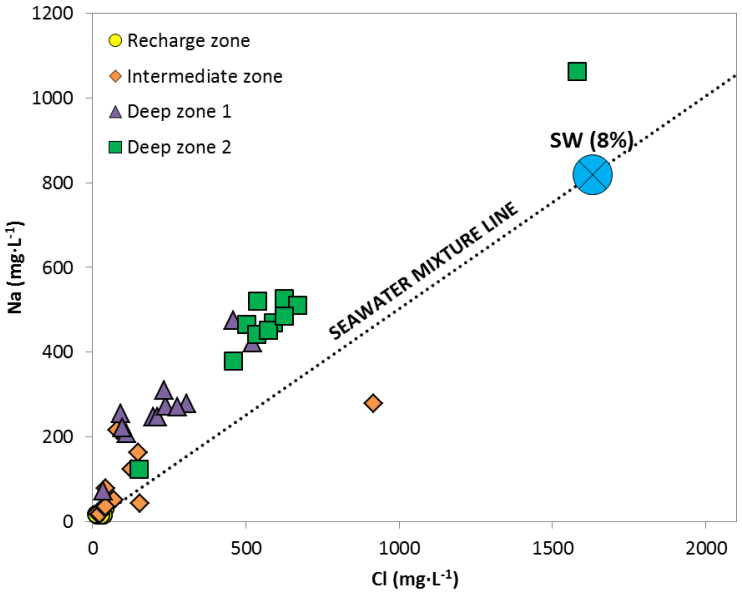

Figure 4.3. Plot of Na vs. Cl in groundwater (mg·L^{-1}). SW= Seawater 8%.

ORIGIN OF MINOR SOLUTES (AS, B AND NH_4)

Of all minor and trace elements/compounds analysed in groundwater, only ammonium, arsenic and boron have anomalously high concentrations that are one order of magnitude higher than those commonly found in average surface water (Gaillardet et al., 2004). Ammonium concentrations of up to 12.8 mg·L^{-1} have been found in the Deep zone 2, and concentrations of 0.18 mg·L^{-1} for arsenic and 3.48 mg·L^{-1} for boron have also been found within this zone. Several natural sources can explain the high ammonium, arsenic and boron concentrations observed in the groundwater. The natural origin is supported by the following: (1) the recharge zone of the aquifer has low ammonium, arsenic and boron concentrations, and high concentrations are only found in the deepest zones located to the SW of the study area; (2) the transit to deeper parts of the aquifer is confined by a thick marl layer (> 200 m) with low permeability, which seals the aquifer system (Figure 2.1 and Figure

2.2); and (3) groundwater residence times >20 ky have been identified in groundwater containing the higher concentrations (Scheiber et al., 2015).

The arsenic mobilization is interpreted as related to the reductive dissolution of Fe-oxyhydroxides. This natural process is well-known and has been observed in reducing aquifers (Berg et al., 2001; McArthur et al., 2001; Ahmed et al., 2004; Halim et al., 2010). Generally, Fe-oxyhydroxides are characterized by a very high specific surface area of ±300 $m^2 \cdot g^{-1}$ (Davis and Leckie, 1978) and a high adsorption capacity, which is capable of adsorbing large amounts of arsenic (van der Zee et al., 2003; Wang et al., 2012). Thus, the reductive dissolution of these minerals involves the release of any arsenic present in groundwater. Instead of mining operations, several observations indicate a geogenic origin in the case of the NP aquifer: 1) goethite gossan deposits are scattered on the surface of the Paleozoic series below the NP strata, with the CLC ore deposit being the most representative; 2) goethite contains up to 0.8% As (CLC, unpublished data); 3) Dissolved Organic Carbon (DOC) concentrations are above the typical values in groundwater (>1 $mg \cdot L^{-1}$), indicating the important role of organic matter in the hydrogeochemical evolution of these waters; 4) arsenic is mostly As(III), which is characteristic of reducing environments; 5) the higher concentrations are scattered across the studied area, and are not directly linked to mining; and (6) historical data obtained before the mining activity show higher As and NH_4 concentrations of up to 0.1 and 5 $mg \cdot L^{-1}$, respectively (CLC, unpublished data).

In many studies where the reductive dissolution of FeOOH has been associated with high arsenic concentrations a moderate relationship between DOC, As and Fe is observed (Anawar et al., 2003; Ahmed et al., 2004; Halim et al., 2009). However, no correlation is found in the studied area (See appendix B). This has been explained in some instances as a non-simultaneous reduction of As and Fe (Islam et al., 2004), or as re-adsorption of As (Nickson et al., 2000). However, the lack of correlation in this case is attributed to massive precipitation of siderite in the NP aquifer. Thermodynamic calculations indicate that groundwater in the Deep zones 1 and 2 are supersaturated and very near to equilibrium with respect to siderite. Moreover, the goethite-made gossan is massively replaced by

siderite (Yesares et al., 2014). The siderites exhibit light $\delta^{13}C$ values (between -13.4 and -47.95 ‰) that are typical of C from organic origin (Capitán, 2006) and have been interpreted as the largest documented occurrence of a microbially derived ore assemblage (Tornos et al., 2014).

The strong correlation of B with NH_4 (R^2=0.91, See appendix B) suggests a common process controlling their concentrations in groundwater. Similarly, the weak correlation observed between As and B and between As and NH_4 indicates that these processes are at least in part different from those concentrating As. Indeed, NH_4 and B show a clear positive correlation with Cl (Figure 4.4 A and B).

Several samples have ammonium, boron, iodide and fluoride concentrations higher than seawater (Figure 4.4). Taking into account the modern seawater concentrations for NH_4, B, I and F, the expected contribution from a maximum of 8% of seawater mixing, and the concentrations found in groundwater samples, enrichment factors of 3200, 9, 140 and 85 are found (Table 4.2). This suggests that an extra source and additional processes are associated with these compounds.

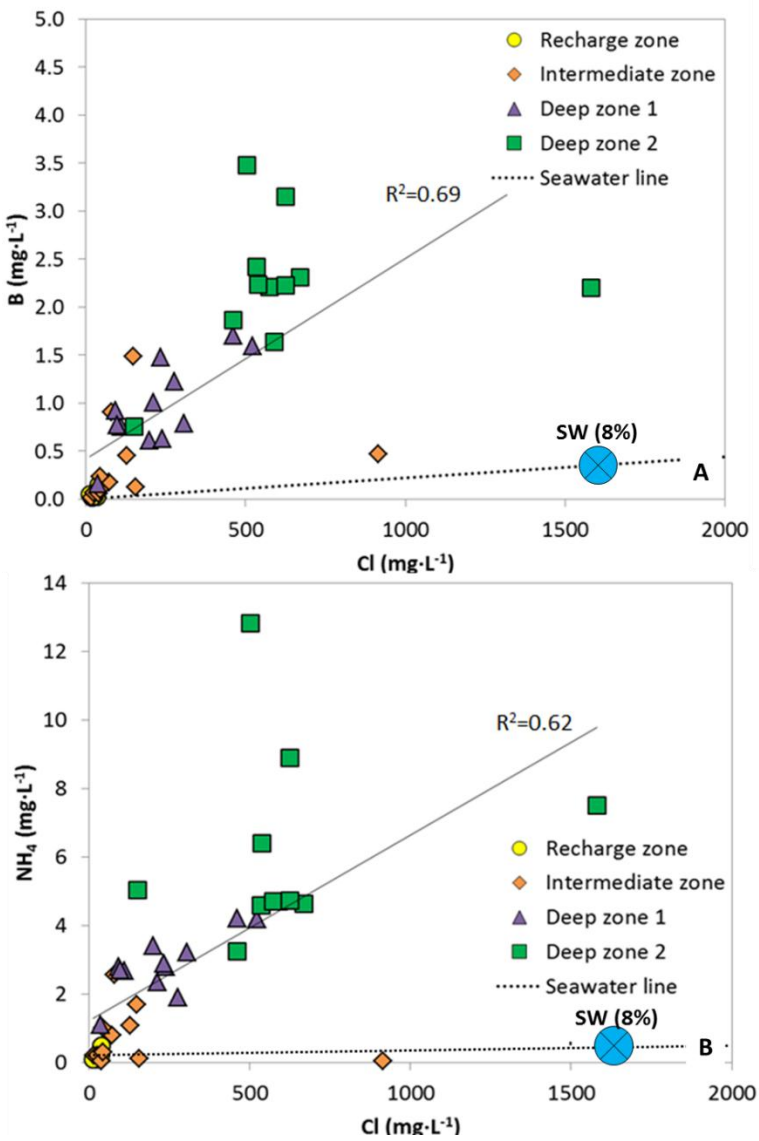

Figure 4.4. Plots of A) boron and chloride and B) ammonium and chloride. SW= Seawater 8%.

Nitrogen is a fundamental nutrient and is a constituent of multiple organisms, so it is generally associated with organic matter in C:N proportions of 16:106 (Redfield, 1934). Iodine is also assimilated by marine organisms, and organic matter is an important source of iodine for this reason (Price and Calvert, 1973; Kennedy and Elderfield, 1987; Worden, 1996). Strong correlations of iodine with ammonium (R^2=0.86) and boron (R^2=0.83) (see appendix B) suggest organic matter degradation as the source for both species in groundwater (Figure

4.5 A and B). In the case of fluoride, the correlations are not so clear, but there is a strong correlation with boron (R^2=0.82) and weaker correlations with ammonium (R^2=0.57) and iodide (R^2=0.39).

	NH_4	**B**	**I**	**F**
Seawater concentration	0.05	4.6	0.06	1
Concentration contribution from 8% of seawater	0.004	0.368	0.0048	0.08
GW samples maximum concentrations	12.8	3.48	0.67	6.79
ENRICHMENT FACTOR	3200	9	140	85

Table 4.2. NH_4, B, I and F concentrations in seawater, mixed water with an 8% contribution of seawater, and groundwater samples ($mg \cdot L^{-1}$). The enrichment factor is calculated under the assumption that groundwater mixes with a maximum of 8% of seawater. Seawater concentrations for NH_4 and B are from Yuan-Hui, 1991, those of I and F are from Truesdall, 2000 and Berner and Berner, 1987, respectively.

This suggestion is confirmed by light $\delta^{13}C$ and $\delta^{15}N_{NH4}$ values found in the groundwater of the deepest zones. The light $\delta^{13}C$ values obtained in the deepest zones (from -6.63 to -11.43 ‰) suggest that the organic matter degradation has an important role in the groundwater chemistry. A detailed and quantitative discussion of the chemical processes affecting the $\delta^{13}C$ values can be found in Scheiber et al. (2015). The nitrogen in the sedimentary rock is accumulated as organic matter during the sedimentation process and is incorporated during the diagenesis process as ammonium. It has been suggested that the $\delta^{15}N_{TOTAL}$ values of sedimentary rocks are representative of $\delta^{15}N_{NH4}$ values (Holloway and Dahlgren, 2002). Under reducing conditions, the organic matter degradation can release high ammonium concentrations (E10). A weak correlation between NH_4 and HCO_3 is observed, but this can be affected by siderite precipitation in the vicinity of the ore.

$$NO_3^- + H_2O + 2CH_2O \leftrightarrow NH_4^+ + 2HCO_3^- \quad \text{(E10)}$$

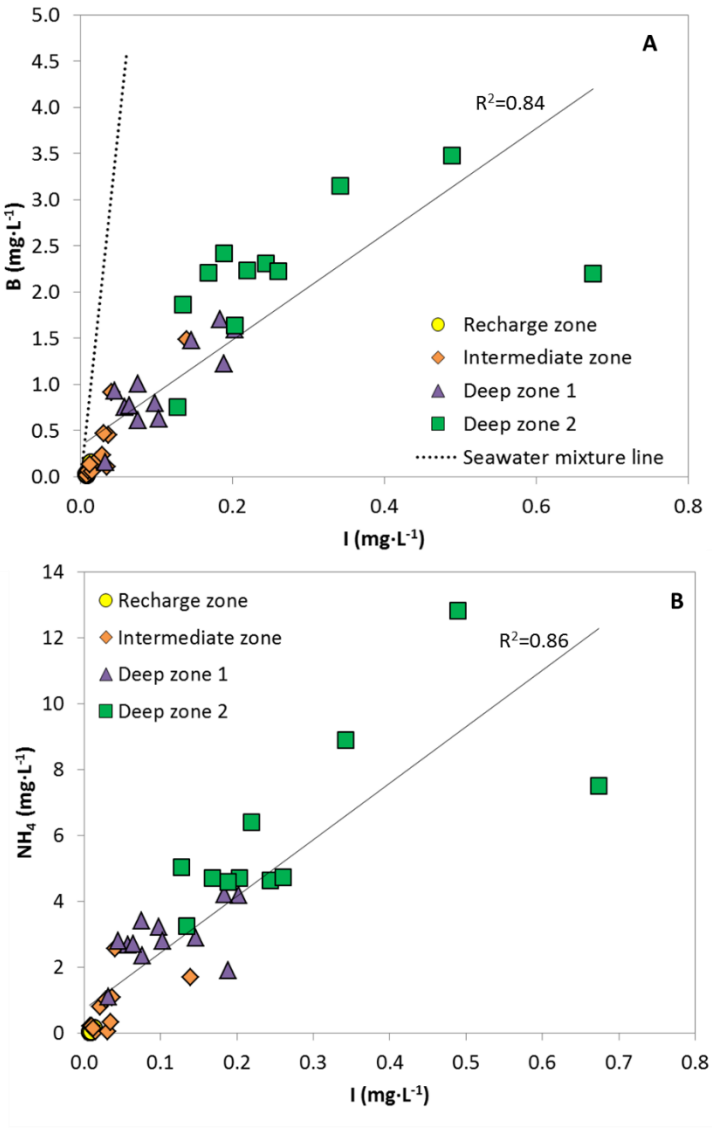

Figure 4.5. Plots of A) boron and iodide, B) ammonium and iodide.

The $\delta^{15}N$ fractionation under laboratory conditions between sedimentary organic matter and pore water ammonium has been investigated by Prokopenko et al., (2006). The results show that pore water $\delta^{15}N_{NH4}$ values (<0.7 ‰) are generally lighter than those of the sedimentary material (≈5 ‰) due to a small isotope fractionation associated with organic matter degradation (Ɛ= -0.7‰ ± 0.2‰). However, the $\delta^{15}N_{NH4}$ values of pore water and sedimentary material in some samples can be quite similar due to the low fractionation

factor. There are several aspects that can vary the isotopic ratios, such as depth, N content, bacterial activity and degree of organic matter degradation (Prokopenko et al., 2006). The groundwater of the NP aquifer has $\delta^{15}N_{NH4}$ values between -3.9 and 0.7 ‰ (Figure 4.6), which are similar to those of the marlstones recovered from North Atlantic cores (Rau et al., 1987), where a range between -2.7 and 2.3 ‰ is observed. Borowski and Paull (2002) reported heavier values of $\delta^{15}N_{NH4+}$ (+3.6 to +4.9‰) in pore water produced by microbial fermentation reactions in deeper marine sediments under sulfate reducing conditions. The similarity between the $\delta^{15}N_{NH4}$ values in groundwater and in marl organic matter found elsewhere suggests that high ammonium concentrations could be derived from organic matter degradation of the bluish marls in the "Gibraleon Fm".

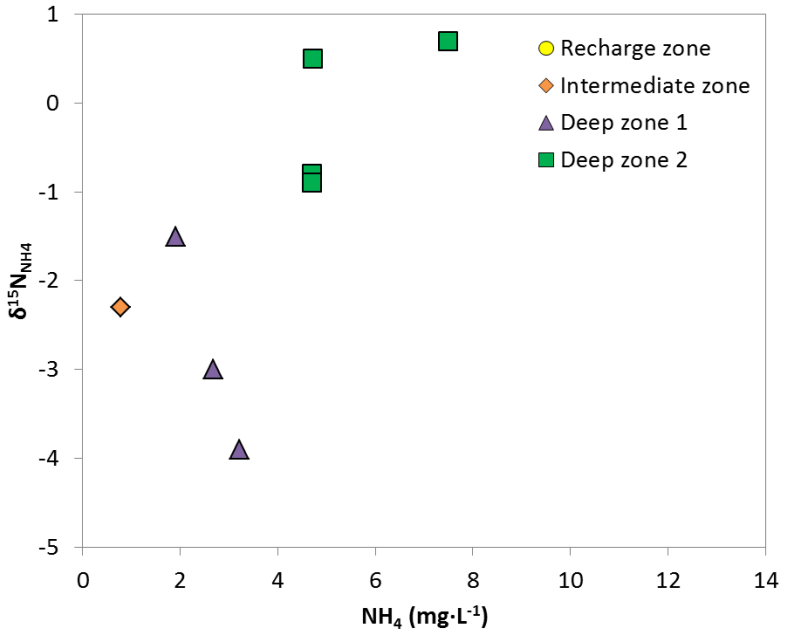

Figure 4.6. Plot of $\delta^{15}N_{NH4}$ vs. NH_4.

High boron contents can be attributed to sorption-desorption processes where seawater B is sorbed onto the surfaces of sediments. Desorption and release to groundwater takes place during the freshening-up stage when fresh continental water displaces seawater in aquifers. The competitive action of HCO_3/CO_3 could drive desorption from mineral surfaces,

producing a B/HCO_3 correlation as observed in aquifers in Bangladesh and Michigan (Ravenscroft and McArthur, 2003). However, no positive correlation between B and HCO_3 has been observed in the studied area, but HCO_3 concentrations are strongly buffered by the dissolution of calcite and precipitation of siderite in the deep zones of the NP aquifer. Therefore, B sorption-desorption cannot be ruled out. An alternative, although similar, explanation for B origin is to assume sorption into solid marine organic matter. Thus, B sorption in the organic matter of soils has been demonstrated to be one order of magnitude more efficient than on mineral surfaces, such as clays and Fe-oxides (Goldberg, 1997). Moreover, oil reservoir brines are commonly enriched in B, so organic matter maturation seems to be a possible source of B during thermal maturation (Williams et al., 2000). The degradation of organic matter by SO_4 from recharge water would account for the release of B to the pore water of the NP aquifer (Figure 4.7).

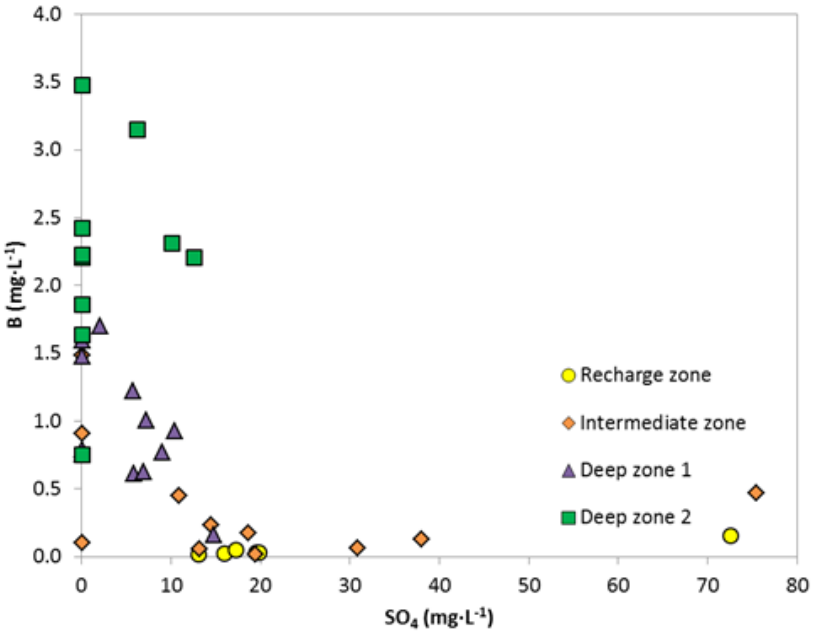

Figure 4.7. Correlation between B and SO_4.

Defining groundwater quality for each defined zones is essential for good management of the NP aquifer. In addition to mining, the main consumption of the groundwater is for

agriculture and drinking water associated with the surroundings villages. Moreover, the aquifer also represents a drinkable water reserve for the city of Seville and its conurbation in severe drought events. Therefore, the guideline defined by the WHO (2008) for drinking water and the USEPA recommendations for irrigation have been used to assess the water quality of the aquifer based on ammonium, arsenic, boron and salinity. The groundwater of the studied area exhibits a clear increase in salinity and loss of quality from NW to SE. Recharge area: In general, the groundwater in this area has acceptable characteristics for drinking water (NH_4, As, B and salinity) and continuous irrigation, except in local cases where high nitrate concentrations related to agriculture has been detected. Intermediate zone: Drinking water and high water quality are found in the NW half of this zone. The intermediate SE half, however, has NH_4 concentrations above the drinking water standards. The salinity and B concentrations allow the use of the water for continuous irrigation of many types of crops. Deep zones 1 and 2: Groundwater from these zones has high concentrations of ammonium, arsenic, boron and salinity and is not suitable for drinking or for continuous irrigation use.

Based on the described water quality data, three different uses of groundwater can be established: drinking and continuous irrigation, irrigation only and none (Figure 4.8). In this paper, only NH_4, As, B and salinity has considered for determining the groundwater quality. Other parameters or compounds not addressed here may affect the delineation of the drinking and continuous irrigation water zone.

Beyond the description of water quality and the classification of aquifer zones, correct management requires the definition of a methodology for discriminating anthropogenic from geogenic origins for the solutes that constrain the water quality, such as As, NH_4 and B. This is particularly necessary in an area of water scarcity and aquifer exploitation by various and often conflicting users. Here, we present evidence that, rather than mining operations, arsenic is related to the reductive dissolution of As-bearing goethite mineralization in a reducing environment, similar to the cases described for SW Asia (Smedley and Kinnibugh, 2002). Evidence of such a process includes the low redox potential,

and the massive precipitation of siderite with light $\delta^{13}C$ values. Moreover, we also demonstrate that NH_4, B, I and F are also of geogenic origin and are correlated. Anomalous concentrations of all such elements have also been previously referred to in an aquitard from northern Mexico (Ortega-Guerrero, 2003), but the relationships among them are not mentioned. A strong correlation of all of these elements with salinity is also observed. However, unlike similar aquifers in Michigan and Bangladesh (Ravescroft and McArthur, 2003; Halim et al., 2010), the concentrations of these elements in the NP aquifer cannot be explained by mixing with seawater, but they require another source. An origin of marine organic matter degradation under a reducing environment is postulated for NH_4, B, I and F. The evidence for organic matter degradation includes the light $\delta^{13}C$ and $\delta^{15}N$ values measured in groundwater. This is in agreement with the origin attributed by Jiao et al. (2010) for the NH_4 and I of pore water in the Pearl River Delta, China, although these authors did not supply direct evidence.

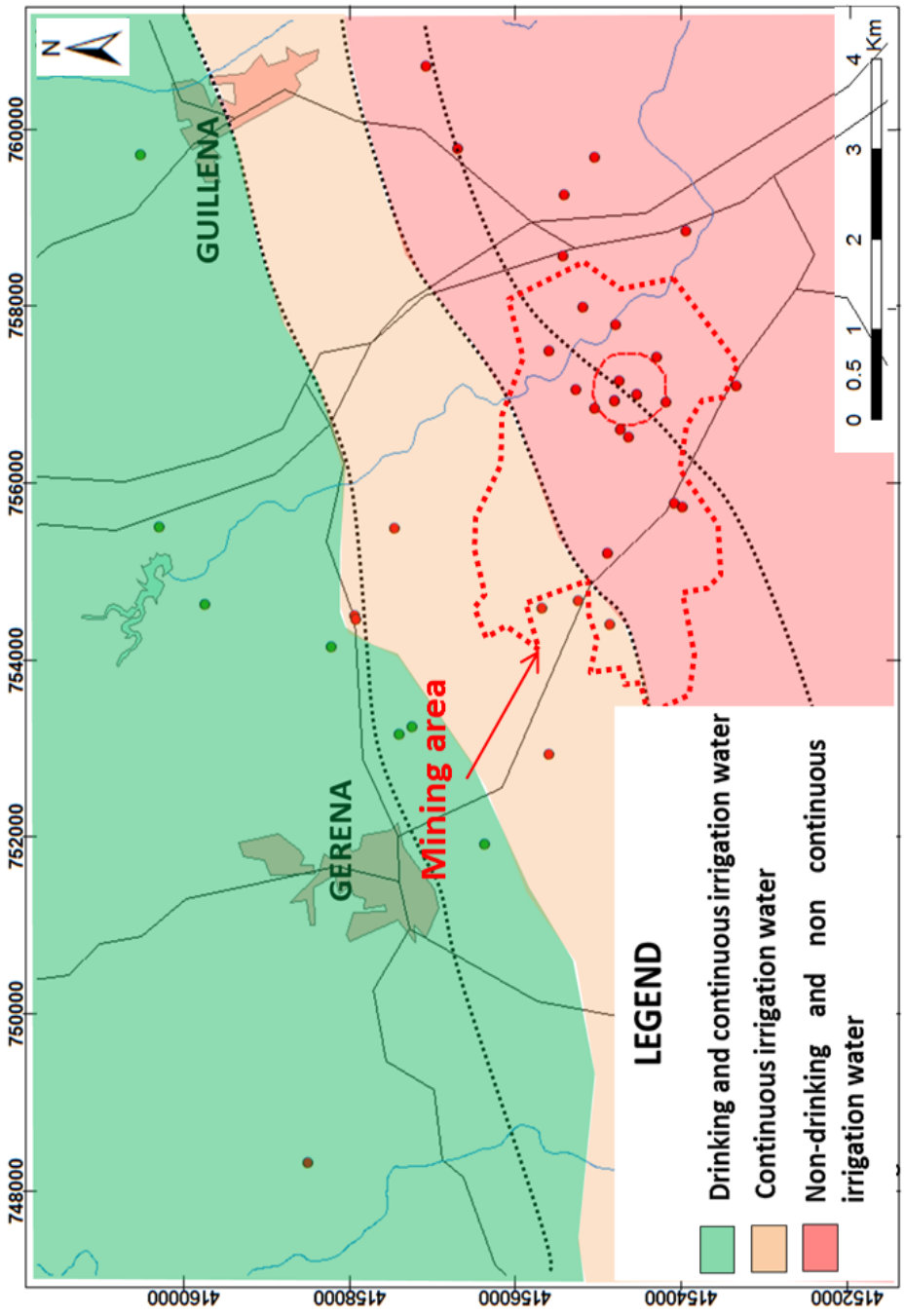

Figure 4.8. Map of groundwater quality from ammonium, arsenic, boron and chloride concentrations. The dashed lines mark the four zones: Recharge, Intermediate, Deep 1 and Deep 2. ETRS_1989_UTM_Zone_29N.

4.4. CONCLUSION

Groundwater flows from NW to SE evolving from Ca-HCO_3 to Na- HCO_3 and finally to Na-Cl type waters with increasing depth. In general, the increased salinity down-flow is a natural characteristic of this system, with two groundwater systems possibly being mixed in different proportions: A) a shallower, faster system associated with recharge in the Cenozoic portion of the NP aquifer, with slightly enriched water stable isotope values, lower Cl/Br ratios and an enrichment in Na due to ion-exchange processes; and B) a deeper, slower system associated with groundwater recharged at the coldest period during last 30 ky, with some remains of marine pore waters of up to 8% and Cl/Br ratios closer to marine-derived values.

High arsenic, ammonium and boron concentrations are found in the deeper zone of the NP aquifer. None of these solutes are found in the recharge area, but their concentrations increase with depth. They appear in zones already isolated from the surface by a thick sequence of low-permeability marls and in groundwater with residence times >30 ky. Therefore, the presence of high arsenic, ammonium and boron concentrations is attributed to geogenic processes. The arsenic distribution follows a different pattern that is not strictly linked to salinity. Arsenic in groundwater is interpreted as originated from the reductive dissolution of As-bearing goethite by dissolved organic matter. Goethite was formed by the oxidation of original Paleozoic ore exposed to atmospheric conditions during the pre-Miocene age. Arsenic in groundwater depends, therefore, on the location of goethite mineralization. The lack of the expected correlation between Fe and As is explained by the massive precipitation of siderite.

Ammonium and boron, together with iodide and fluoride, clearly increase with chloride from NW to SE and are interpreted as being the result of degradation of marine solid organic matter by sulfate dissolved in the recharge water. The light $\delta^{15}N_{NH4}$ values confirm that its origin is linked to marine organic matter. Related to management implications, three zones of groundwater quality were defined based on the ammonium, arsenic, boron and salinity

data: the first zone, which is closer to the recharge area, contains water of human drinkable quality; the second zone downflow contains groundwater suitable for continuous irrigation but not for drinking, due to its high ammonium concentrations; and the third zone contains groundwater of elevated salinity (up to 5940 $\mu S \cdot cm^{-1}$) and high ammonium, arsenic and boron concentrations not being usable.

The accurate investigation of the interactions between water, organic matter and rock is indispensable for the correct determination of the origin of water quality in areas with high human pressure on aquifers.

CHAPTER 5. QUANTIFICATION OF PROPORTIONS OF DIFFERENT WATER SOURCES IN A MINING OPERATION

5.1. INTRODUCTION

Evaluating the potential composition of drained or collected water related to mining activities is important in relation to pollution risks and the development of management alternatives. Water collected in galleries and open pit bottoms normally comes from different sources, e.g., surface runoff, surface water drainage systems, and groundwater. Evaluating how much water comes from each source is usually necessary for several reasons. First, overall water fluxes can be best evaluated when the relative importance of each source is known because some may be easier to estimate than others. Second, pollution risks and geochemical processes are dependent on the chemical signatures of water sources. Finally, treatment plant design, management alternatives, administration regulations and other decisions can be best supported when the relative importance of each source is known. For

example, drained water can be used as irrigation water for roads to reduce dust suspension levels, for the leaching of mine waste tips, for mineral processing, or for recharging aquifers.

To evaluate the composition of such water in early stages of mining activities or in the operational phase, it is necessary to (1) identify and characterize, on a hydrochemical basis, different water sources (end-members) and (2) perform a mass (salt) water balance. Mass water balance and mixing models are widely used in all branches of hydrology. While it is recognized that there are always uncertainties involved in the evaluation of end-member concentrations and mixing ratio evaluations, it is conventionally assumed that (1) concentrations of end-members are different and accurately known, (2) the required number of species to be used through mass balance tests grows with the number of potential sources, and (3) selected species behave conservatively. Under these conditions, the estimation of groundwater mixing ratios has been applied to quantify interactions between groundwater and surface water bodies. For instance, Beyerle et al. (1999) measured degrees of river infiltration to a shallow aquifer using $^{3}H/^{3}He$, noble gases and CFCs; Shaw et al. (2014) investigated sources mixed in the Merced River to understand streamflow and groundwater generation patterns; Liu et al. (2004) used mixing methods to determine the sources and pathways that control the quantity and quality of streamflows draining high elevation catchments in Colorado; and Hitchon and Friedman (1969) and Jørgensen et al. (2008) employed mixing methods to calculate freshwater and seawater mixing ratios. Additionally, Nakaya et al. (2007), Usunoff and Guzmán-Guzmán (1989) and Ramos-Leal et al. (2007), among others, have used mixing methods to differentiate between shallow and deep groundwater aquifers.

Even when the applied mixing conceptual model is considered correct and when water flows are well-stated, there are certain problems with water mass balance applications. (1) The mass balance may not close. This issue can be a result of data errors and can occur at any stage of sampling and analysis in both source and mixed water. (2) Water reactions that were not previously considered or evaluated can emerge. (3) The concentration range of a

species can overlap with any other end-member. In this case, working with many species is necessary. However, concentrations of mixed samples are likely to be less uncertain than those of end-members. This lower level of uncertainty suggests that it is possible to use actual concentration data to impose constraints on valid end-members compositions. Thus, multivariate statistical analysis techniques are required to solve the following problems: (1) the number of end-members is high; (2) potential data errors prevent a closed balance; (3) there are numerous mixtures with common end-members; and (4) there are numerous mixtures for which we wish to calculate end-member percentage contributions. To address these specified difficulties, Carrera et al. (2004) and Vázquez-Suñe et al. (2010) developed and applied a multivariate statistical analysis method to perform mixing ratio calculations while acknowledging the uncertainties of end-members compositions. A more detailed description of the proposed methodology can be found in Carrera et al. (2004). This method is applied in Jurado et al. (2013) and Tubau et al. (2014), who use mixing methods to identify and quantify sources and processes shaping water quality levels in urban aquifers. Cánovas et al. (2012) studied the impacts of releases from a freshwater reservoir into the acidic Tinto River, identifying metal transport mechanisms involved.

Cobre Las Cruces (CLC) is an open pit copper mine highlight in Europe located in southern Spain. It is located in the Guadalquivir Valley, a semiarid region where groundwater is a valuable resource that sustains the population and that supports traditional agricultural systems. The CLC open pit captures a significant amount of rain-derived surface runoff. Moreover, despite the presence of an external pumping well ring system (DRS) that drains the open pit (Baquero et al., 2016), the deepest parts of the open pit receive some groundwater discharge from two different aquifers, Cenozoic sandstones and Palaeozoic metamorphic rock that host ore deposits. The Cenozoic sandstone aquifer presents low degrees of mineralization and is of a Ca-Na-HCO_3^- water type. This water is used for agricultural and human consumption and is strictly regulated by the local water authority. In contrast, water from the Paleozoic aquifer is older, presents high degrees of mineralization and is of a Na-Cl water type (Scheiber et al., 2015). Due to the quality of this

water, it cannot be used for any activities, and no legal regulations control it. These features have spurred considerable controversy regarding the management of the two aquifers related to their potential uses, quality and quantity limits and risks assessment (pollution and resources withdrawal). Further, the involvement of the regional and state government and criticism from the public and from environmental groups have generated uncertainties surrounding mining activity.

The main objective of this study is to propose an approach based on multivariate statistical methods for computing the mixing ratios of different water sources (end-members) related to mining operations. To ensure its applicability, the approach is applied to the CLC open pit, for which it is necessary to define the volume of water extracted from the Cenozoic aquifer, which the CLC must compensate for via artificial recharge in compliance with current regulations. This approach will serve as a useful tool for groundwater management in mining sites where it is necessary to assess or quantify the contributions of different water sources that could define drained water compositions during several stages of mining operation.

5.2. MATERIAL AND METHODS

MIXING CALCULATION

To determine the end-members composition and their proportion in each water sample, the proposed methodology involves: A) Identifying different water sources (end-members) involved; B) Hydrochemically characterizing different end-members and mixed water involved; C) Selecting chemical species to be used in the evaluation; D) Defining the standard deviation of each species in both samples and end-members; E) Introducing all of this information into the MIX code; F) Computing the end-member compositions and mixing ratios obtained; G) Iterating the process by re-evaluating the end-member and tracer selection practices based on the results of previous steps.

The MIX code (used to calculate mixing ratios) is based on the maximum likelihood method for estimating rates of mixing and accounts for uncertainties in known end-member concentrations (Carrera et al., 2004).

In our case, the mixing ratio of open pit water is calculated using two models: the regional and open pit models. For the regional model, chemical and isotope compositions of 28 samples collected from wells, piezometers and springs in the area are used to obtain the best estimates of Cenozoic and Paleozoic groundwater compositions and the most discriminant components. Then, monthly water samples from the open pit for 2014 to 2016 together with runoff samples are used to characterize runoff end-members and calculate the mixing ratios in the open pit

SAMPLING AND ANALYTICAL METHODS

Three types of analytical data are used in the calculations: (1) regional data obtained from samples taken during two field campaigns in February 2012 and September 2013 (Scheiber et al., 2016; Scheiber et al., 2015); (2) historical data (2014-2016) obtained from open pit water and provided by the CLC; and (3) runoff samples collected from rainfall events from 2014. The 28 regional samples were analysed during field campaigns to determine general chemistry features and isotope compositions of the different types of sampling points, e.g., wells, piezometers, drains, and springs. Before collecting samples, sampling points were purged once field parameters had stabilized. Physico-chemical parameters such as temperature (°C), pH, Specific Conductance (SC, $\mu S \cdot cm^{-1}$), Eh and dissolved oxygen (DO, $mg \cdot L^{-1}$) were measured in situ using a closed flow cell.

Complete analyses and further information on the analytical methods can be found in appendix A and B.

INDEPENDENT RUNOFF ESTIMATION

A balance of open pit water is generated to acquire independent runoff values for the open pit and to compare them with values obtained from the MIX calculation. This calculation is based on the curve number method (Mishra and Singh, 2013). It takes into account parameters such as soil characteristics, soil use, vegetation cover and proximity to previous rain periods. An empirical curve that relates precipitation and runoff is obtained. This curve has two parts: 1) a threshold of precipitation below which all rain is retained in the soil with no runoff and 2) points beyond this threshold where the runoff level increases with precipitation. In our case, a curve number of 93 corresponding to low permeable naked ground and firm roads was used. These values are corrected by slopes of greater than 3% and with a value that is dependent on previous soil moisture levels. Further information on this methodology can be found in appendix C.

5.3. RESULTS AND DISCUSSION

REGIONAL MIXING CALCULATION

REGIONAL CONCEPTUAL MODEL

In previous works, study areas have been divided into 4 zones based on geochemical and isotopic features: recharge, intermediate, deep 1 and deep 2 zones (Scheiber et al., 2016; Scheiber et al., 2015). Each zone corresponds to groundwater with different hydrochemical characteristics. The recharge zone is related to water that has recently infiltrated the northern part of the study area where outcropping materials form the Cenozoic aquifer. The intermediate zone corresponds to groundwater from the Cenozoic aquifer. Finally, the two deep zones are associated with groundwater from the Paleozoic aquifer.

Hydrogeochemical variables of regional groundwater samples can be found in appendix B.

ESTIMATING OF REGIONAL END-MEMBERS NUMBER

First, EMMA (End-Member-Mixing-Analysis) methodology was used to determine the number of end-members needed to explain a significant proportion of the variability in the regional samples composition. Hydrochemistry data were obtained from the February 2012 regional field campaign, and we used 28 samples for this analysis. Initially, 14 chemical components were selected for the EMMA analysis: Total Inorganic Carbon (TIC), Cl, NH_4, Na, B, Ca, ^{13}C, I, Br, ^{2}H, $^{87}Sr/^{86}S$, Specific Conductivity (SC), Sr and ^{18}O. Four different EMMA analyses were performed to evaluate the selected species (Figure 5.1)

The first EMMA analysis (A1) considered all 14 species, and a total of variance of 83% was obtained with three eigenvectors. The first eigenvector explains 58% of the variance, and most of the components contribute positively with the exception of Ca, ^{13}C, ^{2}H and ^{18}O; the largest contributing components are Na, Cl, NH_4 and B. The second eigenvector explains 16% of the variance and Ca, Sr, ^{18}O, I, ^{2}H and HCO_3 contribute most. The third eigenvector provides 9% of the total variance, and its contributions are attributable to ^{13}C, Sr and HCO_3. For the second analysis EMMA (A2) $^{87}Sr/^{86}Sr$ was not considered, and the three eigenvectors explain 86% of the total variance. A minor increase in the main contributing components for each eigenvector produces an increase in the total variance of 60% (first eigenvector), 17% (second eigenvector) and 10% (third eigenvector). The EMMA third analysis (A3) does not consider $^{87}Sr/^{86}Sr$, ^{2}H and ^{18}O and the total variance increases by up to 87% with three end-members. In general, this increase is due to a greater contribution by the ions, particularly to characteristic ions of each eigenvector (Cl, Na, HCO_3, Ca, and NH_4). Finally, the last EMMA analysis (A4) explains most of the total variance at 92% excluding $^{87}Sr/^{86}Sr$, ^{2}H, ^{18}O, ^{13}C and Sr. This increase is due to major contributions of components of the third eigenvector, particularly those of HCO_3 and Ca. This analysis (A4) generates the best results of the analyses conducted (A1, A2 and A3). The EMMA analysis determines that 3 end-members and nine components (TIC, Cl, NH_4, Na, B, Ca, I, Br and SC) are needed to explain 92% of the variability in the sample.

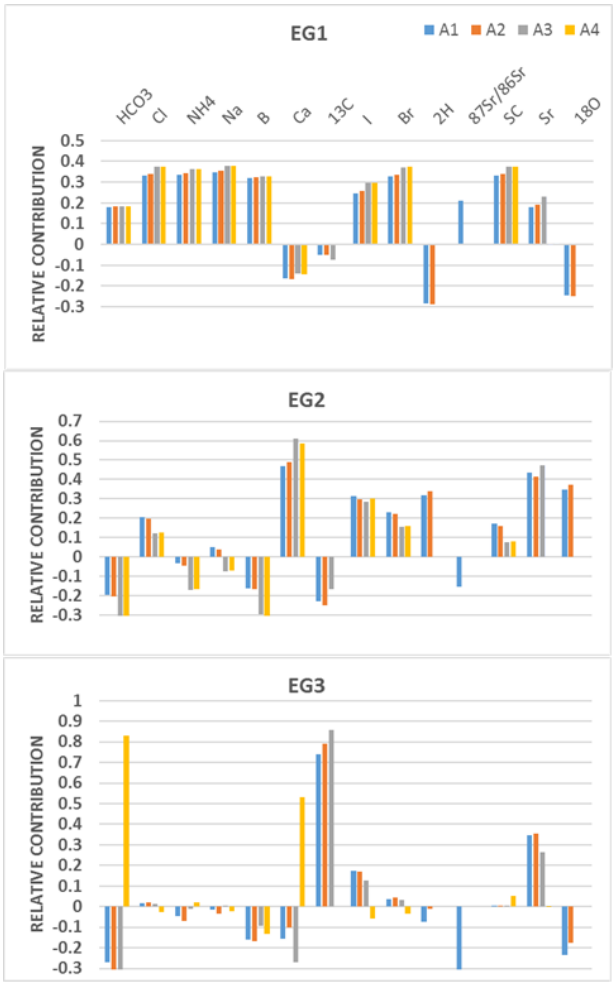

Figure 5.1. Eigenvectors 1, 2 and 3 resulting from processing the data with EMMA.

ESTIMATION OF REGIONAL END-MEMBER COMPOSITIONS

A previous conceptual model must be used to identify potential end-members. We used piper diagrams to identify three possible end-members consistent with the EMMA analysis (Figure 5.2). End-member 1 has a Ca-HCO_3 composition and corresponds to recharge water (R) associated with eigenvector 2. End-member 2, which is related to eigenvector 3, is of a Na-HCO_3 type that corresponds to groundwater from the Cenozoic aquifer (CN), which is affected by a Ca-Na exchange process. Finally, end-member 3, which is linked to eigenvector 1, has a Na-Cl composition and corresponds to groundwater from the Paleozoic aquifer (PZ).

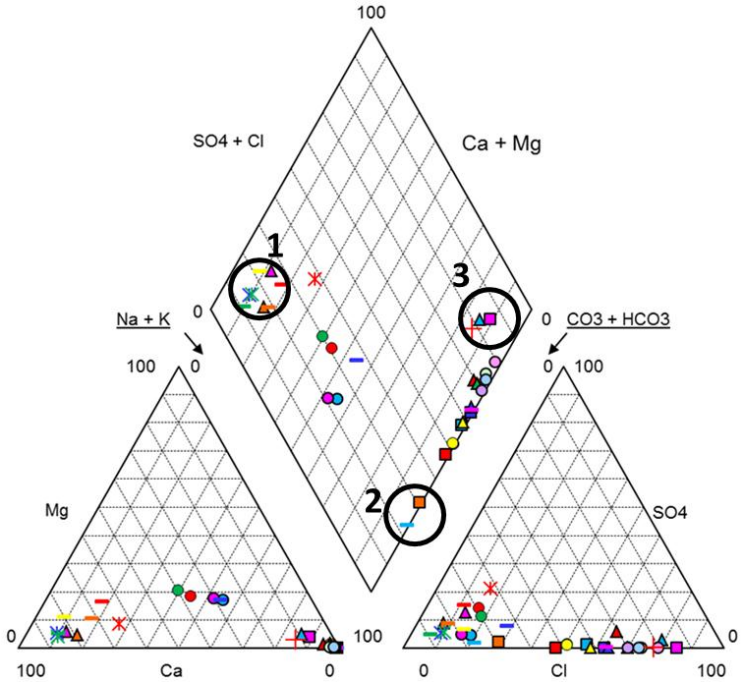

Figure 5.2. Piper diagram of the regional samples and potential end-members. (1) Recharge water, (2) Cenozoic water and (3) Paleozoic water.

We used MIX software to determine the proportion of each water source analysed with respect to potential end-members defined with the minimum error value from regionally available data provided through the two field campaigns.

In the MIX code, uncertainty is quantified from covariance matrices. It is necessary to assume a standard deviation for every species when defining the reliability of measurements and results. Moreover, the standard deviations of less conservative tracers in observation points were made relatively higher to decrease their weights in the calculation. When applying standard deviations, sampling and analytical errors must be taken into account. Standard deviation values applied ranged between 10% and 25%, depending on the species considered (Table 5.1).

	TIC	Cl	NH_4^+	Na	B	Ca	I	Br	SC
Standard deviation (%)	25	10	15	10	15	25	15	15	10

Table 5.1. Standard deviation value applied to each species.

Table 5.2 shows the chemical compositions of end-members as inputs and outputs of MIX calculations. The input data were obtained from regional field campaigns, and end-member compositions were recalculated by MIX. Note that end-members calculated by MIX are mathematical entities resulting from the minimization of errors between measured and calculated concentrations of each component and the final objective function. The difference between the input and output data are considered through the assumed deviation. Determining whether to use a conservative or reactive degree for each species involves carrying out iterative runs of MIX and comparing the predicted and observed values, as shown below.

INPUT END-MEMBERS COMPOSITION									
END-MEMBER	**TIC**	**Cl**	**NH_4^+**	**Na**	**B**	**Ca**	**I**	**Br**	**SC**
R	268	19	0.08	15	0.02	103	0.008	0.09	903
PZ	399	1349	9.63	979	2.20	70	0.64	5.41	5817
CN	270	91	2.83	256	0.93	1	0.04	0.42	1441
OUTPUT END-MEMBERS COMPOSITION									
R	283	14	0.07	11	0.02	90	0.007	0.10	721
PZ	474	1337	10.582	1107	2.54	40	0.63	5.42	5798
CN	305	94	1.32	186	0.76	1	0.05	0.44	1271

Table 5.2. Chemical composition of the end-members used for mix calculation. Units expressed in $mg \cdot L^{-1}$ and $\mu S \cdot cm^{-1}$.

MIXING RATIOS CALCULATION FOR THE REGIONAL MODEL

Nine components selected by EMMA analysis (A4) were included systematically in the MIX model (TIC, Cl, NH_4, Na, B, Ca, I, Br and SC). The concentrations of these species should present broad levels of variability between the different end-members. Based on the previously defined components and standard deviation values, the mixing ratios of the regional water samples were calculated. Adjustments to this analysis was performed by introducing the species by minor deviation values. Systematically, these deviations were adjusted such that the measured and calculated concentrations were similar, and particularly for the conservative species. Figure 5.3 shows the measured versus calculated values obtained from the MIX model. Species such as Cl, Na, I, Br and SC show a 1:1 relationship, denoting that their concentrations are only dependent on mixing processes.

For species such as TIC, NH_4^+, B and Ca, however, the measured value is higher than the computed value due to water-rock reactions of carbonate dissolution or organic matter degradation, which have been identified in previous studies (Scheiber et al., 2016; Scheiber et al., 2015). Then, the uncertainty assigned to Ca and HCO_3 species was increased (Table 5.1).

After calibration, the spatial distribution of the mixing ratios was obtained (Figure 5.4). End-member recharge was consistently present in sampling points close to the recharge aquifer area. Along the NW-SE flow lines, groundwater had a Na-HCO_3 composition approaching the Cenozoic end-member. The deepest sampling points located to the southeast showed compositions rich in sodium and chloride close to the Paleozoic end-member. As an additional output, regional mixing calculations allowed for the best estimation of the end-member compositions (Table 5.2). Two of these end-members (PZ and CN) were then used for subsequent mixing calculations at the open pit scale.

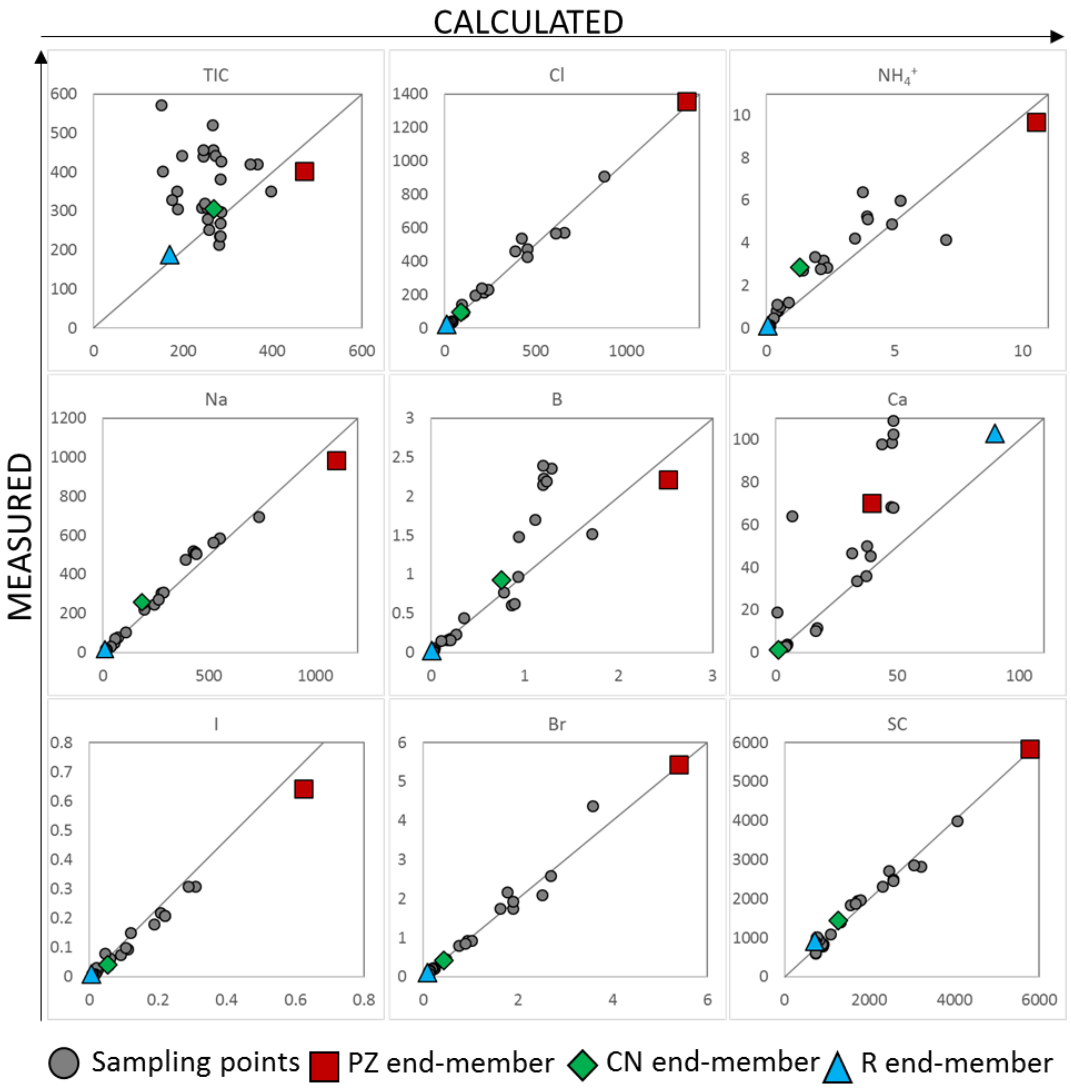

Figure 5.3. Measured versus calculated concentrations of the regional model.

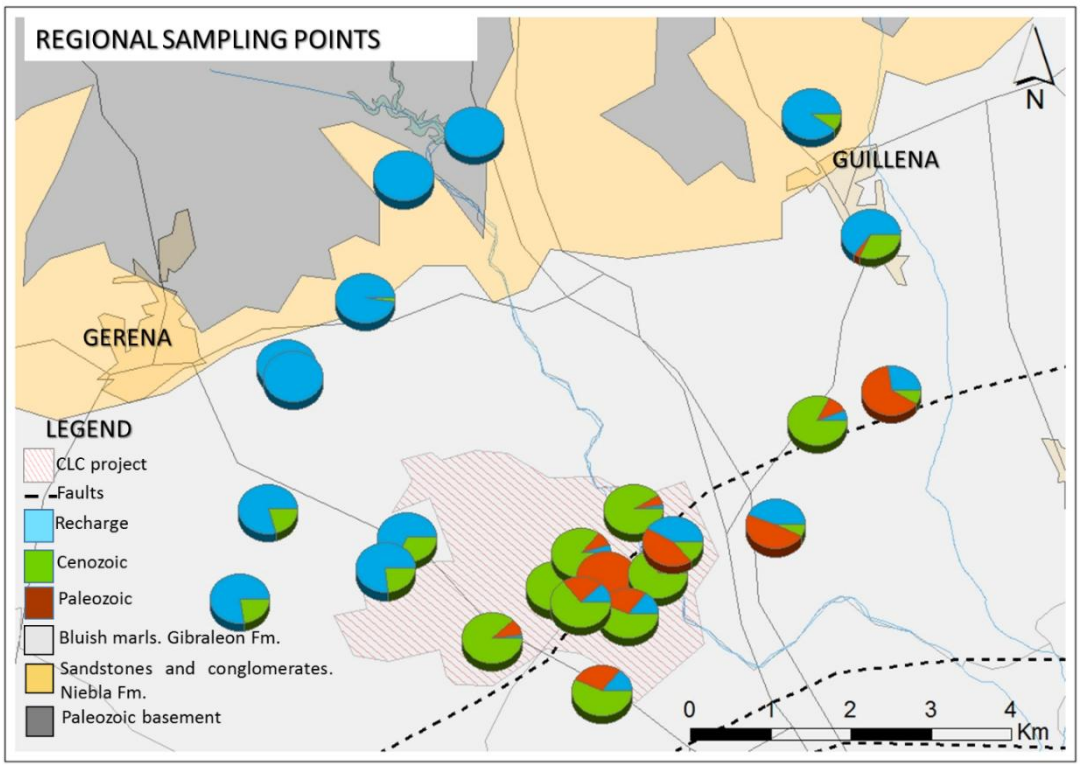

Figure 5.4. Spatial distribution of mixing ratios evaluated from the 28 samples of the regional model

OPEN PIT MIXING CALCULATION

The main goal of this section is to calculate the mixing ratios of water accumulated in the CLC open pit during the hydrological years of 2014-2015 and 2015-2016 (September to August).

LOCAL CONCEPTUAL MODEL

The elevation of the bottom of the CLC open pit reached 160 mbsl (m below sea level) in August 2016. The Las Cruces open pit water is mainly composed of three end-members: Cenozoic and Paleozoic end-members, which correspond to 2 different groundwater bodies, and runoff water (Figure 5.5). The runoff water is rainwater that flows down the slope of the

open pit. Two types of runoff water can be distinguished: No Contact Water (NCW) and Contact Water (CW). NCW is runoff water intercepted by a drainage system installed in the open pit at 105 mbsl. This water is subjected to sedimentation treatment before being returned to the environment (in this case, to surrounding streams). CW is runoff that reaches the open pit and that has been in contact with the ore body (Figure 5.5). Water from the open pit bottom is pumped out and sent to a permanent water treatment plant, where it undergoes reverse osmosis and meets the required quality levels so it can be returned to the aquifer through reinjection wells. As only this aquifer is regulated, CLC must compensate for open pit water drained from the Cenozoic aquifer.

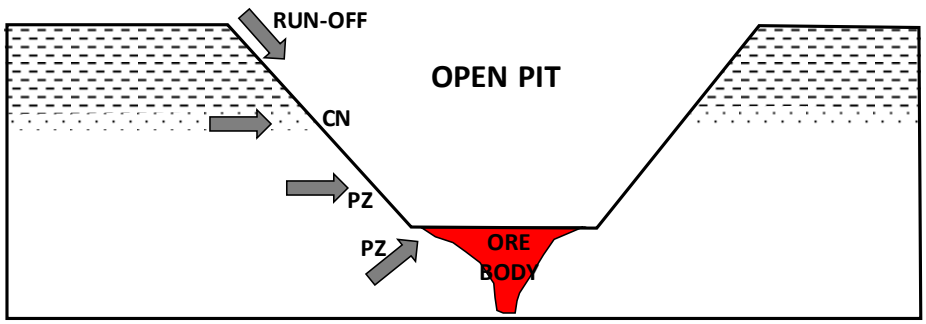

Figure 5.5. Conceptual model of the CLC open pit.

ESTIMATING THE LOCAL END-MEMBERS NUMBER AND THEIR COMPOSITION

In this case, 18 species analyzed monthly are available in the CLC database: NH_4, TIC, B, Ca, Cl, Cu, S.C., F, Mg, Ni, NO_3, pH, K, Na, SO_4, Zn, ^{2}H and ^{18}O. The Piper diagram shows the contributions of each end-member to the composition of the open pit water (Figure 5.6). As was expected for the distance and residence times of groundwater, the regional recharge end-member is not involved in the chemical composition of the open pit water. The new end-member corresponds to runoff water from rainwater flowing through the walls of the open pit to bottom out. The drainage system implemented inside the open pit intercepts part of the runoff water at different depths of the open pit. Part of the runoff water reaches the bottom and shapes the chemical composition of the open pit water. The runoff end-

member was calculated from the arithmetic mean of samples collected from deep sampling points of the drainage system. It should be noted that the open pit water's chemistry is affected by weathering products of massive sulfide ore deposits serving as a new source of solutes (LEACH). These chemical changes are characterized by an increase in SO_4 and metal concentrations. This effect is observable in the Piper diagram where a new source of SO_4 masks effects of the Cenozoic end-member (CN) in the open pit water composition (Figure 5.6). Therefore, to prevent effects of the new source of solutes, our MIX calculation did not incorporate the new components (sulfate and metals).

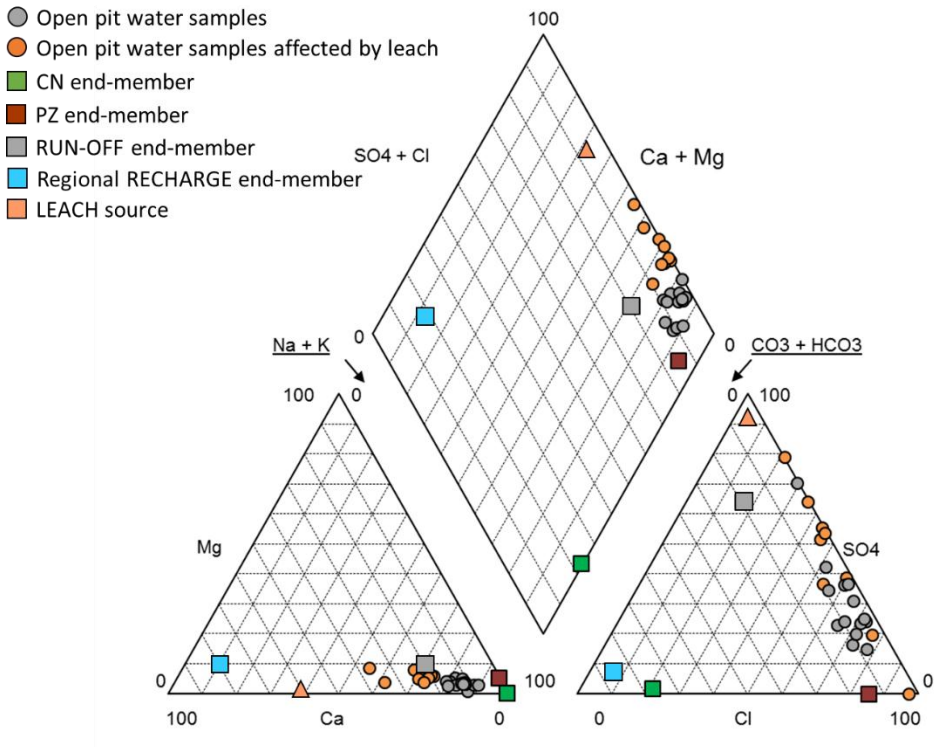

Figure 5.6. Piper diagram of open pit water samples and the identified end-members.

As was done for the regional mixing calculation, the first step of the EMMA calculation involved determining the number of end-members needed to explain the maximum percentage of variability in the samples. Based on the conceptual model, 9 species characteristics of each end-member were used for the EMMA analysis: TIC, Cl, SC, Na, NH_4,

F, B, NO_3 and Mg (Figure 5.7). According to the EMMA analyses, three end-members were needed to explain 84% of the mixture compositions. The first eigenvector contributes 44% of the total variance and components making the strongest contributions are Na, Cl and SC. The second eigenvector explains 26% of the variance (HCO_3, NH_4 and F). Finally, the third eigenvector contributes the remaining 14% where NO_3 and Mg are the species that contribute most.

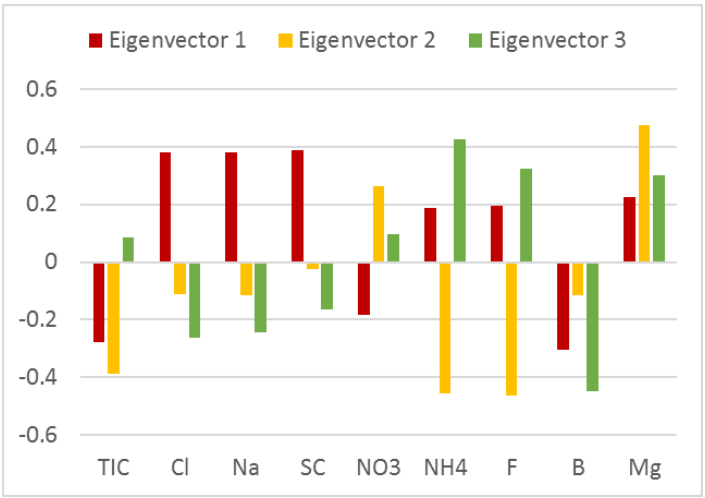

Figure 5.7. Local eigenvectors 1, 2 and 3 resulting from EMMA analysis.

Conservative species are those that facilitate calculation mixing ratios such as Cl, Na and SC but that also consider other species which, for residence times in the system, can be considered to exhibit conservative behaviour and to be representative or exclusive of some end-members. Precipitation and calcite dissolution processes can affect bicarbonate, but the analysed water samples have compositions of close to equilibrium with calcite (saturation index of between 0.09 and 0.35).

The NH_4 species behaves as a conservative element, as its oxidation involves a slow process mediated by microorganisms (Archaea). In addition to oxygen supplies, these microorganisms require a solid substrate for their development. It is for this reason that the nitrification process described in the literature refers in all cases to the unsaturated zone of

the soil (Leininger et al., 2006 and Parkhold et al., 2000). Then, as a result of this mechanism, oxidation is rapid in an unsaturated zone while the oxidation of NH_4 in the free water table occurs slowly. Another process that may affect NH_4 is volatilization. However, this process requires the previous step to NH_3, which only occurs under pH levels of above 9 (Parkhurst and Appelo, 1999). These pH values are much higher than those measured in the open pit water. Another process that can affect concentrations of NH_4 is exchanges with other cations present in clays. This process requires the interaction of water with clay minerals that can form in water retained by the same but very rarely in water that runs through a superficial course. For these reasons, NH_4 is considered to behave as a conservative element.

With respect to NO_3, NO_3 decline (denitrification) is also mediated by microorganisms (bacteria). The process requires that abundant organic matter volumes are available as well as the presence of an anoxic environment and solid support for bacterial biofilm (Rivetta et al., 2008). These conditions could occur in the open pit water if no water renewal processes were occurring and if dissolved organic matter was available. No accumulated organic matter was observed in the open pit water and concentrations of dissolved organic matter do not exceed a value of 1 mg/L. No other processes considered could affect concentrations of NO_3, and thus concentrations of this solute are presumed conservative. F- levels are also considered to be conservative as the water is clearly subsaturated in Fluorite, which is not found in the lithology of the open pit.

Table 5.3 shows the input and output chemical compositions of end-members used for the MIX local calculations and standard deviation applied.

INPUT END-MEMBERS COMPOSITION									
STANDARD DEVIATION (%)	25	10	10	10	20	15	15	15	20
END-MEMBER	**TIC**	**Cl**	**Na**	**SC**	**NO_3**	**NH_4**	**F**	**B**	**Mg**
CN	350	1479	1161	5837	0.1	8.0	4.4	2.2	23
PZ	382	93	234	1460	0.1	2.7	2.9	0.7	0.1
RUN-OFF	49	134	347	2280	48	0.6	0.7	0.4	37
OUTPUT END-MEMBERS COMPOSITION									
CN	333	93	234	1459	0.1	2.6	1.3	0.8	0.1
PZ	334	1482	1173	5783	0.1	7.9	4.8	2.3	32
RUN-OFF	52	133	355	3027	44	0.6	0.7	0.4	45

Table 5.3. Input and output chemical composition of the end-members selected for the open pit mix calculation and standard deviation applied. Units expressed in $mg \cdot L^{-1}$ and $\mu S \cdot cm^{-1}$.

MIXING RATIOS CALCULATION OF THE OPEN PIT MODEL

Figure 5.8 shows the measured and calculated values obtained from the local MIX model. Species such as Cl, Na, SC, NO_3, NH_4, F, B and Mg have a 1:1 relationship, showing that their content depends on mixing processes. However, for species such as TIC, measured values are lower than computed values due to chemical processes that occur in the open pit. However, this component is characteristic of the Cenozoic and Paleozoic end-members and can be used to differentiate runoff end-members. This is related to pH variations occurring in the open pit water. In some months, the pH oscillated between 3.30 and 6.5. Within this pH range, the main species of dissolved inorganic carbon is CO_2 (aq), which is easily transferred to the atmosphere, thus decreasing concentrations of HCO_3 dissolved. To take advantage of these HCO_3 values, we increased the standard deviation for these months. On the other hand, pH values of the open pit water ranged from 7.4 to 8.9 for the remaining months, and the most prominent carbonated species is HCO_3, which is stable in solutions and which was calculated as conservative. Therefore, we assume that such reactions occur very slowly.

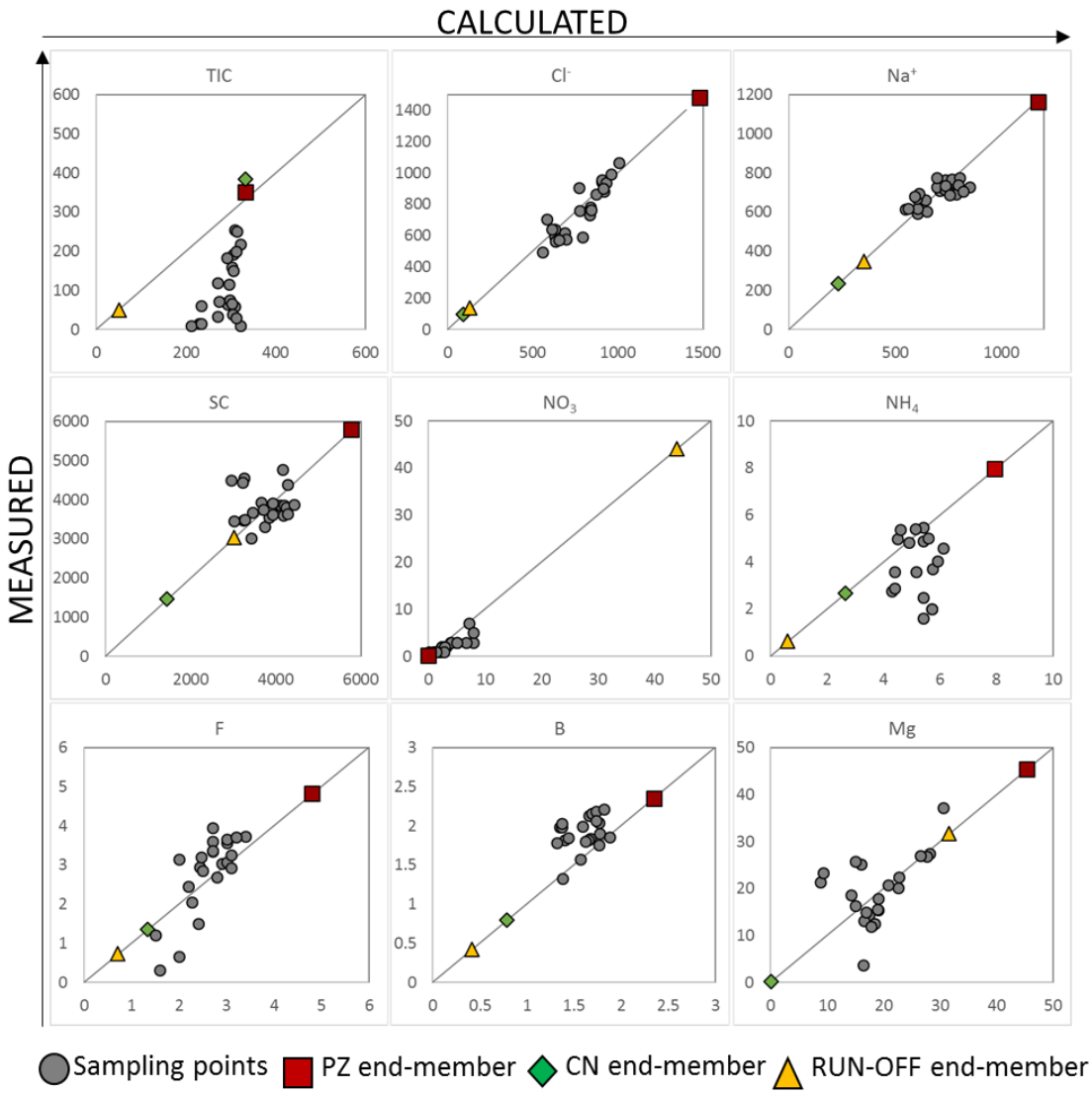

Figure 5.8. Measured concentrations versus calculated concentrations of the local model.

Mixing ratios obtained for each hydrologic year are represented in Figure 5.9. Note how contributions of the Paleozoic increase over the time period. This may be related to a deepening of excavations and to stronger contributions from Paleozoic aquifer water. The fraction of runoff water reaching the open pit bottom has decreased considerably due to a

slight decrease in annual rainfall levels and due to stronger drainage system operations that intercept runoff and that lead this water out of the open pit.

Table 5.4 shows the monthly evolution of mixing proportions obtained from the mixing calculation for each hydrological year.

	HYDROLOGICAL YEAR 2014-15			HYDROLOGICAL YEAR 2015-16		
MONTH	**PZ**	**CN**	**RUNOFF**	**PZ**	**CN**	**RUNOFF**
sep	40	29	31	60	35	5
oct	37	22	41	54	41	5
nov	41	30	29	37	53	10
dec	28	47	25	57	35	8
jan	36	33	31	59	34	7
feb	43	57	0	50	46	4
mar	32	41	27	61	33	6
apr	47	36	17	54	40	6
may	41	59	0	54	30	16
jun	49	51	0	60	30	10
jul	56	44	0	67	31	2
aug	59	41	0	64	34	3

Table 5.4. Monthly evolution of mixing proportions (%) for each hydrological year.

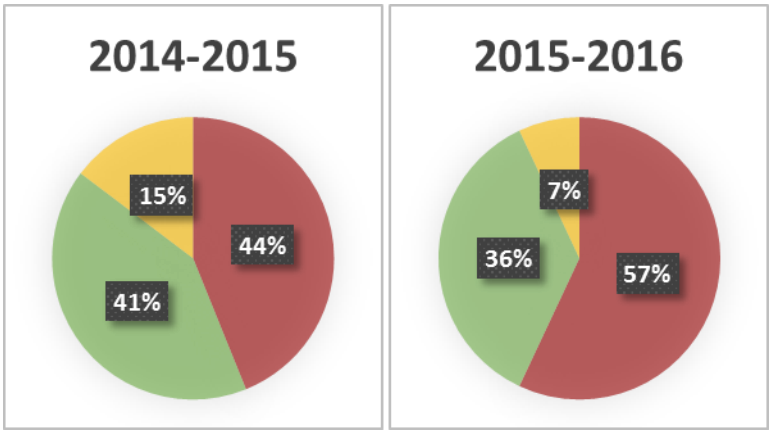

Figure 5.9. Mixing ratios calculated for the hydrological years 2014-2015 and 2015-2016.

RUNOFF END-MEMBER. MASS BALANCE

To carry out the mass balance described above, the following information is needed:

(1) Daily rainfall information. These data were obtained from the meteorological station operating within the mine and were compared with data recorded at other meteorological stations in the village of Guillena.
(2) The CW and NCW areas were calculated from an open pit map provided for CLC.
(3) Runoff and not CW volume. This was calculated from water intercepted by the drainage system installed in the open pit.
(4) Monthly water volumes that accumulate within the open pit.

We thus acquired information independent of runoff values in the open pit and compared them with values obtained from the MIX calculation (Table 5.5). Runoff values (% and m^3) obtained from the water balance are similar to values obtained from the MIX calculation.

The monthly water balance of the open pit can be found in appendix C.

Hydrologic year	VOLUME OPEN PIT WATER (m^3)	RUNOFF MIX (%)	VOLUME RUNOFF MIX (m^3)	RUNOFF CURVE METHOD (%)	VOLUME RUNOFF CURVE METHOD (m^3)
2014-2015	1239120	15	185868	16	199292
2015-2016	1569033	7	105560	8	126417

Table 5.5. Runoff data both in % and volume obtained from the water balance and the MIX calculation.

ERROR ESTIMATION

The error introduced in MIX for each component and analysed sample integrates the precision and accuracy of the analysis instruments.

The analytical error was estimated at ± 5% of the concentration measured for cations and at SC, ± 10% for anions and traces. For specific cases indicating that species used in the

calculations are not conservative (i.e., HCO_3 for months with pH <6), an increment of uncertainty was assigned to remove their weights from the calculations. Due to the impossibility of estimating initial uncertainty values for each component at each end and of transferring this uncertainty through all mathematical operations performed by MIX, an estimate based on bootstrapping was used (Efron, B., 1979). This technique is frequently used in statistics to approximate the variance or confidence interval of a statistical analysis when closed analytic expressions cannot be obtained. In turn, a large number of calculation results are obtained by varying initial conditions and by extracting the variance of the result set. In our case, 1,000 iterations of the MIX were performed so that initial values of these extremes were varied within the range defined by the deviation applied for each extreme water sample and species. The errors obtained ranged from ±2 to ±6 for the Paleozoic end-member, from ±3 to ±4 for the Cenozoic end-member and at ±2 for the runoff end-member.

5.4. CONCLUSION

We used multivariate statistical methods to evaluate the mixing ratios of water that forms open pit water. The MIX code is a valuable tool used to perform such calculations.

We apply this method to an open pit copper mine in southern Spain at the regional and local scales.

The regional mixing model must be used to estimate the compositions of PZ and CN end-members used for mixing calculations at the open pit scale.

Open pit mixing calculations were performed for 3 end-members: Paleozoic (PZ), Cenozoic (CN) and runoff with 9 components (TIC, Cl, SC, Na NH_4, F, B, NO_3 and Mg). Not including components such as SO_4^{-2}, Cu, and Zn in the calculation curtailed effects of a new source of solutes resulting from the open pit water leaching of weathering products from massive sulfide ore reserves.

As a result, we show that open pit mixing ratios for each end-member have evolved from 15 to 7% for the runoff end-member, from 36% to 41% for the Cenozoic end-member and from 44 to 57% for the Paleozoic end-member. Using an open pit water balance, we independently obtained information on term runoff. Runoff calculated from the water balance represents 16% (2014-2015) and 8% (2015-2016), a percentage similar to that calculated by the MIX calculations.

The proposed methodology serves as a useful tool for groundwater management in sites where the contributions of each water input that forms a mix must be determined and particularly for mining operations.

CHAPTER 5

CHAPTER 6. GROUNDWATER-GOSSAN INTERACTION AND THE GENESIS OF THE SECONDARY SIDERITE ROCK AT LAS CRUCES ORE DEPOSIT (SW SPAIN)

6.1. INTRODUCTION

The weathering profile developed in Volcanogenic-Hosted Massive Sulfide (VHMS) has been extensively studied worldwide in terms of its composition, structure and genesis (Crawford et al., 1992; Doyle and Allen, 2003; Galley et al., 2007; Large, 1992). The formation and characteristics of this profile depend on such factors as rock host type, climate, relief, sulfide assemblage, groundwater level, pH, and Eh. However, a common weathering profile can be defined in three differentiated zones: primary, cementation and oxidation zones (Nickel, 1984; Scott et al., 2001b; Thornber and Wildman, 1984). The upper part of the oxidation

zone could constitute what is known as “gossan”. The gossan is mainly composed of oxides and oxyhydroxides of Fe as goethite and hematite with jarosite in minor proportions. This typical gossan mineralogy is found in most worldwide deposits, for example in the Australian Woodlawn and Currawong mine (Scott et al., 2001a), in deposits from the Spanish-Portuguese Iberian Pyritic Belt (IPB) (Almodóvar et al., 1997; Kosakevitch et al., 1993; De Oliveira et al., 2011; Velasco et al., 2013; Viñals et al., 1995), or in the Flambeau mine in the U.S. (Ross, 1997).

The IPB, with over 1,600 million tonnes of massive sulfides, is one of the most important metallogenic provinces in the world. The IPB is a metallogenic province 250 km long and 30-50 km wide, extending from south of Lisbon (Portugal) to Seville (Spain) (Figure 2.1). It contains half of the worldwide giant volcanogenic massive sulfide deposits and more than 100 mines, most of them inactive, and it represents 22% of worldwide VHMS deposits (Tornos, 2006). The IPB has been extensively studied based on genesis, structure, mineralogy, and petrology (Leistel et al., 1997; Marcoux, 1997; Sáez et al., 1996; Strauss and Madel, 1974; Tornos et al., 2000). Most gossans of the IPB are in the present-day surface except for those of Las Cruces in SW Spain and the Lagoa Salgada in Portugal, which are covered by Cenozoic sediments. The Las Cruces cementation zone is exceptionally rich in copper, with 6.2% Cu grade and initial reserves of 17.6 Mt (Yesares et al., 2014a). Moreover, the deposit has important resources of 2 Mt of gossan with 4.5% lead, 5% g/t gold and 115 g/t silver in the supergene profile (Yesares et al., 2014a). Part of the Las Cruces secondary deposit has also sparked an interest in the scientific community because of the uniqueness of its mineralogical composition (Blake, 2008; Capitán Suárez, 2006; Knight, 2000; Miguélez et al., 2011; Miguelez et al., 2011; Moreno C., 2003; Tornos et al., 2014; Yesares et al., 2014a). The mineralogy mainly consists of siderite with galena, calcite, goethite, *hema*tite and precious metals. A comparable case has only been reported in the South Urals (Belogub et al., 2003). The genesis of this mineralogy is the subject of controversy and several hypotheses have been proposed. Knight (2000) considered that the secondary enrichment was multi-genetic and related to events ranging from alteration by a seawater hydrothermal

system during primary deposition (Carboniferous) to post-Tertiary weathering. Blake (2008) proposed that fluctuating oxidizing and reducing conditions, coupled with biogenic processes in groundwater, provided a suitable mechanism for the formation of the secondary deposit composition. Tornos et al. (2017) suggested that anaerobic microbial activity was responsible for the uncommon mineralogy of the Las Cruces secondary deposit and proposed that siderite, galena and iron sulfides in red/black rocks were formed in a natural bioreactor where microbial sulfate reduction was coupled to methane oxidation. These post-Miocene processes occurred below a thick impermeable marl unit from Cenozoic deposits in the Guadalquivir river basin. Conversely, Capitán Suárez (2006) proposed for the Las Cruces gossan an evolution controlled by the Miocene transgressive–regressive episodes that affected the area. Yesares et al. (2014) proposed that the formation of the secondary deposit was related to the circulation of surficial waters flowing downwards through the Cenozoic sediments.

The main objective of this chapter is to quantitatively discuss the feasibility of a genetic model of the Las Cruces siderite rock resulting from the interaction of a previous gossan with groundwater whose composition was similar to that of present day groundwater. To reach this objective, we 1) characterized the hydrochemistry and isotopes of present day groundwater, 2) quantified the groundwater flow rate through the gossan by performing a hydrogeological numerical model, and 3) quantified the biogeochemical interaction of groundwater flow through the gossan rocks by reactive transport numerical modelling.

6.2. SITE DESCRIPTION

ORE DEPOSIT DESCRIPTION

The Las Cruces ore deposit is a sulfide massive body enclosed in Paleozoic rocks. The deposit was exhumed in Miocene time, and the Paleozoic rocks and the massive sulfides were weathered under subaerial conditions. Consequently, a supergene profile was developed in the upper part of the sulfide massive composed of the primary mineralization area and

secondary mineralization area (Figure 6.1). The primary area of the Las Cruces deposit is composed of unaltered sulfides and integrates a sulfide massive body and stockwork mineralization. The main minerals in the massive body are pyrite, chalcopyrite, sphalerite and galena, whereas the stockwork is composed of pyrite and chalcopyrite, similar to other sulfide massive deposits in the IPB (García de Miguel, 1990; Marcoux et al., 1996). The secondary mineralization area consists of cementation and oxidation zones. The cementation zone is enriched in chalcocite. Tornos et al. (2017) differentiated 2 zones in the secondary deposit: (1) a basal "Black rock" mainly composed of iron sulfides, galena, calcite and quartz and (2) a "Red rock" mostly composed of siderite, galena and residual goethite, which constitutes most of the volume. Mineralogical details and textural features are described in Yesares et al. (2015), who described textures of replacement of Fe-oxyhydroxides by siderite and sulfides. The oxidation zone has a peculiarity in its composition where the original gossan (upper part of the oxidation zone) composed of goethite and haematite has been replaced by siderite, galena and iron metastable sulfides such as greigite and smythite (Tornos et al., 2014). Note that part of the CLC deposit has a heterogeneous structure with siderite-rich rocks, galena-rich rocks and siderite and galena rich rocks. Some isotopic studies have reported data about the Las Cruces ore deposit and have helped to improve our understanding of the formation of this deposit. For example, $\delta^{13}C$ values of the siderite were provided by Capitán Suárez (2006) and Tornos et al. (2014) and ranged from -47.9 to -13.4‰ and -41.7 to -17.6‰, respectively. Capitán Suárez (2006) interpreted these values as linked to biomass and concluded that the low values indicated a soil-related origin. However, Tornos et al. (2014) proposed that these values can only be derived by biologically mediated methanotrophy or anaerobic oxidation of methane (AOM) or of low molecular weight organic compounds. Moreover, Knight (2000) and Tornos et al. (2014) presented $\delta^{34}S$ values for both primary and secondary mineralization, which will be discussed below.

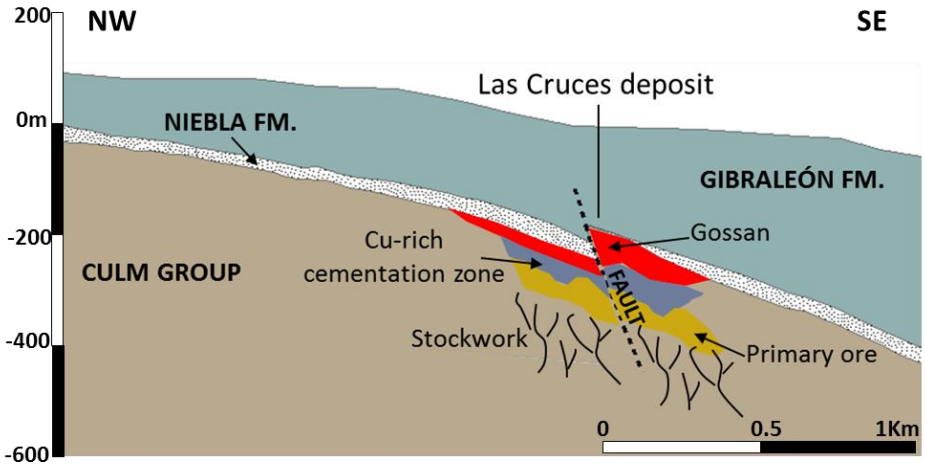

Figure 6.1. Scheme of supergene weathering profile in VMHS of Las Cruces deposit and Cenozoic cover.

AQUEOUS PHASE CHARACTERIZATION

The conglomerate and sand strata of the Niebla formation, together with a narrow layer of weathered Paleozoic basement, constitutes an aquifer. The upper part of fractured Paleozoic basement also constitutes a zone of moderate permeability. These aquifers outcrop to the north of the study area and constitute the recharge zone. The Niebla Fm. dips southward and is confined by the overlying marls of the Gibraleon Fm. that reach a thickness of hundreds of metres (Figure 2.1). Five zones can be differentiated based on their transmissivity values: (1) the zone that corresponds to the marls of the Gibraleon Fm.; (2) the sands and conglomerates of the Niebla formation; (3) the weathered part of the upper Paleozoic formation; (4) the Paleozoic rocks; and (5) the faults (Figure 2.2A). The approximately 10 to 30m thick Niebla Fm. has transmissivity values that range between 10 and 500 m^2/d and its storage coefficient values are on the order of 10^{-2} within the unconfined zone and between 10^{-3} and 10^{-5} in the confined areas (CHG, 2012), and it is sealed near the recharge zone by the low transmissivity (<5 m^2/d) marls of the Gibraleon Fm. (CHG, 2012). No previous values have been measured for the Paleozoic, the weathered Paleozoic and the main faults. Following the groundwater head inventory and prior to mine operations,

groundwater regional flow was mostly from the northwest to the southeast (Figure 2.2B). There was an abnormal change of gradient in the area around the mine site attributed to an elevation of the basement paleorelief where the Niebla Fm. disappears and the marl layer rests directly on the Paleozoic (Figure 2.2A and B). The main recharge of the aquifer is by rainwater infiltration in the outcropping zone (NW). The groundwater residence time, estimated from ^{3}H, ^{14}C and ^{36}Cl analyses, confirms the existence of some recharge of the Niebla aquifer from the underlying Paleozoic. A residence time up to 30,000 years was obtained for the groundwater close to the Las Cruces deposit (Scheiber et al., 2015). The total estimated annual recharge is 32 hm^3 (25 mm/y) for an area of 1,300 km^2. The discharge is 34 hm^3/y and corresponds to agricultural and consumption extraction (CHG, 2012; Navarro et al., 1993). Note that the Niebla aquifer was artesian south of the outcropping area prior to mining and agricultural extraction (IGME, 1984). Another important fact is the role of the main fault system as a possible discharge zone. Several data items, such as high groundwater temperatures (up to 37.5 °C) detected in areas near faults, confirm the presence of upward flows along these faults.

HYDROCHEMICAL SETTING

The groundwater chemistry was detailed by Scheiber et al. (2016) and is summarized as follows. Groundwater shows an evolution along flow lines from the NW to SE direction (Figure 2.2). Groundwater initially is of the Ca-HCO_3^- type then switches to the Na-HCO_3^- and Na-Cl types downstream near the recharge zone. An excess in Na concentrations with respect to seawater ratios is observed towards deeper portions of the aquifer related to a Na-Ca exchange process that occurs within dispersed clay layers in the NP aquifer. There is also an increase in pH and specific conductivity (SC) and a decrease of Eh values downstream. Near the Las Cruces ore, the groundwater has basic pH values up to 10.6 (Figure 6.2A), and the SC reaches values from 1,000 up to 5,940 $\mu S \cdot cm^{-1}$. Dissolved Organic Carbon (DOC) concentration ranges from 2.86 up to 15.9 $mg \cdot L^{-1}$ in the deepest area (Figure 6.2B). These values are above the typical values in groundwater of <1 $mg \cdot L^{-1}$ (Kalbitz et al., 2000). Complete analyses can be found in appendix B. The negative Eh values (Figure 6.2A),

together with the decreasing sulfate concentration and the presence of H_2S, suggest that this is an environment with reducing conditions. Values of $\delta^{34}S$ and $\delta^{18}O$ of the sulfate molecule range between -17.2 to 20.4‰ (CDT) and 1.9 to 18.1‰ (V-SMOW), respectively, for samples near the mining site. Thode and Monster (1970) proved that sulfur and sulfides that originated by biological sulfate reduction are characterized by heavier isotopic values, with slopes between 0.22 and 0.28 in a plot of $\delta^{18}O$ *vs.* $\delta^{34}S$. This tendency towards higher $\delta^{18}O$ and $\delta^{34}S$ values and the clear depletion of sulfate concentration is consistent with sulfate reduction shown in Figure 6.3. Moreover, high ammonium (up to 12.8 $mg{\cdot}L^{-1}$), boron (up to 3.48 $mg{\cdot}L^{-1}$) and iodide (up to 0.67 $mg{\cdot}L^{-1}$) concentrations are found in parts of the deep Niebla and Paleozoic aquifers (Figure 6.2C) and increase towards the deepest areas close to the ore body. The high NH_4, B and I concentrations have been attributed to the anoxic decomposition of marine organic matter (Whitehead, 1974; Goldberg et al., 1993; Scheiber et al., 2016). Moreover, the $\delta^{13}C$ values of dissolved inorganic carbon (DIC) are approximately -10‰ near the ore. All these facts indicate that the organic matter occurs along a groundwater flow path. From the groundwater characteristics described above, we can postulate that the current groundwater can induce the replacement of goethite at the expense of DOC (represented as CH_2O). The reaction increases the pH and releases Fe^{2+} and HCO_3^-, which promotes siderite precipitation and results in a replacement of goethite by siderite by the following reaction:

$$CH_2O + 4\,FeOOH + 7\,H^+ \rightarrow 4\,Fe^{2+} + HCO_3^- + 6H_2O \qquad \text{(E11)}$$

Arsenic concentration, present as As(III), ranges from below the limit detection to 0.18 mg/L and has also been found locally in some wells from the deepest Niebla aquifer. The presence of As(III) also suggests the dissolution of the As-bearing goethite in a reducing environment. The low amount of Fe (< 10 ppb) detected in groundwater can result from siderite precipitation. Indeed, thermodynamic calculations performed with PHREEQC software and the Wateq4 database (Parkhurst and Appelo, 2013) indicate that groundwater close to the ore body is supersaturated and very close to equilibrium with respect to siderite (Figure 6.2D).

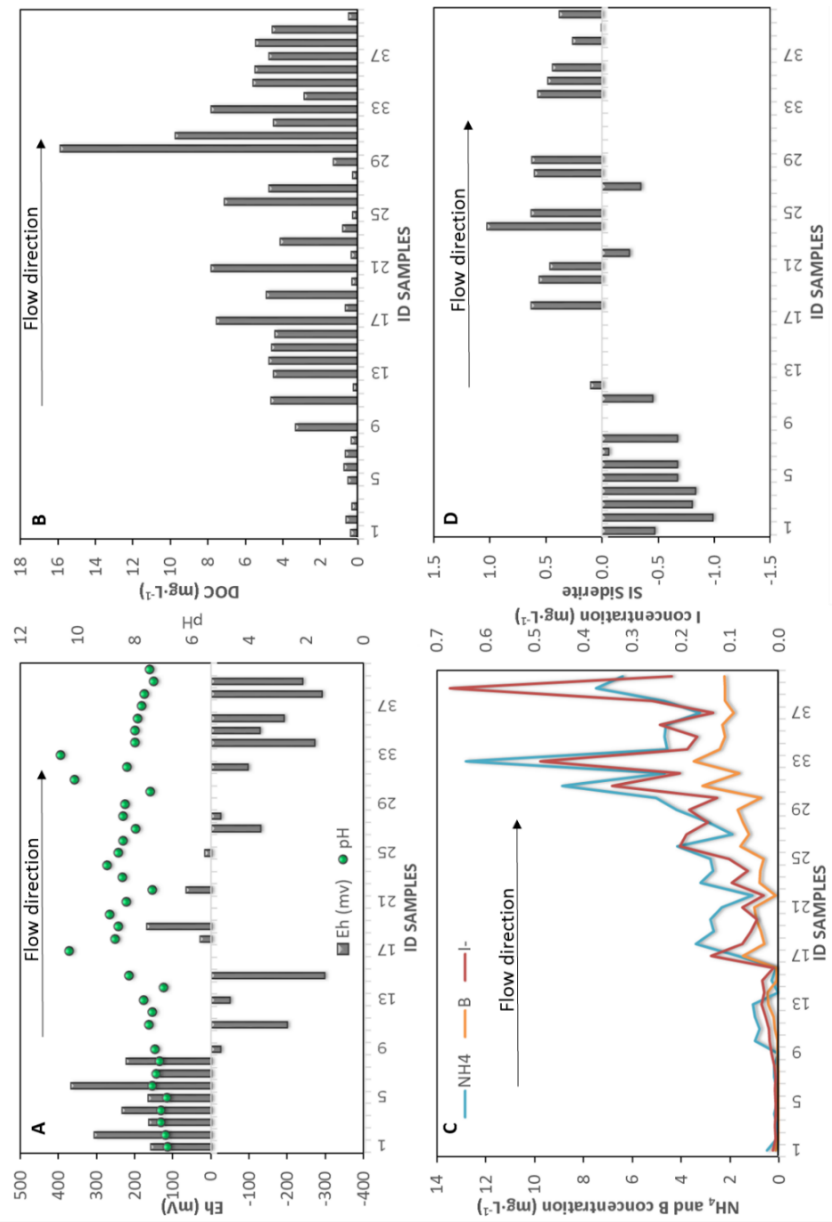

Figure 6.2. (A) Eh and pH values of groundwater; (B) Dissolved Organic Carbon concentration of groundwater; (C) NH_4, B and I concentration and (D) Saturation index of siderite. The location of the samples is shown in Figure 2.2B.

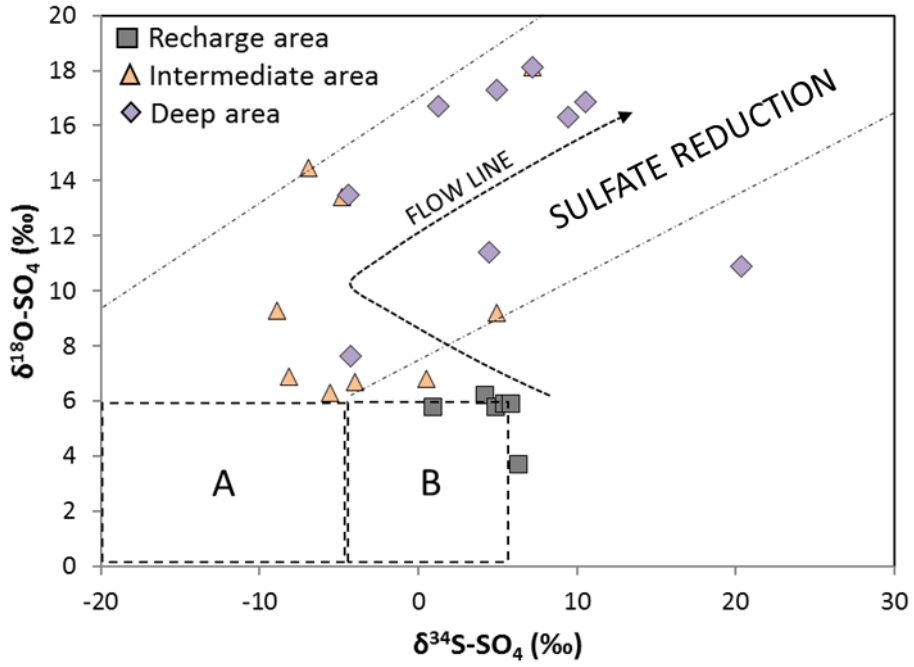

Figure 6.3. Representation of the isotopic content of sulfates in groundwater. Legend: (A) Sulfate derived from sedimentary rock, (B) Sulfate derived from magmatic sulfide. Figure modified from Scheiber et al. (2015)

SOLID PHASE CHARACTERIZATION

Another aspect to consider is that groundwater transports a very low content of Pb (< 1 ppb) and thus an additional source of the element to form galena is assumed to be present in the initial gossan. Minerals from the jarosite family rich in lead, such as plumbojarosite or beudantite, have very often been described as the mineral limiting the low Pb concentrations of massive sulfide oxidation sites, particularly in the Iberian Pyrite Belt (Figueiredo and Pereira da Silva, 2011; Nieto et al., 2003). However, these minerals have not been identified in the oxides remaining in the Las Cruces siderite rock.

To determine the origin of Pb, three samples rich in goethite were analysed by Electron microprobe (EPMA). Pb, As, Cu, Fe, S and Sb in goethite were quantified (Figure 6.4 and Figure 6.5). The complete analyses are found in appendix B.

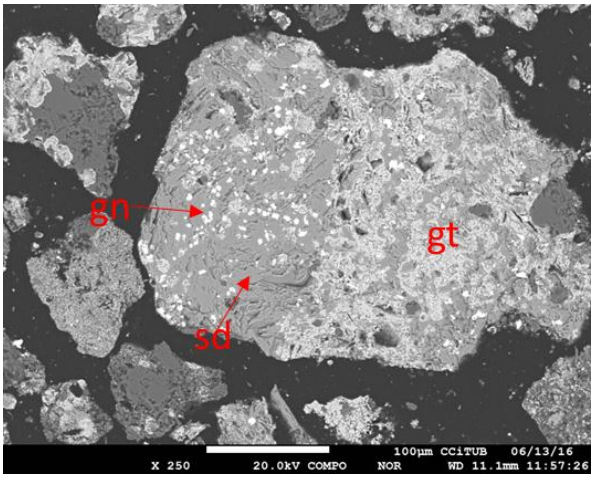

Figure 6.4. Electron microprobe images of secondary deposit fragments. Goethite (gt) replaced by siderite (sd) and galena (gn).

The EPMA analyses in goethite suggested that this mineral is the main source of Pb and Sb that subsequently formed galena and Pb-sulfosalts and for As found in groundwater in some wells from the deep zone.

GOETHITE	
No. Of data=53	**Average±Standard deviation**
As_2O_5	0.387 ± 0.15
Fe_2O_3	93.304 ± 1.27
PbO	0.946 ± 0.14
SO_3	0.364 ± 0.07
Sb_2O_5	0.209 ± 0.12

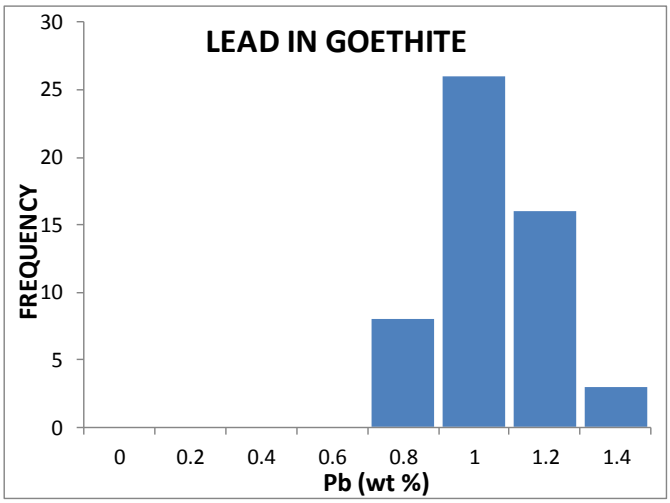

Figure 6.5. Results from electron microprobe analyses of goethite (N= 53) and frequency histogram of lead in goethite.

The presence of As, Pb and Sb in goethite has been extensively described. Fe-oxyhydroxides are characterized by a very high specific surface area of ±300 $m^2 \cdot g^{-1}$ and a high adsorption capacity capable of adsorbing large amounts of metals and metalloids (Davis and Leckie, 1978). Many studies related to As adsorption on goethite are available (Bowell, 1994; Dixit and Hering, 2003; Fendorf et al., 1997; Goldberg and Johnston, 2001). Lead adsorption on goethite has been investigated by Forbes et al. (1976), Hiemstra and Van Riemsdijk (1999), Coughlin and Stone (1995), and Bargar et al. (1997), among others. Several studies have also investigated the Sb adsorption mechanism on Fe-oxyhydroxides by laboratory experiments (Leuz et al., 2006; Tighe et al., 2005). No mineral phases other than goethite have been identified by X-ray diffraction; however, the atomic Pb/S ratio close to 1 (0.96) and the narrow dispersion of the Pb and S contents suggest that these elements could be present as nanoinclusions of a Pb:S 1:1 phase anglesite homogeneously distributed in goethite.

Additionally, sulfur isotope data provide valuable information about the environmental conditions of ore formation and the sources of sulfur. Our values fell between the range reported by Knight (2000) and Tornos et al. (2017) for galena from the Las Cruces deposit and were significantly higher than the values reported for other sulfides from the IPB (Table 6.1). The similarity between the $\delta^{34}S$ values of the secondary mineralization of the Las Cruces deposit and those of groundwater sulfate suggests that the current galena composition can be explained by groundwater and gossan interaction. Indeed, the sulfate reduction increased the $\delta^{34}S_{SO4}$ of groundwater along its transit through the aquifer. Therefore, the $\delta^{34}S_{SO4}$ values of groundwater from the deep zone close to the Las Cruces deposit were as high as 10‰ and up to 20‰ (Figure 6.3 and Table 6.1). Then, the complete reduction of SO_4 and the subsequent precipitation of galena would produce a solid with high $\delta^{34}S$ values. Therefore, the heavy $\delta^{34}S_{SO4}$ of galena suggests a high influence of the sulfur carried by groundwater.

ORE DEPOSIT	$\delta^{34}S$ MIN.	$\delta^{34}S$ MAX.	DATA SOURCE
Agua Teñidas	-5.6	+3.6	Velasco et al. (1998)
Aljustrel	-20.4	+4.0	
Aznalcollar	-6.0	+4.4	
Concepción	-1.4	+9.2	
Cueva de la Mora	+2.5	+7.1	
La Zarza	-7.3	+7.8	
Lousal	-8.3	+5.5	
Monte Romero	+3.3	+9.0	
Neves Corvo	-11.1	+6.0	
Rio Tinto	-14.1	+12.4	
San Miguel	-3.9	+9.2	
Sotiel	-34.2	+6.7	
Tharsis	-26.8	+3.5	
Aznalcollar	-6.0	+4.4	Almodóvar et al. (1997)
Tharsis	-10.7	+3.5	Kase et al. (1990)
Tharsis	-11.5	+0.0	Tornos et al. (1998)
Las Cruces secondary deposit	**+11.9**	**+25.9**	**Tornos et al. (2014)**
Las Cruces secondary deposit	**+3.5**	**+21.7**	**Knight (2000)**
Las Cruces secondary deposit	**+10.2**	**+13.5**	**This work.**

Table 6.1. Summary of sulfur isotope data of some massive sulfide deposits from the Iberian Pyrite Belt

6.3. QUANTITATIVE MODELING AND DISCUSSION

NUMERICAL FLOW MODEL

The main purpose of quantitative modelling was to apply a semi-quantitative approach to the flow that recently circulated through the original gossan. The flow rate value obtained was used to perform reactive transport modelling. To achieve this purpose, a 2D numerical flow model in steady conditions based on piezometric data prior to mining activity was applied. TRANSIN software (Medina and Carrera, 2003) was used for the modelling process using its graphical interface VISUAL TRANSIN (UPC (2003), http://h2ogeo.upc.edu/en/investigation-hydrogeology/software). The model corresponded to a NW-SE vertical section 25 km in length and 1.2 km thick. Based on the data described in the preceding sections, the following boundary conditions were imposed: (C1) prescribed the head at the SE boundary; (C2) prescribed the recharge in the Paleozoic outcrop (1.2 m^3y^-

[1], CHG (2012)) and (C3) in the Niebla formation outcrop (0.3 m^3y^{-1}, CHG (2012)); and (C4) prescribed mixed conditions that represent the artesian zone in the marl surface close to the recharge area (IGME, 1984). The model was discretized in the five transmissivity zones based on the geologic differences defined in section 2.2: the Gibraleón Fm. (T1), the Niebla Fm. (T2), the weathered Paleozoic (T3), Paleozoic schists and volcanics (T4) and faults (T5).

TRANSIN solves the flow equation by applying the finite element method and the inverse problem using automatic calibration. A finite element mesh of 4,752 nodes and 8,947 triangular elements was defined. The model calibration was performed by fitting the measured and calculated groundwater levels, the applied hydraulic parameters and their uncertainty range and the mass balance consistency. The transmissivity data from CHG (2012) and the piezometric levels from previous mining activity (Figure 2.2) were used in the calibration process. The starting and calibrated values of transmissivity and recharge are listed in Table 6.2.

ZONE	**DESCRIPTION**	**TRANSMISSIVITY m^2d^{-1}**	
		Reference	**Calibrate**
T1	Gibraleon Fm.	<5	0.2
T2	Niebla Fm.	10-500	20
T3	Weathered Paleozoic	-	3.5
T4	Paleozoic materials	-	0.04
T5	Faults	-	0.02
ZONE	**DESCRIPTION**	**RECHARGE m^3y^{-1}**	
R1	Paleozoic	1.2	
R2	Niebla Fm.	0.3	

Table 6.2. Calibrated transmissivity values of the five different materials used in the flow model. Initial reference values from CHG (2012). Recharge values used for the numerical flow model (CHG, 2012).

The correlation between computed and measured head is shown in Figure 6.6, which shows an average error lower or equal to 2.5 m. The adjustment was considered acceptable

because the highest errors corresponded to the areas most distant from the ore deposit. The mass balance expressed as an annual average value model is shown in Table 6.3. For a steady-state flow, inputs were equal to outputs.

ZONE	PRESCRIBED HEAD	PRESCRIBED FLOW	LEAKAGE
C1	-1.5	-	-
C2	-	1.2	-
C3	-	0.3	-
C4	-	-	-0.34E-05
FLOW MASS BALANCE ERROR			**0.12E-10**

Table 6.3. Mass balance obtained from the modelling process (m^3d^{-1}). Water inflow is expressed by positive values and negative values instead express water outflow.

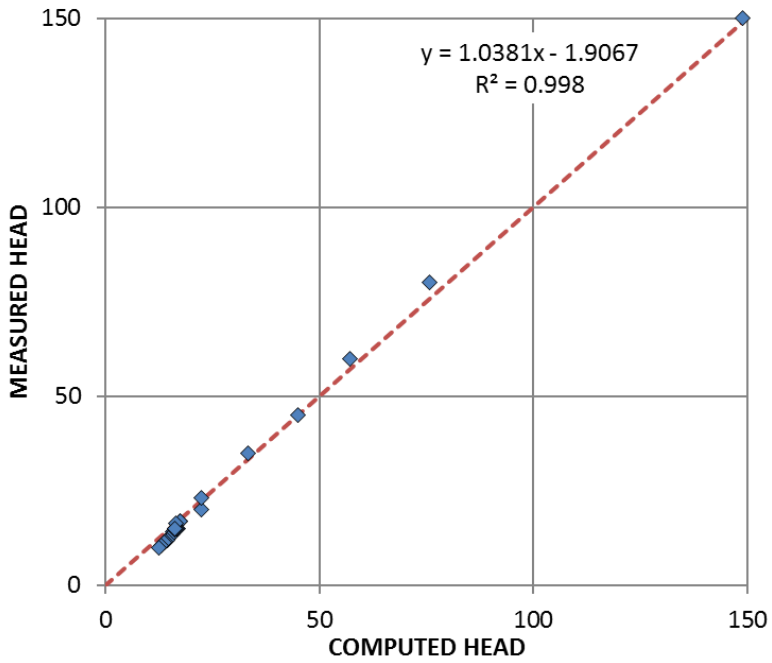

Figure 6.6. Correlation between computed and measured hydraulic heads obtained from the numerical flow model.

The piezometric map of the cross section from NW to SE was thus obtained from the model (Figure 6.7). As expected, the flow was from the recharge area to the southeast. There were areas where the flow in the Paleozoic rocks had an upward component; this behaviour was

mainly detected close to the principal faults where the flow was up to the faults and the groundwater from the discharged to the Niebla aquifer. The main output of the flow modelling was that the unitary flow that circulates upwards through the gossan was 1.35 $m^3m^{-2}y^{-1}$. This value was used in the reactive transport model.

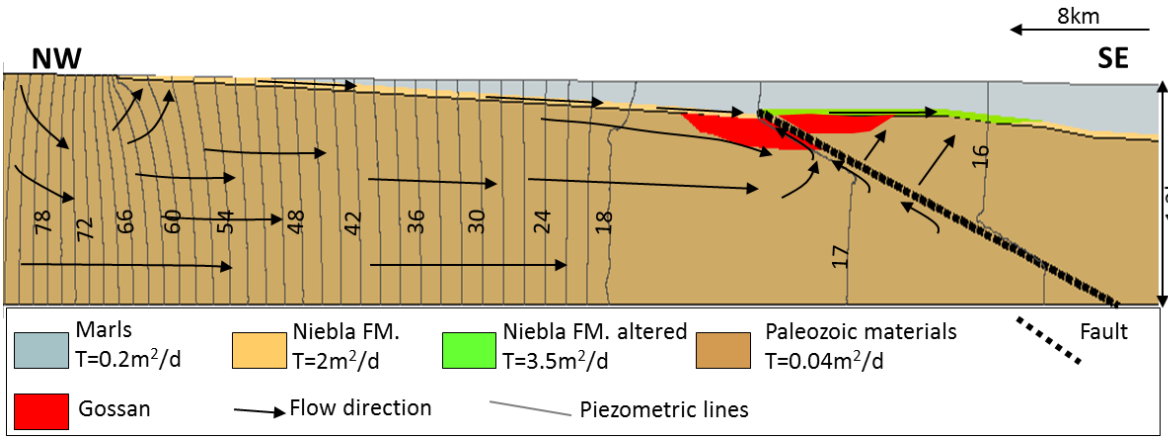

Figure 6.7. Cross section piezometric map of the study area as result of the numerical flow model results. The labels in the isopotential lines correspond to groundwater levels in masl (meters above sea level)

REACTIVE TRANSPORT MODEL

INITIAL AND BOUNDARY CONDITIONS

The main goal of this section is to evaluate the feasibility of the conceptual model proposed and to estimate the time required for the formation of the siderite rock. Groundwater-mineral interaction was modelled with the computer software RETRASO (Saaltink et al., 1998), which is based on a full coupling of the multicomponent solute transport equations with chemical reaction equations, either under equilibrium or kinetic laws.

A 1D reactive transport model representing a 10-m long flow line circulating from the base to the top of the gossan was considered. The entire domain was initially composed of goethite (0.7 volume fraction) and refractory silicates (0.01). We assumed that goethite

includes hematite because hematite is less reactive than goethite. A porosity of 0.3 has been estimated for the original gossan (Emmons and Laney, 1926; Kelly, 1958). Based on the analysis of goethite, Pb was included in the stoichiometric formula of goethite. However, for the sake of simplicity Sb and As were not included in the calculations. The upstream boundary condition was prescribed flow (1.35 $m^3 \cdot m^{-2} \cdot y^{-1}$) obtained from the groundwater flow model. The chemical composition of initial and inflow water (Table 6.4) corresponded to the groundwater composition upstream of the secondary deposit. The domain was discretized into 20 elements. Calculations were performed at 25°C, the temperature of present day groundwater in the wells near the deposit.

pH	Ca	DIC	Cl	Fe (II)	Na	S(II)	S(VI)	Pb	DOC
7.8	2.50E-05	6.41E-03	4.47E-02	8.98E-08*	4.63E-02	3.13E-06	1.31E-04	4.84E-09*	2.86E-04

Table 6.4. Chemical composition of groundwater from the deep aquifer used as initial and inflow water (mol·L^{-1}). *Detection Limit.

A total of eleven primary aqueous species, fifteen aqueous complexes and five minerals were selected to describe the geochemical model (Table 6.5). A summary of all the reactions and kinetic formulations used for the reactive transport model is found in Table 6.5. Aqueous species were selected from the most abundant species in previous aqueous speciation modelling. Thermodynamic data were those of the Wateq4f database included in the PHREEQC code (Parkhurst and Appelo, 2013). In addition to initial goethite, neoformed minerals were selected from among the most representative observed in the present-day secondary deposit mineralogy. Mackinawite was selected as a first step for greigite and smythite formation (Rickard, 2006). Minerals were assumed to precipitate in equilibrium.

PRIMARY AQUEOUS SPECIES	Ca^{+2}, HCO_3^-, H^+, Cl^-, Fe^{+2}, $Fe(OH)_3$, Na^+, HS^-, SO_4^{-2}, $PbCO_3$, CH_2O		
AQUEOUS COMPLEXES	$CaCO_3$, $NaCO_3^-$, $NaHCO_3$, $CaHCO_3^+$, CO_2, CO_3^{-2}, $FeCO_3$, $FeHCO_3^+$, $Fe(OH)_4^-$, Fe^{+3}, OH^-, H_2S, $NaSO_4^-$, $Pb(CO_3)_2^{-2}$, Pb^{+2}		
MINERALS	Goethite ($Fe_{0.996}Pb_{0.004}OOH$), Calcite, Galena, Siderite, Mackinawite		
REACTION	**FORMULATION**	**k**	
R_1: $Ca^{2+} + HCO_3^- \rightarrow CaCO_3 + H^+$	EQUILIBRIUM		
R_2: $2CH_2O + 4FeOOH + 7H^+ \rightarrow 4Fe^{2+} + HCO_3^- +$	$r_{OM\_FeOOH}=k_{OM\_FeOOH}\cdot([CH_2O]/k^*+[CH_2O])\cdot(\Omega-1)$	$1.38E^{-10}$	[1]
R_3: $Pb^{2+} + HS^- \rightarrow PbS\ (s) + H^+$	EQUILIBRIUM		
R_4: $Fe^{2+} + HCO_3^- \rightarrow FeCO_3 + H^+$	EQUILIBRIUM		
R_5: $2CH_2O + SO_4^{2-} \rightarrow HS^- + 2HCO_3^- + H^+$	$r_{OM\_SO4}=k_{OM\_SO4}\cdot[CH_2O]\cdot(SO^{2-}{}_4/k_{SO4}+ SO^{2-}{}_4)$	$3.17E^{-8}/1E^{-4}$	[2]
R_6: $1/8H_2S+FeOOH+1/4H^+ \rightarrow Fe^{2+}+1/8SO_4^{2-}$	$r_{H2S\text{-}FeOOH}= k_{H2S\text{-}FeOOH}\cdot[H_2S]$	$1E^{-5}$	[3]
R_7: $Fe^{2+} + HS^- \rightarrow FeS + H^+$	EQUILIBRIUM		

Table 6.5. Primary and secondary aqueous species, mineralogical composition and reactions used for the reactive transport model. [1] Liu et al. (2001); [2] Canavan et al. (2006) and [3] Torres et al. (2014).

Reactions involving organic matter were modelled based on experimental kinetic laws. The replacement of goethite by siderite at the expense of DOC has been investigated by several authors (Torrent et al.,1987; Schwertmann,1991; Liu et al.,2001; Zachara et al., 2001 and Crosby et al.,2007); however, only a few studies, for example Torrent et al. (1987) and Liu et al. (2001), contain the data necessary to obtain dissolution rates normalized to surface area and can be used in reactive transport modelling. Torrent et al. (1987) measured the goethite reductive dissolution in dithionite and obtained a dissolution rate of $4.6E^{-10}$ mol $m^{-2}\cdot s^{-1}$. Liu et al. (2001) performed a comprehensive study of goethite reduction in batch cultures of the groundwater bacterium Shewanella putrefaciens at neutral pH. To match the experimental values, they proposed a Monod-type expression where the rate depends on the FeOOH

surface and the concentration of lactate used as electron donors and on the thermodynamics of the solution with respect to goethite.

In the reactive transport model, the kinetic expression for goethite dissolution proposed by Liu et al. (2001) was used as follows:

$$R = k\sigma \frac{[DOC]}{k^* + [DOC]}(\Omega - 1) \quad \text{(E12)}$$

where R is the goethite dissolution rate (mol m^{-3} s^{-1}), k is the dissolution rate constant (mol m^{-2} s^{-1}), σ is the specific reactive surface area or the area of water-mineral contact (m^{-2} m^{-3}), k* is an experimental semi-reaction constant with value 0.52 mol m^{-3} proposed by Liu et al. (2001), and Ω is the saturation of the solution with respect to goethite (ion activity product divided by the equilibrium constant). A value of 1.38E^{-10} mol m^{-2}·s^{-1} was obtained for k from the initial dissolution experimental values (Ω<<1) of Liu et al. (2001). The σ parameter has a large uncertainty that depends on the flow structure. Therefore, a sensitivity analysis of the reactive transport results as a function of this parameter is discussed below. Similar kinetic expressions have also been used to describe the sulfate-reduction at DOC expense (Torres et al., 2014) and the reductive dissolution of goethite by H_2S (Canavan et al., 2006).

RESULTS

The results obtained from the reactive transport model show that the goethite replacement by siderite occurred at the expense of organic matter oxidation that decreased with distance from the inflow because of its consumption along the flow path (Figure 6.8 A and B). Because the rate depends on DOC concentration (equation E12), goethite replacement also vanished with distance. Goethite replacement also decreased with time because the reactive surface (σ in E12) shrank with the goethite mass. As observed in Figure 6.8, most of the siderite was replaced in 0.8 Ma. Goethite replacement released iron and lead to the groundwater. Galena and then mackinawite precipitated close to the inflow boundary because of its low solubility product. The FeS consumed most of the available Fe^{2+}, reducing the precipitation of siderite, which again increased in the second part of the system (Figure 6.8 C, D and E). In the basic

case, calcite did not precipitate in the calculations because of the low assumed concentration of Ca in the inflow groundwater. Porosity was slightly depleted with time in most of the system (Figure 6.8 F) because of the higher molar volume of siderite with respect to goethite and the precipitation of sulfides. However, porosity increased to almost 0.5 at the inflow boundary of the system because no mackinawite formed. A period of 1 Ma was necessary to replace 80% of the goethite initially assumed. By comparing the flow and goethite dissolution rates, the mass of sulfur carried by groundwater was up to two orders of magnitude higher than that released by goethite dissolution. This explains the heavier values of $\delta^{34}S_{SO4}$ measured in galena, close to the values of groundwater and far from those of massive sulfides in the IPB (Table 6.1).

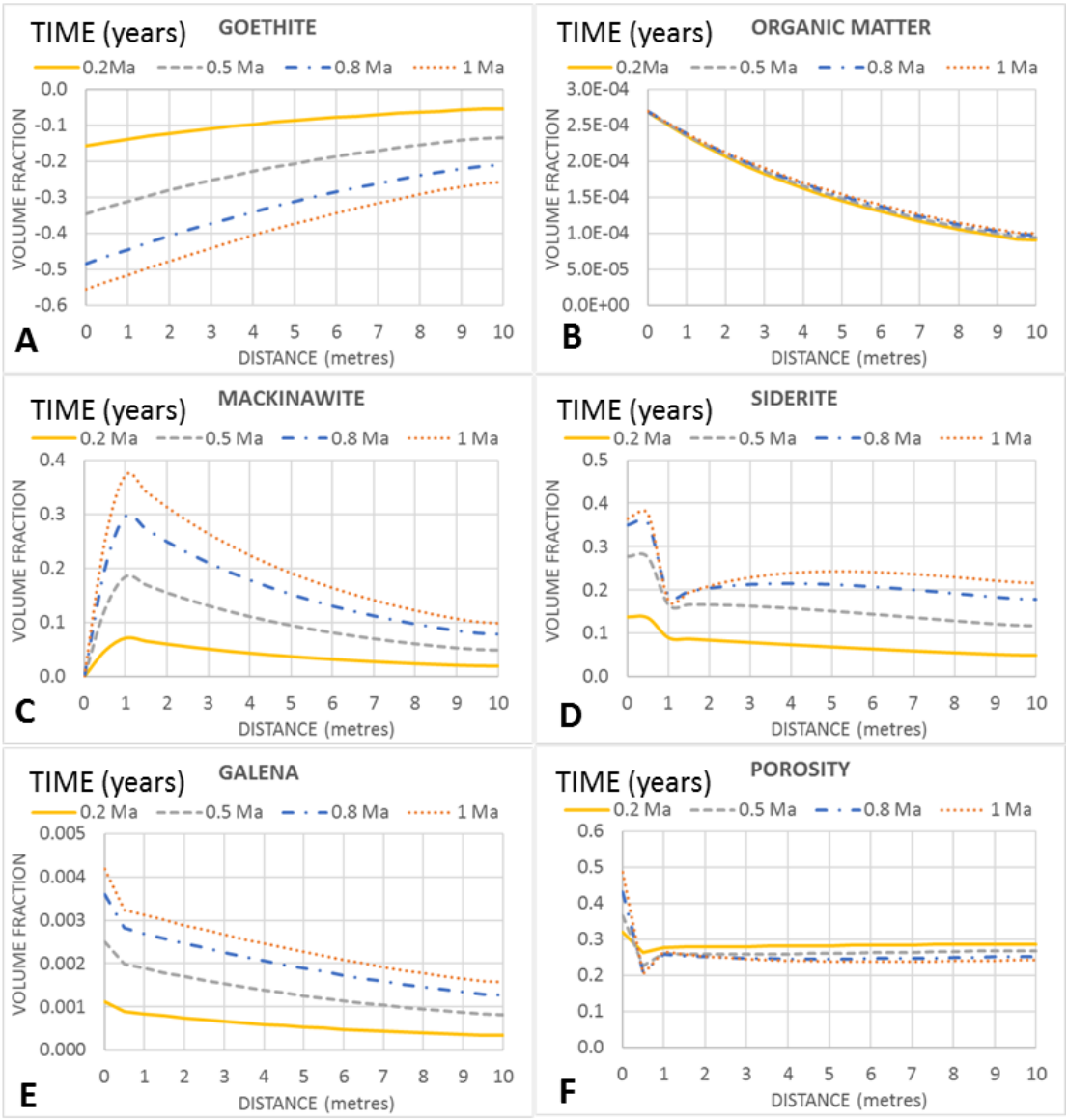

Figure 6.8. Results of the reactive transport base model.

SENSITIVITY ANALYSIS

Some of the parameters used in the described calculations (the base model) are not well known. Therefore, we investigated the impacts of changing the values of these parameters on the results. The reactive surface area, the groundwater flow rate and the DOC concentration in the inflow water had major impacts on the results and were selected for sensitivity analysis. Other parameters, such as the concentration of solutes other than DOC in the inflow water, led to a slight and expected modification of the results. The increase of Ca in the inflow water, within the range of the low concentrations measured in groundwater, thus led to precipitation of minor calcite at the expense of siderite (not represented).

The reactive surface area is the most uncertain parameter in reactive transport modelling because it depends on the structure of the flux (i.e., the wetted surface of the minerals). The value of 10 m^2 m^{-3} for rock used in the base case corresponded to a flow through fractures separated by 0.20 m. Two more cases were tested, with rock reactive surface areas of 1 m^2 m^{-3} (corresponding to a fracture every 2 m, fracture-controlled flux) and 50 m^2 m^{-3} (corresponding to fractures every 0.04 m, pervasive flux).The results are plotted in Figure 6.9. The decrease of the reactive surface area (σ=1) produced a dramatic decrease in the replacement of goethite. Consequently, the small amount of Fe^{2+} released was precipitated as mackinawite that inhibited the formation of siderite, in clear disagreement with observations. The increase of the reactive surface area (σ=50) enhanced the goethite replacement, and the high amounts of Fe^{2+}, Pb^{2+} and DIC allowed the precipitation of siderite and galena. Porosity was drastically depleted to below 0.1 at the end of the system, perhaps modifying the flow structure, as will be discussed below.

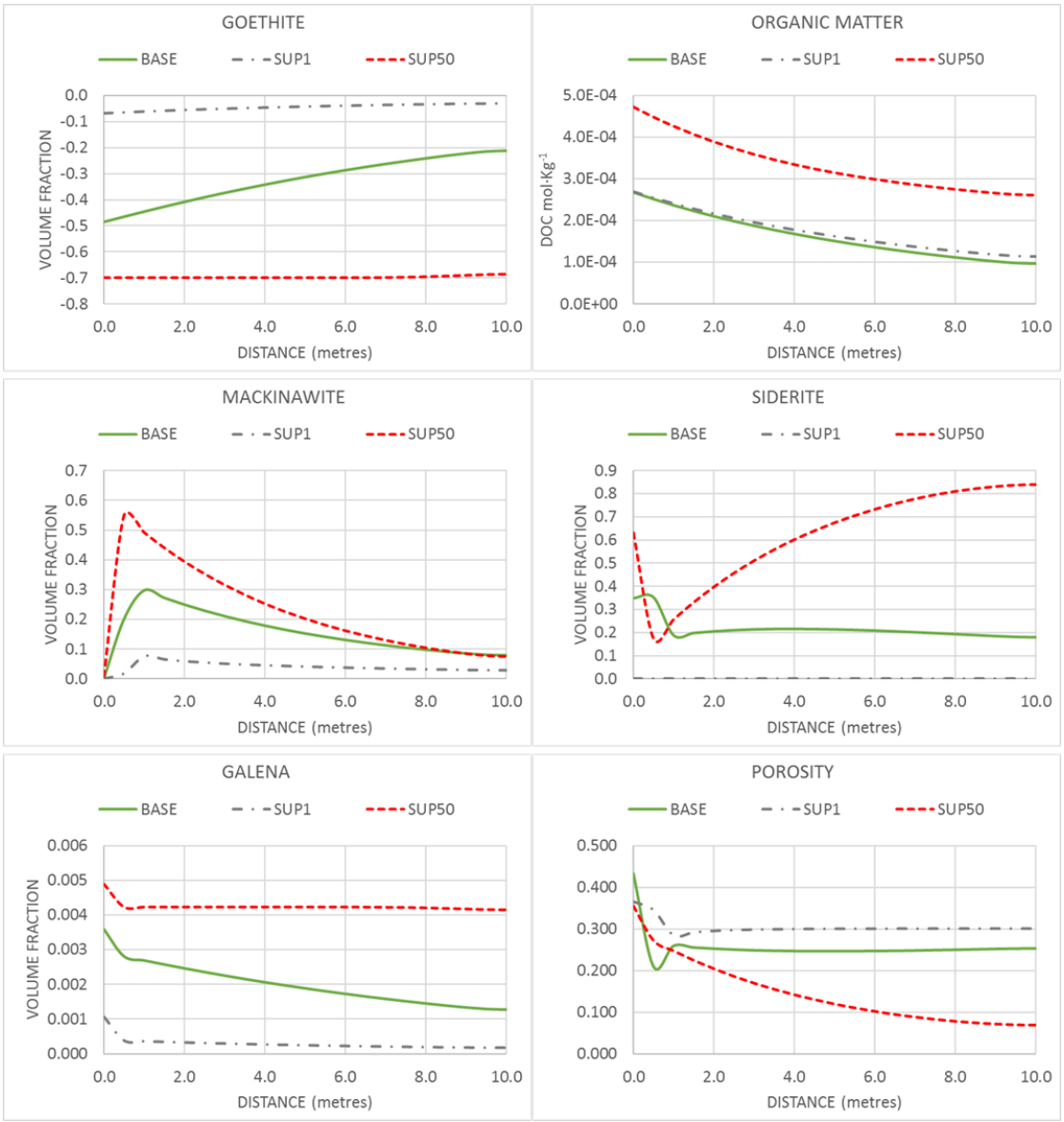

Figure 6.9. Sensitivity analysis of the reactive transport model based on the specific reactive surface area, σ_{BASE}=10 $m^2 \cdot m^{-3}$, σ=1 $m^2 \cdot m^{-3}$ and σ=50 $m^2 \cdot m^{-3}$ for each mineral. Elapsed time of 0.8 Ma.

The groundwater flow rate could also have varied in the past with respect to the present-day value. For example, changes in pluviometry or in sea level during the Holocene could have led to changes in groundwater flow. The impacts of flows half and twice that of the base case were tested. The results are plotted in Figure 6.10.

A flow rate reduction (the flow divided by two) did not produce major changes with respect to the base model but decreased the galena and mackinawite precipitation because most sulfur was supplied by the groundwater flux. A flow rate increase (double) produced the opposite effect. However, the resulting mineral zonation was similar in all cases (Figure 6.10).

Finally, the DOC concentration from the different wells close to the deposit area varied widely. The impact of the lower and higher DOC concentrations on the results of the model were tested, and the results are plotted in Figure 6.11. Changes in DOC concentration led to very distinct results. Indeed, the lower DOC concentration (1 $mg \cdot L^{-1}$) led to a very low amount of goethite replacement and no precipitation of mackinawite, in disagreement with observations. The higher DOC concentration (15 $mg \cdot L^{-1}$) caused faster goethite replacement (sulfate reduction rates). Therefore, all the Fe, Pb and DIC released was precipitated as mackinawite and galena in the first 3 m, and precipitation of siderite was entirely inhibited and delayed to the second 7 m of the system. The complete replacement of goethite occurred in less than 0.8 Ma. Porosity increased to values near 0.5 close to the input; the “black rock” was mainly formed by sulfides, and the “red rock” formed by siderite as described by Tornos et al. (2017) thus became distinct. This result suggests that DOC concentration in past groundwater was probably higher that the average of the values recorded in present day samples.

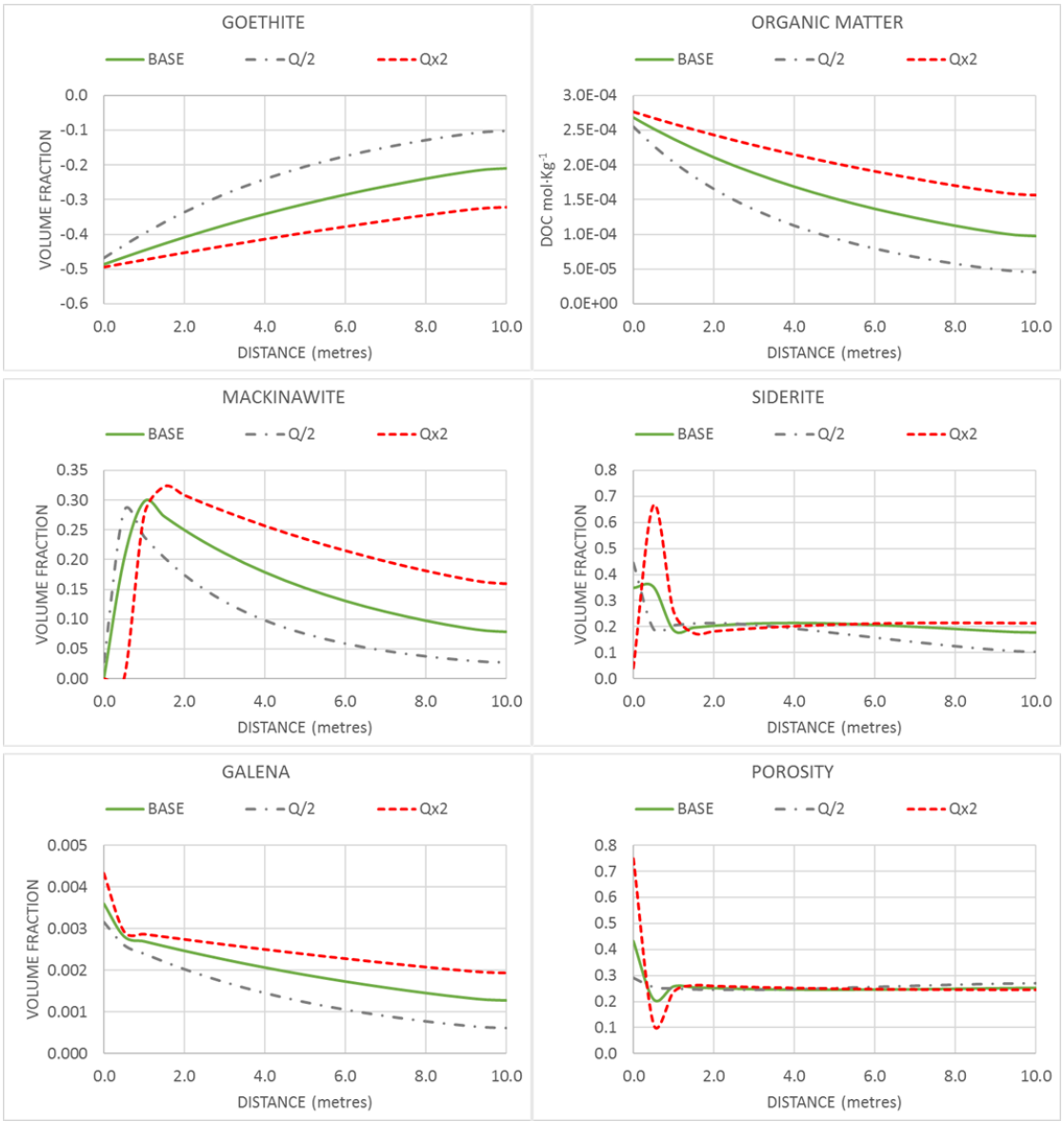

Figure 6.10. Sensitivity analysis of the reactive transport model based on the flow rate value, Q_{BASE}=1.35 $m^3 \cdot m^{-2} \cdot y^{-1}$, Q/2=0.675 $m^3 \cdot m^{-2} \cdot y^{-1}$ and Q*2=2.7 $m^3 \cdot m^{-2} \cdot y^{-1}$ for each mineral. Elapsed time of 0.8 Ma.

In the previous calculations, changes in porosity were low and no changes in the hydraulic properties of the rock were assumed. However, the porosity increased up to 0.8 at the inflow in several calculations. The upsurge in porosity could have caused the mechanical collapse

of the rock and an apparent increase in deformation at the base of the system, as was described by Yesares et al. (2015). In contrast, porosity in the second half of the system approached 0.05 in cases of high surface area and/or DOC concentration (15 mg·L^{-1}). In such a case, reactions leading to an increase in the volume of the solid phase become difficult. Therefore, more realistic modelling would assume that replacement reaction rates are constrained to maintain the solid volume (Ayora et al., 1998), and the following stoichiometry would occur instead of:

(E13)

$$FeOOH + 0.459HCO_3^- + 1.041H^+ + 0.25CH_2O \rightarrow 0.709FeCO_3 + 1.5H_2O + 0.291Fe^{2+}$$

The resulting model would reduce the siderite precipitated without a virtual decline in porosity (Figure 6.11). The final resulting texture would be an isomorphic replacement of goethite with siderite, which has been extensively described in Las Cruces siderite rock (Tornos et al., 2017; Yesares et al., 2015).

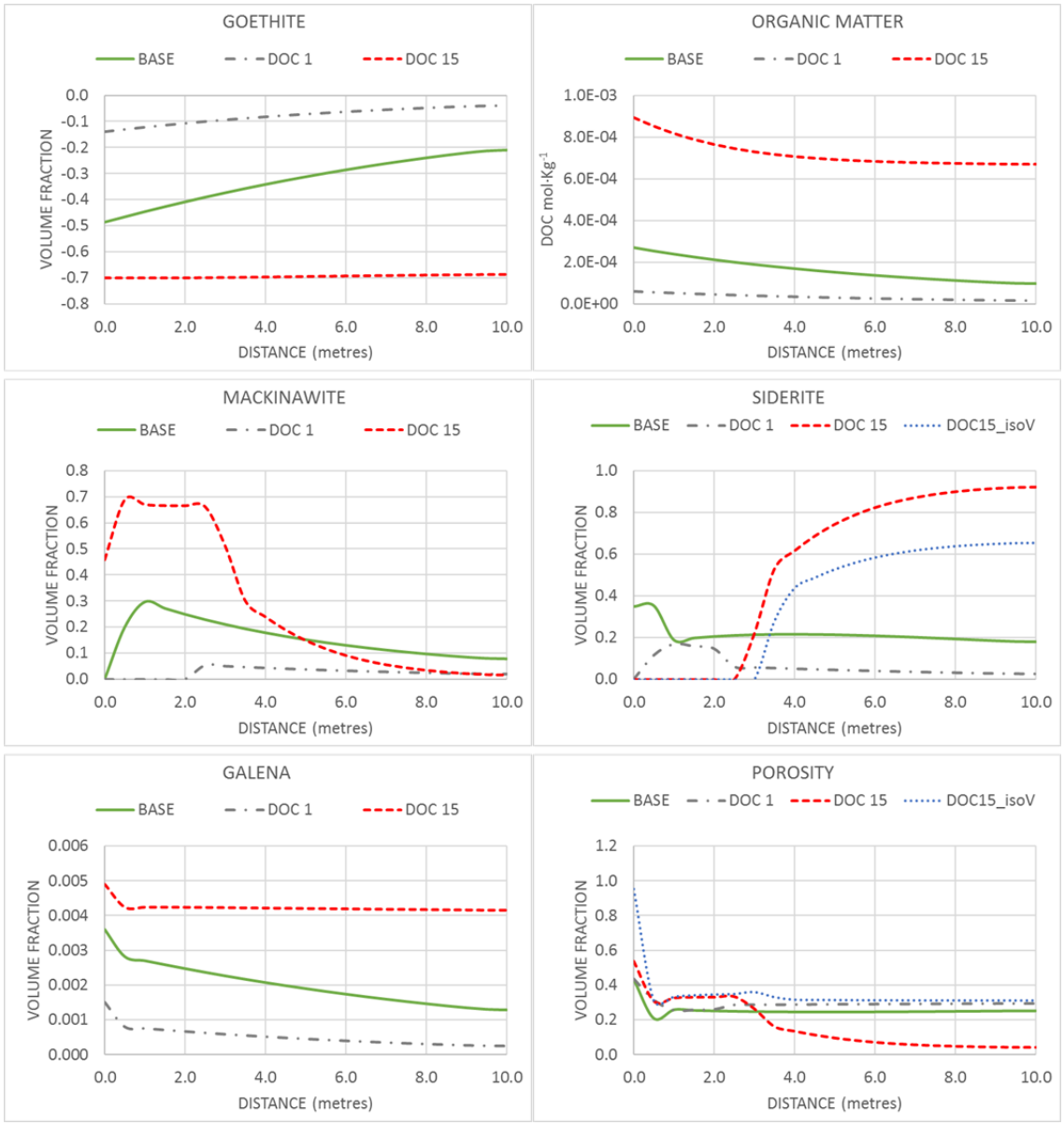

Figure 6.11. Sensitivity analysis of the reactive transport model based on the organic matter concentration, DOC_{BASE}=4.5 mg·L^{-1}, DOC1 = 1 mg·L^{-1} and DOC15=15 mg·L^{-1} for each mineral. Elapsed time of 0.8 Ma

6.4. CONCLUSIONS

This paper quantitatively and qualitatively demonstrated that the reduction of gossan minerals at the expense of the organic matter dissolved in present day groundwater could have formed the unusual mineralogy of part of the Las Cruces deposit.

A reactive transport 1D model was developed and applied to calculate the interaction between the present-day groundwater and a goethite gossan. The obtained results showed that goethite replacement occurred at the expense of organic matter oxidation and siderite, galena and iron sulfides thus precipitated. Less than 1 Ma was required to replace the goethite initially assumed. This is consistent with the continuity in the functioning of the hydrogeological system from the lower-Pleistocene (1.8 Ma). The goethite dissolution was the major source of the Pb, As and Sb recorded in galena and of the As found in water from wells. Porosity tended to increase at the inflow boundary and may have caused the mechanical collapse of the rock. In the rest of the system, the higher volume of siderite with respect to goethite tended to reduce the porosity. However, volume constraints may have induced the observed isomorphic replacement to maintain the porosity and the hydraulic permeability of the final rock. The mass of sulfur carried by groundwater was up to two orders of magnitude higher than that released by goethite dissolution, which explains the high values of $\delta^{34}S_{SO4}$ values measured in galena that are close to those of groundwater.

We concluded from the sensitivity analysis that the groundwater flux was pervasive rather than channelized through fractures in the Las Cruces deposit. More interestingly, DOC concentration in past groundwater was probably higher than the average of the values recorded in present day samples. Indeed, high DOC concentration produced a mineral zonation formed by Fe-sulfides and siderite that agreed with the observations described by Tornos et al. (2017) of black rock (formed manly by iron sulfides) and red rock (formed mainly by siderite).

The results from the reactive transport model were also supported by the following evidence observed both in the groundwater and in the rock: (A) low Eh values, the presence of H_2S

and the high sulfate isotope values, which indicated that the groundwater had reducing conditions; (B) high ammonium, boron, iodide and DOC concentrations together with the low $\delta^{13}C$ values for both groundwater and siderite, which showed the important role of organic matter oxidation; and (C) the chemical equilibrium of groundwater with siderite, which indicated the precipitation of this mineral.

CHAPTER 7. GENERAL CONCLUSIONS

This thesis aims to provide a tool for the sustainable management and protection of groundwater resources affected by mining activities. The methodology is based on a combination of hydrochemical, isotopic, multivariate statistical and modelling techniques that evaluate the impact of mining activities on groundwater to determine the origin of the chemical constituents of regional and mining waters and assist in the management of groundwater used in mining activity.

At the beginning of this thesis, a series of issues were raised to be addressed throughout the research work:

- ***Is groundwater renewable or a fossil resource?***

  The combination of geochemical, isotopic and dating techniques has allowed the (1) division of the study area into four zones, the recharge, intermediate, and deep (1 and 2) zones; (2) identification of the chemical processes that play an important role in this system, including calcite dissolution, Ca-Na cation exchange, mixing between fresh water and ancient seawater trapped in the porosity and SO_4^{-2} and iron oxide reduction; and (3) distinction of a strip zone with short-turnover (renewable) groundwater and another with almost steady (non-renewable) groundwater.

  This enhances the understanding of groundwater system dynamics and lends support to the sustainable management and protection of groundwater resources.

- ***What is the origin of groundwater chemistry?***

  Combined geochemical and isotopic techniques have allowed differentiation of the geogenic/anthropogenic origin of the high concentration of ammonium, arsenic and boron in groundwater. This approach has confirmed that these anomalous concentrations are attributed to geogenic processes such as the reductive dissolution of As-bearing goethite and the degradation of marine solid organic matter by sulfate dissolved in recharge water.

- ***Is groundwater suitable for human use without treatment? If not, what are the limitations?***

  Based on the described water quality data, three zones of groundwater quality were defined based on ammonium, arsenic, boron and salinity data. The first zone, which is closer to the recharge area, contains water of sufficient quality for human consumption; the second zone downflow contains groundwater suitable for continuous irrigation but not for drinking without treatment due to its high ammonium concentrations; and the third, deeper zone contains groundwater of

elevated salinity (up to 5940 $\mu S \cdot cm^{-1}$) and high ammonium, boron and local arsenic concentrations that is not usable for any public use as drinking water or irrigation.

- ***Is the use of groundwater in mining activity sustainable?***

  A multivariate statistical approach has allowed evaluation of the contributions from each water input (runoff, Cenozoic and Paleozoic end-members) that mixes in the open pit water of the CLC. This approach allowed determination of the fraction of water extracted from the Cenozoic aquifer and the amount required to be compensated for the CLC use to fulfil the regulations that aim to preserve the water resources of the Cenozoic aquifer.

- ***What is the effect of the groundwater-ore mineralogy interaction?***

  Reactive transport modelling has quantitatively and qualitatively confirmed that the reduction of initial iron oxides (gossan) at the expense of organic matter dissolved in present day groundwater can form the unusual mineralogy found in the Las Cruces deposit (massive siderite with galena and iron sulfides) in a time span of 10^5 years. The sensitivity analysis concluded that the DOC concentration in past groundwater was likely higher than the average of the values recorded in present day samples. Indeed, a high DOC concentration would produce a mineral zonation formed by Fe-sulfides and siderite that agrees with observations.

REFERENCES

Abad de los Santos M., 2007. La transgresión tortoniense en el margen pasivo de la cuenca del Guadalquivir: respuesta estratigráfica e implicaciones paleontológicas. Published PhD Thesis. Universidad de Huelva. 527 pp.

Ahmed, K.M., Bhattacharya, P., Hasan, M.A., Akhter, S.H., Alam, S.M.M., Bhuyian, M.A.H., Imam, M.B., Khan, A.A, Sracek O., 2004. Arsenic enrichment in groundwater of the alluvial aquifers in Bangladesh: an overview, Appl. Geochem.181–200.

Alberto, M. C. R., Arah, J. R. M., Neue, H. U., Wassmann, R., Lantin, R. S., Aduna, J. B., & Bronson, K. F., 2000. A sampling technique for the determination of dissolved methane in soil solution. Chemosphere-Global Change Science, 2(1), 57-63.

Alcalá, F.J., Custodio, E., 2008. Using the Cl/Br ratio as a tracer to identify the origin of salinity in aquifers in Spain and Portugal. Journal of Hydrology, 359(1–2): 189-207.

Almodóvar, G. R., Sáez, R., Pons, J. M., Maestre, A., Toscano, M., & Pascual, E., 1997. Geology and genesis of the Aznalcóllar massive sulphide deposits, Iberian Pyrite Belt, Spain. Mineralium Deposita, 33(1-2), 111-136.

Anawar, H. M., Akai, J., Komaki, K., Terao, H., Yoshioka, T., Ishizuka, T., Safiullah, S., and Kato, K., 2003. Geochemical occurrence of arsenic in groundwater of Bangladesh: sources and mobilization processes: Journal of Geochemical Exploration, v. 77, no. 2-3, p. 109-131.

Andre, L., Franceschi, A., Pouchan, P., Atteia, O., 2005. Using geochemical data and modelling to enhance the understanding of groundwater flow in a regional deep aquifer, Aquitaine Basin, south-west of France. Journal of Hydrology, 305(1-4): 40-62.

Appelo, C.A.J., 1994. Cation and proton exchange, pH variations, and carbonate reactions in a freshening aquifer. Water Resources Research, 30(10): 2793-2805.

Appelo, C.A.J., Postma, D., 2005. Geochemistry, groundwater and pollution (Second Edition). CRC Press: 1-668.

Aravena, R., Evans, M.L., and Cherry J.A., 1993. Stable isotopes of oxygen and nitrogen in source identification of nitrate from septic systems. Ground Water 31, 180-186

Atkinson, A.P., Cartwright, I., Gilfedder, B.S., Hofmann, H.,Unland, N.P., Cendón, D.I., and Chisari, R., 2013. A multi-tracer approach to quantifying groundwater inflows to an upland river; assessing the influence of variable groundwater chemistry. Hydrological Processes. DOI: 10.1002/hyp.10122

Ayora, C., Taberner, C., Saaltink, M., Carrera, J., 1998. The genesis of dedolomites: a discusion based on reactive transport modeling. Journal of Hydrology, 209(1): 346-365.

Azcue, J.M., Murdoch, A., Rosa, F., Hall, G.E.M., 1994. Effects of abandoned gold mine tailings on the arsenic concentrations in water and sediments of Jack of Clubs Lake, BC. Environ. Technol. 15, 669–678.

Ball, J.M., Nordstrom, D.K., 2001. User's manual for WATEQ4F with revised thermodynamic database and test cases for calculating speciation of major, trace and redox elements in natural waters. U.S. Geological Survey Water Resources. Investigation Report 91-183.

Baquero, J.C., de los Reyes, M.J., Custodio, E., Scheiber, L., and Vázquez-Suñé, E., 2017. Groundwater Management in Mining. The Drainage and Reinjection System in Cobre Las Cruces (Spain). Modern Environmental Science and Engineering.

Bargar, J., Brown, G., Parks, G., 1997. Surface complexation of Pb (II) at oxide-water interfaces: I. XAFS and bond-valence determination of mononuclear and polynuclear Pb (II) sorption products on aluminum oxides. Geochimica et Cosmochimica Acta, 61(13): 2617-2637.

Belkin, H.E., Zheng, B., Finkelman, R.B., 2000. Human health effects of domestic combustion of coal in rural China: a causal factor for arsenic and fluorine poisoning. In:2nd World Chinese Conf. Geological Sciences, Extended Abstr., August 2000, Stanford Univ.,pp.522 .524.

Belogub, E., Novoselov, C., Spiro, B., Yakovleva, B., 2003. Mineralogical and S isotopic features of the supergene profile of the Zapadno-Ozernoe massive sulphide and Au-bearing gossan deposit, South Urals. Mineralogical Magazine, 67(2): 339-354.

Bentley, H.W., Phillips, F.M., Davis, S.N., Habermehl, M.A., Airey, P.L., Calf, G.E., Elmore, D., Gove, H.E., Torgersen, T., 1986. Chlorine 36 dating of very old groundwater: 1. The Great Artesian Basin, Australia. Water Resources Research, 22(13): 1991-2001.

Berg, M., Tran, H. C., Nguyen, T. C., Pham, H. V., Schertenleib, R., and Giger, W., 2001. Arsenic contamination of groundwater and drinking water in Vietnam: A human health threat: Environmental Science & Technology, v. 35, no. 13, p. 2621-2626.

Bernard, R., Taran, Y., Pennisi, M., Tello, E., & Ramirez, A., 2011. Chloride and Boron behavior in fluids of Los Humeros geothermal field (Mexico): A model based on the existence of deep acid brine. Applied Geochemistry, 26(12), 2064-2073.

Berner, E.K., Berner, R.A., 1987. The global water cycle: geochemistry and environment. Prentice-Hall.

Beyerle, U., Aeschbach-Hertig, W., Hofer, M., Imboden, D. M., Baur, H., and Kipfer, R., 1999. Infiltration of river water to a shallow aquifer investigated with 3 H/3 He, noble gases and CFCs. Journal of Hydrology, 220(3), 169-185.

Blake, C., 2008: The mineralogical characterisation and interpretation of a precious metal-bearing fossil gossan, Las Cruces, Spain: Published PhD Thesis. Cardiff University. 207 p.

Borowski., W.S. and Paull., C.K., 2000. Data report: nitrogen isotopic composition of pore-water ammonium, Blake ridge, site 9971. In: Paull, C.K., Matsumoto, R., Wallace, P.J., and Dillon, W.P. (Eds.), 2000. Proceedings of the Ocean Drilling Program, Scientific Results, Vol. 164-171.

Bouchaou, L., Michelot, J.L., Vengosh, A., Hissou, Y., Qurtobi, M., Gaye, C.B., Bullen, T.D., Zuppi, G.M. 2008. Application of multiple isotopic and geochemical tracers for investigation of recharge, salinization, and residence time of water in the Souss-Massa aquifer, southwest of Morocco. Journal of Hydrology, 352(3-4): 267-287.

Bowell, R., 1994. Sorption of arsenic by iron oxides and oxyhydroxides in soils. Applied Geochemistry, 9(3): 279-286.

Canavan, R. W., Slomp, C. P., Jourabchi, P., Van Cappellen, P., Laverman, A. M., & Van den Berg, G. A., 2006. Organic matter mineralization in sediment of a coastal freshwater lake and response to salinization. Geochimica et Cosmochimica Acta, 70(11), 2836-2855.

Cánovas, C. R., Olias, M., Vazquez-Suñé, E., Ayora, C., & Nieto, J. M., 2012. Influence of releases from a fresh water reservoir on the hydrochemistry of the Tinto River (SW Spain). Science of the Total Environment, 416, 418-428

Capasso, G. and S. Inguaggiato, 1998. "A simple method for the determination of dissolved gases in natural waters. An application to thermal waters from Vulcano Island." Applied Geochemistry 13(5): 631-642.

Capitán Suárez, M. A., 2006. Mineralogía y geoquímica de la alteración superficial de depósitos de sulfuros masivos en la faja pirítica ibèrica. Departamento de geología, Universidad de Huelva (UHU): 368.

Carrera, J., Vázquez-Suñé, E., Castillo, O., Sánchez-Vila, X., 2004. A methodology to compute mixing ratios with uncertain end-members. Water Resources Research, 40(12): n/a-n/a.

Cartwright, I., Weaver, T., Cendón, D.I., Swane, I., 2010. Environmental isotopes as indicators of inter-aquifer mixing, Wimmera region, Murray Basin, Southeast Australia. Chemical Geology, 277(3–4): 214-226.

Cartwright, I., Weaver, T.R., Cendón, D.I., Fifield, L.K., Tweed, S.O., Petrides, B., Swane, I., 2012. Constraining groundwater flow, residence times, inter-aquifer mixing, and aquifer properties using

environmental isotopes in the southeast Murray Basin, Australia. Applied Geochemistry, 27(9): 1698-1709.

Carvalho, D.d., 1976. Considerações sobre o vulcanismo da região de Cercal-Odemira. Suas relações com a faixa piritosa. Com Serv Geol Portugal, 60: 215-238.

Cendón, D.I., Hankin, S.I., Williams, J.P., Van der Ley, M., Peterson, M., Hughes, C.E., Meredith, K., Graham, I.T., Hollins, S.E., Levchenko, V., Chisari, R., 2014. Groundwater residence time in a dissected and weathered sandstone plateau: Kulnura–Mangrove Mountain aquifer, NSW, Australia. Australian Journal of Earth Sciences, 61(3): 475-499.

Cerling, T.E., Solomon, D.K., Quade, J., Bowman, J.R., 1991. On the isotopic composition of carbon in soil carbon dioxide. Geochimica Et Cosmochimica Acta, 55(11): 3403-3405.

Chen, J. Y., Tang, C. Y., Shen, Y. J., Sakura, Y., and Fukushima, Y., 2004. Nitrate pollution of groundwater in a wastewater irrigated field in Hebei Province, China: Wastewater Re-Use and Groundwater Quality, no. 285, p. 23-27.

CHG, 2012. Confederación Hidrográfica del Guadalquivir. Propuesta de Proyecto de Plan Hidrológico de la Demarcación Hidrográfica del Guadalquivir. Sevilla.

CLC, 2005. Valoración ambiental del estado pre-operacional EVA-0, Sevilla, Diciembre 2005, 77 pag. http://www.cobrelascruces.com/index.php/documentos-de-interes/.

Cloutier, V., Lefebvre, R., Savard, M., Bourque, É., Therrien, R., 2006. Hydrogeochemistry and groundwater origin of the Basses-Laurentides sedimentary rock aquifer system, St. Lawrence Lowlands, Québec, Canada. Hydrogeology Journal, 14(4): 573-590.

Coetsiers, M., Walraevens, K., 2009. A new correction model for 14C ages in aquifers with complex geochemistry – Application to the Neogene Aquifer, Belgium. Applied Geochemistry, 24(5): 768-776.

Coughlin, B.R., Stone, A.T., 1995. Nonreversible adsorption of divalent metal ions (MnII, CoII, NiII, CuII, and PbII) onto goethite: effects of acidification, FeII addition, and picolinic acid addition. Environmental science & technology, 29(9): 2445-2455.

Craig, H., 1961. Isotopic variations in meteoric waters. Science, 133(346): 1702-&.

Crawford, A., Corbett, K., Everard, J., 1992. Geochemistry of the Cambrian volcanic-hosted massive sulfide-rich Mount Read Volcanics, Tasmania, and some tectonic implications. Economic Geology, 87(3): 597-619.

Cresswell, R.G., Bauld, J., Jacobson, G., Khadka, M.S., Jha, M.G., Shrestha, M.P., Regmi, S., 2001. A first estimate of ground water ages for the deep aquifer of the Kathmandu Basin, Nepal, using the radioisotope chlorine-36. Ground Water, 39(3): 449-457.

Criaud, A., Fouillac, C., 1989. The distribution of arsenic(III) and arsenic(V) in geothermal waters: Examples from the Massif Central of France, the Island of Dominica in the Leeward Islands of the Caribbean, the Valles Caldera of New Mexico, USA, and southwest Bulgaria. Chem. Geol. 76, 259–269.

Crosby, H.A., Roden, E.E., Johnson, C.M., Beard, B.L., 2007. The mechanisms of iron isotope fractionation produced during dissimilatory Fe (III) reduction by Shewanella putrefaciens and Geobacter sulfurreducens. Geobiology, 5(2): 169-189.

Currell, M., Cartwright, I., Raveggi, M., & Han, D., 2011. Controls on elevated fluoride and arsenic concentrations in groundwater from the Yuncheng Basin, China. Applied Geochemistry, 26(4), 540-552.

Currell, M., Cendón, D., Cheng, X., 2013. Analysis of environmental isotopes in groundwater to understand the response of a vulnerable coastal aquifer to pumping: Western Port Basin, south-eastern Australia. Hydrogeology Journal, 21(7): 1413-1427.

Custodio, E., Llamas M.R. (eds.) 1976. Hidrología subterránea [Groundwater hydrology]. Ediciones Omega, Barcelona: 1-2350.

Custodio, E.,Bruggeman, G.A. 1987. Groundwater problems in coastal areas. Studies & Reports in Hydrology 45. UNESCO, Paris: 1-576.

Custodio, E., Custodio-Ayala, J. 2013. Interpretación simplificada de la evolución del tritio en acuíferos con mezcla exponencial [Symplified interpretation of tritium evolution in aquifers with exponential mixing]. In: X Simposio de Hidrogeología, Granada, Hidrogeología y Recursos Hidráulicos. Asociación Española de Hidrogeólogos, Madrid, XXX: 427-436.

Dansgaard, W., 1964. Stable isotopes in precipitation. Tellus, 16(4): 436-468.

Davis, J. A., and Leckie, J. O., 1978. Effect of adsorbed complexing ligands on trace metal uptake by hydrous oxides. Environmental Science & Technology, 12(12), 1309-1315.

Davis, S.N., Whittemore, D.O., Fabryka-Martin, J., 1998. Uses of chloride/bromide ratios in studies of potable water. Ground Water, 36(2): 338-350.

De Oliveira, D. P. S., Matos, J. X., Rosa, C. J. P., Rosa, D. R. N., Figueiredo, M. O., Silva, T. P., Reiser, F. K. M., 2011. The Lagoa Salgada Orebody, Iberian Pyrite Belt, Portugal. Economic Geology, 106(7), 1111-1128.

Dixit, S., Hering, J.G., 2003. Comparison of arsenic (V) and arsenic (III) sorption onto iron oxide minerals: implications for arsenic mobility. Environmental science & technology, 37(18): 4182-4189.

Dogramaci, S.S., Herczeg, A.L., 2002. Strontium and carbon isotope constraints on carbonate-solution interactions and inter-aquifer mixing in groundwaters of the semi-arid Murray Basin, Australia. Journal of Hydrology, 262(1-4): 50-67.

Douglas, A.A., Osiensky, J.L., Keller, C.K., 2007. Carbon-14 dating of ground water in the Palouse Basin of the Columbia river basalts. Journal of Hydrology, 334(3–4): 502-512.

Doyle, M.G., Allen, R.L., 2003. Subsea-floor replacement in volcanic-hosted massive sulfide deposits. Ore Geology Reviews, 23(3): 183-222.

Durán Valsero, Juan José, 2002. Los sistemas kársticos de la provincia de Málaga y su evolución: contribución al conocimiento paleoclimático del Cuaternario en el Mediterráneo occidental. PhD Thesis, Complutense University of Madrid, Spain. 404 pp.

Edmunds, W., Fellman, E., Goni, I., Prudhomme, C., 2002. Spatial and temporal distribution of groundwater recharge in northern Nigeria. Hydrogeology Journal, 10(1): 205-215.

Edmunds, W. M., Dodo, A., Djoret, D., Gaye, C. H., Goni, I. B., Travi, Y., and Gasse, F., 2004. Groundwater as an archive of climatic and environmental change: Europe to Africa. In Past climate variability through Europe and Africa (pp. 279-306). Springer Netherlands.

Edmunds, W.M., 2009. Palaeoclimate and groundwater evolution in Africa-implications for adaptation and management. Hydrological Sciences Journal-Journal des Sciences Hydrologiques, 54(4): 781-792.

Efron, B., 1979. Computers and the theory of statistics: thinking the unthinkable. SIAM review, 21(4), 460-480.

Ellis, A.J., Mahon, W.A.J., 1977. Chemistry and Geothermal Systems. Academic Press, New York.

Emmons, W.H., Laney, F.B., 1926. Geology and ore deposits of the Ducktown mining district, Tennessee. Govt. Print. Off.

Escudero, R. B., 1994. Cuaternario aluvial dela depresión del Guadalquivir: episodios geomorfológicos y cronología paleomagnética.

Fabryka Martin, J., Davis, S.N., Elmore, D., 1987. Applications of 129I and 36Cl in hydrology. Nuclear Instruments and Methods in Physics Research Section B: Beam Interactions with Materials and Atoms, 29(1–2): 361-371.

Fendorf, S., Eick, M.J., Grossl, P., Sparks, D.L., 1997. Arsenate and chromate retention mechanisms on goethite. 1. Surface structure. Environmental science & technology, 31(2): 315-320.

Fernandes, P. G., Carreira, P. M., 2008. Isotopic evidence of aquifer recharge during the last ice age in Portugal. Journal of hydrology, 361(3), 291-308.

Fernández-Caliani, J. C. and E. Galán (1991). Las pizarras de la faja piritica Ibérica (zona sur-Portuguesa): geología, mineralogía y aplicaciones industriales. Estudios Geológicos, Vol 47, No 5-6 (1991) doi:10.3989/egeol.91475-6425.

Fifield, L.K., Ophel, T.R., Bird, J.R., Calf, G.E., Allison, G.B., Chivas, A.R., 1987. The chlorine-36 measurement program at the Australian National University. Nuclear Instruments and Methods in Physics Research Section B: Beam Interactions with Materials and Atoms, 29(1–2): 114-119.

Figueiredo, M.-O., Pereira da Silva, T., 2011. The positive environmental contribution of jarosite by retaining lead in acid mine drainage areas. International journal of environmental research and public health, 8(5): 1575-1582.

Forbes, E., Posner, A., Quirk, J., 1976. The specific adsorption of divalent Cd, Co, Cu, Pb, and Zn on goethite. Journal of soil science, 27(2): 154-166.

Frengstad, B., Banks, D., Siewers, U., 2001. The chemistry of Norwegian groundwaters: IV. The pH-dependence of element concentrations in crystalline bedrock groundwaters. Science of the Total Environment, 277(1–3): 101-117.

Gaillardet, J., Viers, J. and Dupre, B., 2004. Trace Elements in River Waters. In: Treatise on Geochemistry. Holland, H.D. and Turekian, K.K. (Editors), Elsevier, Amsterdam. 5: 225-272.

Galley, A.G., Hannington, M., Jonasson, I., 2007. Volcanogenic massive sulphide deposits. Mineral deposits of Canada: a synthesis of major deposit-types, district Metallogeny, the evolution of geological provinces, and exploration methods: Geological Association of Canada, Mineral Deposits Division, Special Publication, 5: 141-161.

García de Miguel, J., 1990. Mineralogía, paragénesis y sucesión de los sulfuros masivos de la Faja Pirítica en el suroeste de la Península Ibérica. Boletin Geológico y Minero, 101(1): 73-105.

Gemici, Ü., Tarcan, G., Helvacı, C., & Somay, A. M., 2008. High arsenic and boron concentrations in groundwaters related to mining activity in the Bigadiç borate deposits (Western Turkey). Applied Geochemistry, 23(8), 2462-2476.

Goldberg, S., Forster, H.S., Heick, E.L., 1993. Boron adsorption mechanisms on metal oxides, clay-minerals, and soils inferred from ionic-strength effects, Soil Sci. Soc. Am. 57 (1993) 704–708.

Goldberg, S., 1997. Reactions of boron with soils. Plant and soil, 193(1-2), 35-48.

Goldberg, S., Johnston, C.T., 2001. Mechanisms of arsenic adsorption on amorphous oxides evaluated using macroscopic measurements, vibrational spectroscopy, and surface complexation modeling. Journal of colloid and Interface Science, 234(1): 204-216.

Grassi, S., Amadori, M., Pennisi, M., & Cortecci, G., 2014. Identifying sources of B and As contamination in surface water and groundwater downstream of the Larderello geothermal–industrial area (Tuscany–Central Italy). Journal of Hydrology, 509, 66-82.

Guendouz, A., Michelot, J.-L., 2006. Chlorine-36 dating of deep groundwater from northern Sahara. Journal of Hydrology, 328(3-4): 572-580.

Halim, M. A., Majumder, R. K., Nessa, S. A., Hiroshiro, Y., Sasaki, K., Saha, B. B., Saepuloh, A., and Jinno, K., 2010. Evaluation of processes controlling the geochemical constituents in deep groundwater in Bangladesh: Spatial variability on arsenic and boron enrichment: Journal of Hazardous Materials, v. 180, no. 1-3, p. 50-62.

Halim, M. A., Majumder, R. K., Nessa, S. A., Oda, K., Hiroshiro, Y., Saha, B. B., Hassain, S. M., Latif, S. A., Islam, M. A., and Jinno, K., 2009. Groundwater contamination with arsenic in Sherajdikhan, Bangladesh: geochemical and hydrological implications: Environmental Geology, v. 58, no. 1, p. 73-84.

Harms-Ringdahl, P., 2007. Identifying possible sources of ammonium ions and arsenic in groundwater in the Nam Du area, Vietnam. MS Thesis, Swedish Univ. Agric. Sci., Dept. Soil Sci. Vol. 82.

Harvey, C., C. Swartz, A. Badruzzaman, N. Keon-Blute, W. Yu, M. Ali, J. Jay, R. Beckie, V. Niedan and D. Brabander, 2003. Response to Comments on Arsenic Mobility and Groundwater Extraction in Bangladesh. Science 300(5619): 584-584.

Herrera, C., Custodio, E., 2000. Utilización de la relación Cl/Br como trazador hidrogeoquímico en hidrología subterránea. Boletín Geológico Minero. Madrid.

Hiemstra, T., Van Riemsdijk, W., 1999. Surface structural ion adsorption modeling of competitive binding of oxyanions by metal (hydr) oxides. Journal of colloid and Interface Science, 210(1): 182-193.

Hinkle, S.R., J.K. Böhlke, J.K. Duff, D.S. Morgan, R.J. Weick., 2007. Aquifer-scale controls on the distribution of nitrate and ammonium in ground water near La Pine, Oregon, USA. Journal of Hydrology 333, 486-503.

Hitchon, B., Friedman, I., 1969. Geochemistry and origin of formation waters in the western Canada sedimentary basin—I. Stable isotopes of hydrogen and oxygen. Geochimica et Cosmochimica Acta, 33(11): 1321-1349.

Holloway, J. M., & Dahlgren, R. A., 2002. Nitrogen in rock: occurrences and biogeochemical implications. Global Biogeochemical Cycles, 16(4), 65-1.

Holmes, R.M., McClelland, J.W., Sigman, D.M., Fry, B., Peterson, B.J., 1998. Measuring 15N-NH4+ in marine, estuarine and fresh waters: An adaptation of the ammonia diffusion method. Mar. Chem. 60, 235–243.

Hughes, C.E. and Crawford, J., 2012. A new precipitation weighted method for determining the meteoric water line for hydrological applications demonstrated using Australian and global GNIP data. Journal of Hydrology. 464–465: 344–351.

Iglesias, M., 1999. Hydrogeochemical characterization of groundwater flow in El Abalario, Doñana, Huelva. PhD Thesis, Universidad Politécnica de Cataluña, Spain.

IGME., 1983. Prospección geotérmica en Andalucía occidental. Instituto Geológico y Minero de España. Madrid (internal report)

Islam, F. S., Gault, A. G., Boothman, C., Polya, D. A., Charnock, J. M., Chatterjee, D., & Lloyd, J. R., 2004. Role of metal-reducing bacteria in arsenic release from Bengal delta sediments. Nature, 430(6995), 68-71.

Jiao, J. J., Wang, Y., Cherry, J. A., Wang, X. S., Zhi, B. F., Du, H. Y., and Wen, D.G., 2010. Abnormally High Ammonium of Natural Origin in a Coastal Aquifer-Aquitard System in the Pearl River Delta, China: Environmental Science & Technology, v. 44, no. 19, p. 7470-7475.

Jiménez, D., Custodio, E., 2008. El exceso de deuterio en la lluvia y en la recarga a los acuíferos en el área circum-mediterránea y en la costa mediterránea española [Deuterium excess in rain and recharge to the aquifers in the Circum-Mediterranean área and in the Spanish coastal area]. Boletín Geológico Minero. Madrid., 119: 21-32.

Jiménez de Cisneros, C. and Caballero, E., 2013. Paleoclimate reconstruction during MIS5a based on a speleothem from Nerja Cave, Málaga, South Spain. Natural Science, 5, 533-540. doi: 10.4236/ns.2013.55067.

Jørgensen, N.O., Andersen, M.S., Engesgaard, P., 2008. Investigation of a dynamic seawater intrusion event using strontium isotopes (87 Sr/86 Sr). Journal of Hydrology, 348(3): 257-269.

Jurado, A., Vàzquez-Suñé, E., Soler, A., Tubau, I., Carrera, J., Pujades, E., and Anson, I., 2013. Application of multi-isotope data (O, D, C and S) to quantify redox processes in urban groundwater. Applied geochemistry, 34, 114-125.

Kalbitz, K., Solinger, S., Park, J.-H., Michalzik, B., Matzner, E., 2000. Controls on the dynamics of dissolved organic matter in soils: a review. Soil Science, 165(4): 277-304.

Kase, K., Yamamoto, M., Nakamura, T., Mitsuno, C., 1990. Ore mineralogy and sulfur isotope study of the massive sulfide deposit of Filon Norte, Tharsis Mine, Spain. Mineral. Deposita, 25(4): 289-296.

Kelly, W., 1958. Topical study of lead-zinc gossans. Bulletin, 46: 42-47.

Kennedy, H. A., and Elderfield, H., 1987. Iodine diagenesis in pelagic deep-sea sediments. Geochimica et Cosmochimica Acta, 51(9), 2489-2504.

Knight, F., 2000. The mineralogy, geochemistry and genesis of the secondary sulphide mineralisation of the Las Cruces deposit, Spain.

Kohl, D. H., Shearer, G. B., and Commoner, B., 1971. Fertilizer Nitrogen -Contribution to Nitrate in Surface Water in a Corn Belt Watershed: Science, v. 174, no. 4016, p. 1331-&.

Kosakevitch, A., Polomero, F., Leca, X., Leistel, J. M., Lenotre, N., Sobol, F. (1993). Contrôles climatique et géomorphologique de la concentration de l'or dans les chapeaux de fer de Rio Tinto (Province Huelva, Espagne). Comptes rendus de l'Académie des sciences. Série 2, Mécanique, Physique, Chimie, Sciences de l'univers, Sciences de la Terre, 316(1), 85-90.

Kulongoski, J.T., Hilton, D.R., Cresswell, R.G., Hostetter, S., Jacobson, G., 2008. Helium-4 characteristics of groundwaters from Central Australia: Comparative chronology with chlorine-36 and carbon-14 dating techniques. Journal of Hydrology, 348(1-2): 176-194.

Large, R.R., 1992. Australian volcanic-hosted massive sulfide deposits; features, styles, and genetic models. Economic Geology, 87(3): 471-510.

Leininger S, Urich T, Schloter M, Schwark L, Qi J, Nicol GW, Prosser JI, Schuster SC, Schleper C, (2016) Archaea predominate among ammonia-oxidizing prokaryotes in soils. Nature 2442: 806-809.

Leistel, J. M., Marcoux, E., Thiéblemont, D., Quesada, C., Sánchez, A., Almodóvar, G. R., Sáez, R., 1997. The volcanic-hosted massive sulphide deposits of the Iberian Pyrite Belt Review and preface to the Thematic Issue. Mineralium Deposita, 33(1-2), 2-30.

Leuz, A.-K., Mönch, H., Johnson, C.A., 2006. Sorption of Sb (III) and Sb (V) to goethite: influence on Sb (III) oxidation and mobilization. Environmental science & technology, 40(23): 7277-7282.

Liu, C., Kota, S., Zachara, J.M., Fredrickson, J.K., Brinkman, C.K., 2001. Kinetic Analysis of the Bacterial Reduction of Goethite. Environmental science & technology, 35(12): 2482-2490.

Liu, F., Williams, M.W., Caine, N., 2004. Source waters and flow paths in an alpine catchment, Colorado Front Range, United States. Water Resources Research, 40(9).

Mahlknecht, J., Garfias-Solis, J., Aravena, R., Tesch, R., 2006. Geochemical and isotopic investigations on groundwater residence time and flow in the Independence Basin, Mexico. Journal of Hydrology, 324(1-4): 283-300.

Manning, B.A., Goldberg, S., 1997b. Adsorption and stability of arsenic (III) at the clay mineral-water interface. Environ.Sci. Technol. 31, 2005–2011.

Manzano, M., Soler, A., Carrera, J. y E. Custodio, 2001. Composición isotópica (δ18O, δ2H y δ34S) de las aguas del área afectada por el vertido minero de Aznalcóllar (SO España). En A. Medina, J. Carrera y L. Vives (Editores) Las Caras del Agua Subterránea. Serie Hidrogeología y Aguas Subterráneas, Nº 1. IGME, Madrid, 477-487.

Marcoux, E., 1997. Lead isotope systematics of the giant massive sulphide deposits in the Iberian Pyrite Belt. Mineral. Deposita, 33(1-2): 45-58.

Marcoux, E., Moelo, Y., Leistel, J., 1996. Compared ore mineralogy and geochemistry of the massive-sulfide and stringers ore deposits of Southern Spain. Mineral. Deposita, 31: 1-26.

Massmann, G., Sültenfuß, J., Dünnbier, U., Knappe, A., Taute, T., and Pekdeger, A., 2008. Investigation of groundwater residence times during bank filtration in Berlin: a multi-tracer approach. Hydrological Processes, 22(6), 788-801.

Mastrocicco, M., Giambastiani, B. M. S., & Colombani, N., 2013. Ammonium occurrence in a salinized lowland coastal aquifer (Ferrara, Italy). Hydrological Processes, 27(24), 3495-3501.

McArthur, J.M., Ravenscroft, P., Safiullah, S., Thirlwall, M.F., 2001. Arsenic in groundwater: testing pollution mechanisms for aquifers in Bangladesh. Water Resour. Res. 37, 109–117.

Medina, A.n., Carrera, J., 2003. Geostatistical inversion of coupled problems: dealing with computational burden and different types of data. Journal of Hydrology, 281(4): 251-264.

Meng, X., & Wang, W., 1998. Speciation of arsenic by disposable cartridges. In Book of posters of the third international conference on arsenic exposure and health effects. Society of Environmental Geochemistry and Health Denver, Colorado.

Meredith, K., Cendón, D.I., Pigois, J.-P., Hollins, S., Jacobsen, G., 2012. Using C-14 and H-3 to delineate a recharge 'window' into the Perth Basin aquifers, North Gnangara groundwater system, Western Australia. Science of the Total Environment, 414: 456-469.

Miguélez, G., Tornos Arroyo, F., Velasco, F., Videira, J.C., 2011. Geology and Cu Isotope Geochemistry of the Las Cruces Deposits (SW Spain). Macla 15: 131-132.

Mishra, S.K., Singh, V., 2013. Soil conservation service curve number (SCS-CN) methodology, 42. Springer Science & Business Media.

Mook, W.G., 2002. Isótopos ambientales en el ciclo hidrológico: principios y aplicaciones. Instituto Geológico y Minero de España, Sevicio de Publicaciones, Serie: Guías y Manuales 1. Madrid: 1-596.

Mook, W.G., Bommerson, J.C., Staverman, W.H., 1974. Carbon isotope fractionation between dissolved bicarbonate and gaseous carbon dioxide. Earth and Planetary Science Letters, 22(2): 169-176.

Moral, F., Balanyá, J. C., Expósito, I., Rodríguez Rodríguez, M., 2013. Análisis geomorfológico de las terrazas fluviales del Bajo Guadalquivir e implicaciones tectónicas.

Moreno, C., Sáez, R., 1990. Sedimentación marina somera en el Devónico del anticlinorio de Puebla de Guzmán, Faja Pirítica Ibérica. Geogaceta, 8: 62-64.

Moreno C., C.M.A., Doyle M., Nieto J.M., Ruiz F., Sáez R., 2003. Edad mínima del gossan de Las Cruces. Geogaceta 33.

Mukherjee, A., Fryar, A.E., 2008. Deeper groundwater chemistry and geochemical modeling of the arsenic affected western Bengal basin, West Bengal, India Appl. Geochem., pp. 863–894.

Nakaya, S., Uesugi, K., Motodate, Y., Ohmiya, I., Komiya, H., Masuda, H., and Kusakabe, M., 2007. Spatial separation of groundwater flow paths from a multi-flow system by a simple mixing model using stable isotopes of oxygen and hydrogen as natural tracers. Water resources research, 43(9).

Navarro, A., Fernández, A., Doblas, J.G., 1993. In: IGME (Ed.), Las aguas subterráneas en España. Instituto Geológico y Minero de España: 255-256.

Nickel, E., 1984. The mineralogy and geochemistry of the weathering profile of the Teutonic Bore Cu-Pb-Zn-Ag sulphide deposit. Journal of Geochemical Exploration, 22(1): 239-263.

Nickson, R.T., McArthur, J.M., Ravenscroft, P., Burgess, W.G., Ahmed, K.M., 2000. Mechanism of arsenic release to groundwater, Bangladesh and West Bengal, Appl.Geochem 403–413.

Nicolli, H.B., Suriano, J.M., Peral, M.A.G., Ferpozzi, L.H., Baleani, O.A., 1989. Groundwater contamination with arsenic and other trace-elements in an area of the Pampa, province of Co´ rdoba, Argentina. Environ. Geol. Water Sci.14, 3–16.

Nieto, J., Capitán, M., Sáez, R., Almodóvar, G., 2003. Beudantite: a natural sink for As and Pb in sulphide oxidation processes. Applied Earth Science: Transactions of the Institutions of Mining and Metallurgy: Section B, 112(3): 293-296

Odezulu, C. I., 2011. Stable hydrogen and oxygen isotopic variations in natural waters in North Florida: implications for hydrological and paleoclimatic studies., University of Florida, Gainesville.

Ortega-Guerrero, A., 2003. Origin and geochemical evolution of groundwater in a closed-basin clayey aquitard, Northern Mexico: Journal of Hydrology, v. 284, no. 1-4, p. 26-44.

Palmucci, W., Rusi, S., 2014. Boron-rich groundwater in Central Eastern Italy: a hydrogeochemical and statistical approach to define origin and distribution. Environmental Earth Sciences, 72(12): 5139-5157.

Park, J., Bethke, C.M., Torgersen, T., Johnson, T.M., 2002. Transport modeling applied to the interpretation of groundwater Cl-36 age. Water Resources Research, 38(5). DOI: 0.1029/2001WR000399, 2002.

Parkhurst, D.L., and Appelo, C.A.J., 2013. Description of input and examples for PHREEQC version 3—A computer program for speciation, batch-reaction, one-dimensional transport, and inverse geochemical calculations: U.S. Geological Survey Techniques and Methods, book 6, chap. A43, 497 p., available only at http://pubs.usgs.gov/tm/06/a43.

Pascual, E., Sáez, R., Toscano, M., Ruiz de Almodóvar, G., Donaire, T., 1994. Petrología y geoquímica de tobas vítreas del área de Aznalcóllar (Faja Pirítica Ibérica). Boletín de la Sociedad Española de Mineralogía, 17(1): 155-156.

Pearson, F.J., 1965. Use of C-13/C-12 ratios to correct radiocarbon ages of material initially diluted by limestone. 6th International Conference Radiocarbon and Tritium Dating, Pulman, Washington.

Plummer, L.N., Eggleston, J.R., Andreasen, D.C., Raffensperger, J.P., Hunt, A.G., Casile, G.C., 2012. Old groundwater in parts of the upper Patapsco aquifer, Atlantic Coastal Plain, Maryland, USA: evidence from radiocarbon, chlorine-36 and helium-4. Hydrogeology Journal, 20(7): 1269-1294.

Price, N. B., & Calvert, S. E., 1973. The geochemistry of iodine in oxidised and reduced recent marine sediments. Geochimica et Cosmochimica Acta, 37(9), 2149-2158.

Prokopenko, M. G., Hammond, D. E., Stott, L., 2006. Lack of Isotopic Fractionation of 15 N of Organic Matter during Long-Term Diagenesis in Marine Sediments, ODP Leg 202, Sites 1234 and 1235.

Quesada, C., 1991. Geological constraints on the Paleozoic tectonic evolution of tectonostratigraphic terranes in the Iberian Massif. Tectonophysics, 185(3): 225-245.

Rambaud, F., 1978. Distribución de focos volcánicos y yacimientos en la banda pirítica de Huelva. Bol. Geol. Min., 89: 223-233.

Ramos-Leal, J. A., Durazo, J., Gonzalez-Moran, T., Juarez-Sanchez, F., Cortes-Silva, A., and Johannesson, K. H., 2007. Hydrogeochemical evidence for regional flow mixing in the La Muralla aquifer, Guanajuato. Revista mexicana de ciencias geologicas, 24(3), 293-305.

Rau, G. H., Arthur, M.A., Dean, W.E., 1987. N-15/N-14 variations in Cretaceous Atlantic sedimentary sequences: Implication for past changes in marine nitrogen biogeochemistry, Earth Planet. Sci. Lett., 82, 269–279.

Ravenscroft, P., McArthur, J.M., Hoque, B.A., 2001. Geochemical and palaeohydrological controls on pollution of groundwater by arsenic, In: Chappell, W.R., Abernathy, C.O., Calderon, R. (Eds), Proc. 4th Int. Conf. on Arsenic Exposure and Health Effects, San Diego, USA, June 2000. Elsevier Science Ltd., Oxford, UK.

Ravenscroft, P., McArthur, J.M., 2003. Mechanism of regional enrichment of groundwater by boron: the examples of Bangladesh and Michigan, USA, Appl. Geochem. 1413–1430.

Redfield, A.C., 1934. On the proportions of organic derivatives in sea water and their relation to the composition of plankton. In: James Johnson Memorial Volume, Liverpool, pp. 177- 192.

Rickard, D., 2006. The solubility of FeS. Geochimica et Cosmochimica Acta, 70(23): 5779-5789.

Rivetta, M.O., Bussb S.R., Morganb P., Smithc J.W.N., Bemmentb C.D. (2008) Nitrate attenuation in groundwater: A review of biogeochemical controlling processes, Water Research, 42: 4215–4232.

Robinson, B., Outred, H., Brooks, R., Kirkman, J., 1995. The distribution and fate of arsenic in the Waikato River System, North Island, New Zealand. Chem. Spec. Bioavail. 7, 89–96.

Ross, A.M., 1997. Supergene gold enrichment of the Precambrian aged Flambeau gossan, Flambeau mine, Rusk County, Wisconsin. Thesis (M.S.), Dept. of Geology and Geophysics, University of Utah, 1997. Includes bibliographical references (leaves [55]-56).

Saaltink, M.W., Ayora, C., Carrera, J. 1998. A mathematical formulation for reactive transport that eliminates mineral concentrations. Water Resources Research, 34: 1649-1656.

Sáez, R., Almodóvar, G., Pascual, E., 1996. Geological constraints on massive sulphide genesis in the Iberian Pyrite Belt. Ore Geology Reviews, 11(6): 429-451.

Sáez, R., Pascual, E., Toscano, M., Almodóvar, G.R., 1999. The Iberian type of volcano-sedimentary massive sulphide deposits. Mineral Deposita, 34(5-6): 549-570.

Salvany, J., Mediavilla, C., Manzano, M., Mantecón, R., 2001. Geología del Valle del Guadiamar y áreas colindantes.

Sancha, A.M., Castro, M.L., 2001. Arsenic in Latin America: occurrence, exposure, health effects and remediation. In: Chapell, W. R., Abernathy, C.O., Calderon, www.aulados.net Temas Ambientales 2007 31 R.L.(eds.). Arsenic Exposure and Health Effects IV. Elsevier, Amsterdam, pp.87-96.

Santos, F.J., López-Gutiérrez, J.M., García-León, M., Schnabel, C., Synal, H.-A., and Suter, M. (2004) Analysis of 36Cl in atmospheric samples from Seville (Spain) by AMS. Nuclear Instruments and Methods in Physics Research Section B: Beam Interactions with Materials and Atoms, 223-22. pp. 501-506. ISSN 0168-583X (doi:10.1016/j.nimb.2004.04.094)

Sapek, A., 2005. Agriculture activities as a source of nitrates in groundwater in Razowska-Jaworek, L., and Sadurski, A., eds., Nitrates in groundwater: Leiden, A.A. Balkema Publishers.

Savage, K. S., Tingle, T. N., O'Day, P. A., Waychunas, G. A., & Bird, D. K., 2000. Arsenic speciation in pyrite and secondary weathering phases, Mother Lode gold district, Tuolumne County, California. Applied Geochemistry, 15(8), 1219-1244.

Scheiber, L., Ayora, C., Vázquez-Suñé, E., Cendón, D. I., Soler, A., Baquero, J. C., 2016. Origin of high ammonium, arsenic and boron concentrations in the proximity of a mine: Natural vs. anthropogenic processes. Science of the Total Environment, 541, 655-666.

Scheiber, L., Ayora, C., Vázquez-Suñé, E., Cendón, D. I., Soler, A., Custodio, E., and Baquero, J. C., 2015. Recent and old groundwater in the Niebla-Posadas regional aquifer (southern Spain): Implications for its management: Journal of Hydrology, v. 523, p. 624-635.

Schermerhorn, L.J.G., 1971. An outline stratigraphy of the Iberian Pyrite Belt. Boletin Geológico y Minero, 82(3-4): 239-268.

Schwertmann, U., 1991. Solubility and dissolution of iron oxides. Plant and Soil, 130(1): 1-25.

Scott, K., Ashley, P., Lawie, D., 2001a. The geochemistry, mineralogy and maturity of gossans derived from volcanogenic Zn–Pb–Cu deposits of the eastern Lachlan Fold Belt, NSW, Australia. Journal of Geochemical Exploration, 72(3): 169-191.

Scott, K.M., Ashley, P.M., Lawie, D.C., 2001b. The geochemistry, mineralogy and maturity of gossans derived from volcanogenic Zn–Pb–Cu deposits of the eastern Lachlan Fold Belt, NSW, Australia. Journal of Geochemical Exploration, 72(3): 169-191.

Sebilo, M., Mayer, B., Grably, M., Billiou, D., & Mariotti, A., 2004. The use of the ammonium diffusion. Method for δ15NNH4+ and δ15NNO3 measurements: Comparison with other techniques. Environmental Chemistry, 1(2), 99-103.

Shaw, G.D., Conklin, M.H., Nimz, G.J., Liu, F., 2014. Groundwater and surface water flow to the Merced River, Yosemite Valley, California: 36Cl and Cl− evidence. Water Resources Research, 50(3): 1943-1959.

SIGEA, 2014. Sistema de Información GeoEstadística de Andalucía. https://www.juntadeandalucia.es/institutodeestadisticaycartografia/SIGEA/principal.html

Silva, J., Oliveira, J., Ribeiro, A., 1990. South Portuguese Zone. Structural outline. Pre-Mesozoic Geology of Iberia, 6(3): 348-363.

Smedley, P.L., 1996. Arsenic in rural groundwater in Ghana. J. Afr. Earth Sci. 22, 459–470.

Smedley, P.L. and D.G Kinniburgh, 2002. A review of the source, behaviour and distribution of arsenic in natural waters. Applied Geochemistry 17, 517-568.

Strauss, G.K., Madel, J., 1974. Geology of massive sulphide deposits in the Spanish-Portuguese Pyrite Belt. Geologische Rundschau, 63(1): 191-211.

Stuiver M, Polach HA., 1977. Discussion: reporting of 14C data. Radiocarbon 19(3):355–63.

Su, C., Wang, Y., Pan, Y., 2013. Hydrogeochemical and isotopic evidences of the groundwater regime in Datong Basin, Northern China. Environ Earth Sci, 70(2): 877-885.

Sukhija, B.S., Reddy, D.V., Nagabhushanam, P., Bhattacharya, S.K., Jani, R.A., Kumar, D., 2006. Characterisation of recharge processes and groundwater flow mechanisms in weathered-fractured granites of Hyderabad (India) using isotopes. Hydrogeology Journal, 14(5): 663-674.

Swartz, C. H., N. K. Blute, B. Badruzzman, A. Ali, D. Brabander, J. Jay, J. Besancon, S. Islam, H. F. Hemond and C. F. Harvey, 2004. Mobility of arsenic in a Bangladesh aquifer: Inferences from geochemical profiles, leaching data, and mineralogical characterization. Geochimica et Cosmochimica Acta 68(22): 4539-4557.

Tamers, M.A., 1975. Validity of radiocarbon dates on ground water. Geophysical Surveys, 2(2): 217-239.

Tang, C., Chen, J., Shindo, S., Sakura, Y., Zhang, W., and Shen, Y., 2004. Assessment of groundwater contamination by nitrates associated with wastewater irrigation: A case study in Shijiazhuang region, China: Hydrological Processes, v. 18, no. 12, p. 2303-2312.

Thode, H.G., Monster, J., 1970. Sulfur isotope abundances and genetic relations of oil accumulations in Middle East basin. Am. Assoc. Pet. Geol., 54: 627–637.

Thompson, J.M., Demonge, J. M., 1996. Chemical Analyses of Hot Springs, Pools, and Geysers from Yellowstone National Park, Wyoming and Vicinity, 1980–1993. US Geol. Surv. Open File Rep. 96–68.

Thornber, M., Wildman, J., 1984. Supergene alteration of sulphides, VI. The binding of Cu, Ni, Zn, Co and Pb with gossan (iron-bearing) minerals. Chemical Geology, 44(4): 399-434.

Tighe, M., Lockwood, P., Wilson, S., 2005. Adsorption of antimony (V) by floodplain soils, amorphous iron (III) hydroxide and humic acid. Journal of Environmental Monitoring, 7(12): 1177-1185.

Tornos, F., 2006. Environment of formation and styles of volcanogenic massive sulfides: the Iberian Pyrite Belt. Ore Geology Reviews, 28(3): 259-307.

Tornos, F., 2000. The Iberian Pyrite Belt. R.R. Large, D.J. Blundell (Eds.), Database on Global VMS Districts, CODES-GEODE: pp. 19-5.

Tornos, F., Clavijo, G.E., Spiro, B., 1998. The Filon Norte orebody (Tharsis, Iberian Pyrite Belt): a proximal low-temperature shale-hosted massive sulphide in a thin-skinned tectonic belt. Mineral. Deposita, 33(1): 150-169.

Tornos, F., Velasco, F., Menor-Salván, C., Delgado, A., Slack, J. F., Escobar, J. M., 2014. Formation of recent Pb-Ag-Au mineralization by potential sub-surface microbial activity. Nature communications, 5.

Tornos, F., Velasco, F., Slack, J. F., Delgado, A., Gomez-Miguelez, N., Escobar, J. M., Gomez, C., 2017. The high-grade Las Cruces copper deposit, Spain: a product of secondary enrichment in an evolving basin. Mineralium Deposita, 1-34.

Torrent, J., Schwertmann, U., Barron, V., 1987. The reductive dissolution of synthetic goethite and hematite in dithionite. Clay Miner, 22(3): 329-337.

Torres, E., Ayora, C., Jiménez-Arias, J. L., García-Robledo, E., Papaspyrou, S., Corzo, A., 2014. Benthic metal fluxes and sediment diagenesis in a water reservoir affected by acid mine drainage: A laboratory experiment and reactive transport modeling. Geochimica et Cosmochimica Acta, 139, 344-361.

Torres, E., C. Mix Alan and D. Rugh Williamk, 2005. "Precise δ13C analysis of dissolved inorganic carbon in natural waters using automated headspace sampling and continuous-flow mass spectrometry." Limnol. Oceanogr.: Methods 3.

Tóth, J., 1999. Groundwater as a geologic agent: An overview of the causes, processes, and manifestations. Hydrogeology Journal, 7(1): 1-14.

Truesdall, V.W., Bale, A.J., Woodward, M., 2000. The meridional distribution of dissolved iodine in near-surface waters of the Atlantic Ocean. Prog. Oceanogr. 45, 387–400. USEPA (2012) Guidelines for water reuse. EPA/600/R-12/618, 643 pp.

Tubau, I., Vàzquez-Suñé, E., Jurado, A., Carrera, J., 2014. Using EMMA and MIX analysis to assess mixing ratios and to identify hydrochemical reactions in groundwater. Science of The Total Environment, 470–471: 1120-1131.

UPC, 2003. Visual Transin code. Universitat Politécnica de Catalunya (UPC).

USEPA, 2012 Guidelines for Water Reuse. (EPA Publication EPA/600/R-12/618). September 2012) U.S. Environmental Protection Agency.

Usunoff, E.J., Guzmán-Guzmán, A., 1989. Multivariate analysis in hydrochemistry: an example of the use of factor and correspondence analyses. Ground Water, 27(1): 27-34.

Van der Zee, C., Roberts, D. R., Rancourt, D. G., & Slomp, C. P., 2003. Nanogoethite is the dominant reactive oxyhydroxide phase in lake and marine sediments. Geology, 31(11), 993-996.

Velasco, F., Herrero, J. M., Suárez, S., Yusta, I., Alvaro, A., Tornos, F., 2013. Supergene features and evolution of gossans capping massive sulphide deposits in the Iberian Pyrite Belt. Ore Geology Reviews, 53, 181-203.

Velasco, F., Sánchez-España, J., Boyce, A. J., Fallick, A. E., Sáez, R., Almodóvar, G. R., 1998. A new sulphur isotopic study of some Iberian Pyrite Belt deposits: evidence of a textural control on sulphur isotope composition. Mineralium Deposita, 34(1), 4-18.

Viñals, J., Roca, A., Cruells, M., Núñez, C., 1995. Characterization and cyanidation of Rio Tinto gossan ores. Canadian metallurgical quarterly, 34(2): 115-122.

Vogel, J.C., 1993. 4 - Variability of Carbon Isotope Fractionation during Photosynthesis. In: Bernard, S., James, R.E., Anthony, E.H., Graham D. FarquharA2 - Bernard Saugier, J.R.E.A.E.H., Graham, D.F. (Eds.), Stable Isotopes and Plant Carbon-water Relations. Academic Press, San Diego, pp. 29-46.

Wallin, B., Gaye, C., Gourcy, L., Aggarwal, P., 2005. Isotope methods for management of shared aquifers in northern Africa. Ground Water, 43(5): 744-749.

Wang, Z.H. Ye, W.S. Shu, W.C. Li, M.H. Wong, C.Y., 2006. Lan Arsenic uptake and accumulation in fern species growing at arsenic-contaminated sites of southern China: field surveys International Journal of Phytoremediation, pp. 1–11

Wang Y, Jiao JJ, Cherry JA., 2012. Occurrence and geochemical behavior of arsenic in a coastal aquifer-aquitard system of the Pearl River Delta, China. Sci Total Environ. 2012 Jun;427-428 286-297. doi:10.1016/j.scitotenv.2012.04.006. PubMed PMID: 22554534.

Welch, A.H., Lico, M.S., Hughes, J.L., 1988. Arsenic in ground-water of the Western United States. Ground Water 26, 333–347.

Wen, X., Wu, Y., Su, J., Zhang, Y., Liu, F., 2005. Hydrochemical characteristics and salinity of groundwater in the Ejina Basin, Northwestern China. Environmental Geology, 48(6): 665-675.

Wendt, I., 1968. Fractionation of carbon isotopes and its temperature dependence in the system CO2-Gas-CO2 in solution and HCO3-CO2 in solution. Earth and Planetary Science Letters, 4(1): 64-68.

Whitehead, D., 1974. The sorption of iodide by soil components. Journal of the Science of Food and Agriculture, 25(1): 73-79.

Whittemore, D.O., 1988. Bromide as a tracer in ground-water studies: geochemistry and analytical determination. Proc. Ground Water Geochem. Conf., Denver National Water Well Assoc. Dublin, Ohio: 339-360.

WHO, 2008. Guidelines for Drinking Water Quality, third ed., World Health Organization, Geneva, Switzerland. 668 pp.

Williams, M., Fordyce, F., Paijitprapapon, A., Charoenchaisri, P., 1996. Arsenic contamination in surface drainage and groundwater in part of the southeast Asian tin belt, Nakhon Si Thammarat Province, southern Thailand. Environ. Geol. 27, 16–33.

Williams, M., 1997). Mining-related Arsenic Hazards: Thailand Case-study. Summary Report. Brit. Geol. Surv. Tech. Rep., WC/97/49.

Williams, L.B., 2000. Boron isotope geochemistry during burial diagenesis. Ph.D. thesis, University of Calgary, Calgary, Alberta, 168 pp.

Williams, A. E., Lund, L. J., Johnson, J. A., Kabala, Z. J. 1998. Natural and anthropogenic nitrate contamination of groundwater in a rural community, California, Environ. Sci. Technol., 32, 32– 39, 1998.

Wilson, F.H., Hawkins, D.B., 1978. Arsenic in streams, stream sediments and ground water, Fairbanks area, Alaska. Environ. Geol. 2, 195–202.

WHO, 2008. World Health Organization. http://www.who.int/whosis/whostat/2008/en/

Worden, R.H., 1996. Controls on halogen concentrations in sedimentary formation waters. Mineralogical Magazine, 60(399): 259-274.

Wunsch, A., Navarre-Sitchler, A. K., and McCray, J. E., 2013. Geochemical implications of brine leakage into freshwater aquifers. Groundwater, 51(6), 855-865.

Yesares, L., Sáez, R., Nieto, J.M., de Almodóvar, G.R., Cooper, S., 2014. Supergene enrichment of precious metals by natural amalgamation in the Las Cruces weathering profile (Iberian Pyrite Belt, SW Spain). Ore Geology Reviews, 58(0): 14-26.

Yesares L., Sáez R, Nieto J.M., Ruiz De Almodovar G., Gómez J.L., Escobar J.M., 2014. The Las Cruces deposit, Iberian Pyrite Belt, Spain. Ore Geology Reviews 66 (2015) 25–46

Yokoyama, T., Takahashi, Y., Tarutani, T., 1993. Simultaneous determination of arsenic and arsenious acids in geothermal water. Chem. Geol. 103, 103–111.

Yuan-Hui, L., 1991. Distribution patterns of the elements in the ocean: A synthesis. Geochimica et Cosmochimica Acta, 55(11), 3223-3240.

Zachara, J.M., Fredrickson, J.K., Smith, S.C., Gassman, P.L., 2001. Solubilization of Fe (III) oxide-bound trace metals by a dissimilatory Fe (III) reducing bacterium. Geochimica et Cosmochimica Acta, 65(1): 75-93.

APPENDIX A. SAMPLING AND ANALYTICAL PROCEDURES

GROUNDWATER SAMPLING AND ANALYTICAL PROCEDURES

Groundwater samples were collected from a total of 40 wells and piezometers during two field campaigns carried out in February 2012 and September 2013. Wells were purged and samples collected after removing three well volumes or once field parameters had stabilized.

- The physico-chemical parameters such as **temperature (ºC), pH, Specific Conductance (SC, µS·cm^{-1}), Eh and dissolved oxygen (DO, mg·L^{-1})** were measured in situ inside a closed flow cell by electrodes specific for the measurement of each parameter. To avoid interference of sunlight in oxygen sensor, which use LDO luminescent technology, the sample was protected by foil (Figure B1).

Figure B1. Measurement of parameters in situ by flow cell.

- Total **alkalinity** was determined in the field by acid-base titration in samples of 5mL previously filtered through a 0.45 µm nylon filter. It has used an Aquamerck Alkalinity kit (Figure B2).

Figure B2. Kit used for alkalinity calculation

- Groundwater samples for **general chemistry** were collected in high-density polyethylene, 25 mL bottles for anions and 50 mL for cation-trace samples, previously filtered through a 0.22 µm nylon filter. Cation-tracer samples were acidified with 1 mL of 20% diluted nitric acid for sample preservation. Anions were analysed by High Performance Liquid Chromatography (HPLC). Equipment: binary pump system WATERS 1525, Conductivity Detector WATERS 432 and automatic sampler WATERS 717 plus. LABORATORY: CSIC-IDAEA and CCiT-UB-Unitat de Medi Ambient. Analytical error: 7%. Detection Limit: 2 mg / L. Cations were analysed by Inductively Coupled Plasma Atomic Emission Spectrometry (ICP-AES). Equipment: Thermo Jarrel-Ash Iris Advantage HS. LABORATORY: CSIC-IDAEA. Analytical error: 5%. Detection limit: 1 mg/L for K, Mg, Na and 0.4 mg/L for the other elements. The total trace elements concentrations were measured by inductively coupled plasma and mass spectrometry (ICP-MS). Equipment: Agilent 7500 CE. Analytical error: 5%. Detection limit: 0.05 µg/L. LABORATORY: CSIC-IDAEA.

- In order to differentiate **arsenite (As (III))** from **arsenate (As(V))** field speciation cartridges were used (Meng et al., 1998). Groundwater samples were collected in high-density polyethylene, 25 mL opaque bottles, previously filtered through a 0.22 µm nylon filter and acidified with 1 mL of 20% diluted nitric acid for sample preservation. The samples were analysed by inductively coupled plasma and mass spectrometry (ICP-MS). Equipment: Agilent 7500 CE. Analytical error: 5%. Detection limit: 0.05 µg/L. LABORATORY: CSIC-IDAEA.

- **Dissolved Organic Carbon (DOC)** samples were collected in 30 ml glass bottles previously muffled. These samples were filtered through a 0.45 µm and acidified with 1 mL of HCl (2N). Bottles were sealed with Parafilm® to minimize any contact with air. DOC was analysed by the catalytic oxidation method at 680 °C using a

Shimadzu TOC-V CSH instrument, with a detection limit of 0.05 mg/L (Figure B3). LABORATORY: CSIC-IDAEA.

Figure B3. Shimadzu TOC-V CSH for DOC calculation

- **NH_4^+ and I^-** concentrations were analysed with ion selective electrodes Orion Orion 9512HPBNWP and Orion 9653BN, respectively and lector Thermo Scientific Orion 4 Star. LABORATORY: CSIC-IDAEA. Analytical error: 2%.

- Samples for **CH_4 and H_2S** gas analysis were collected in 250 mL glass bottles with septum cap and stored in an upside-down vertical position according with Capasso and Inguaggiato, (1998) (Figure B4). The CH_4 in the gas phase was determined using a Trace GC Ultra ThermoFisher Scientific chromatograph, with a detection limit of 0.58 mg/L and analytical error from ±0.001 to ±0.009 $mg \cdot L^{-1}$. The CH_4 dissolved in water was calculated by the liquid gas partition coefficient (Alberto et al., 2000). The H_2S content in the liquid phase was analysed by ionic chromatography with a DIONEX model IC5000, and with a variable wavelength detector with a detection limit of 0.005 $mg \cdot L^{-1}$ S_2 and an analytical error of 5%. LABORATORY: Catalan Institute for Water Research ICRA (Girona).

Figure B4. Sample for CH_4 and H_2S gas analysis

- Water samples were collected for **δ^2H and $\delta^{18}O$** analysis in 50 mL high-density polyethylene bottles previously filtered through a 0.45 µm nylon filter. A Wavelength Scanned Cavity Ringdown Spectroscopy (WS-CRDS) instrument was used for δ^2H and $\delta^{18}O$ in water. The analytical precision is ±0.8 ‰ for δ^2H and ±0.3 ‰ for $\delta^{18}O$. LABORATORY: Applied Mineralogy and Environmental group at Barcelona University (UB).

- Samples for **$\delta^{13}C_{DIC}$** were stored in 25 mL muffled glass bottles without headspace and sealed with Parafilm® to minimize any contact with air previously filtered through a 0.45 µm nylon filter. A gas-bench system using the conventional H_3PO_4 method was used for $\delta^{13}C_{DIC}$ analysis (Torres et al.,2005). Isotopic results are given in δ notation against V-SMOW and V-PDB standards. The analytical precision is ±0.3 ‰ for $\delta^{13}C_{DIC}$. LABORATORY: Applied Mineralogy and Environmental group at Barcelona University (UB).

- To determine **$\delta^{34}S$ and $\delta^{18}O$ in sulfate**, 2L samples in polyethylene terephthalate (PET) bottles were collected, acidified with HCl, with an excess of barium chloride solution added to precipitate $BaSO_4$. The precipitation was carried out at elevated temperature (≈100 ° C) to prevent the formation of $BaCO_3$. After settling, the precipitate was recovered by filtration through a 3-µm filter and dried at room temperature. The $\delta^{34}S_{SO4}$ was analyzed in a Carlo Erba Elemental Analyzer (EA) coupled in continuous flow to a Finnigan Delta C IRMS. $\delta^{18}O_{SO4}$ was analyzed in duplicate with a ThermoQuest TC/EA unit (high temperature conversion elemental analyzer) with a Finnigan Matt Delta C IRMS. The analytical error is 0.1 to 0.6 for $\delta^{34}S$ and 0.1 to 0.8 for $\delta^{18}O$. LABORATORY: Applied Mineralogy and Environmental group at Barcelona University (UB).

- The samples for **$\delta^{15}N_{NH4+}$** were collected in high-density polyethylene bottles of 250 mL capacity, previously filtered through a 0.22 µm nylon filter and preserved by adding H_2SO_4 (10%) to keep pH below 5.5. At the laboratory, over the water sample a filter-pack is placed by the ammonia trap. Filter-packs consist a 1 cm-diameter GF/D filter (WHATMAN) acidified with 30 µL of 8N H_2SO_4, sandwiched between two 2.5 cm diameter 10 µm pore-size Teflon membranes. Two mL of Na(OH) 5N solution was added in order to increase pH to a value above 12 pH units causing NH_4^+ to convert to NH_3. The bottle was quickly sealed and placed in an orbital shaker during 7 days at room temperature in order to favour the NH_3 diffusion into the headspace. NH_3 was then trapped into the filter and converted to $(NH_4^+)_2\,SO_4$. After one week, the filter-pack was placed in an acid-washed glass bottle and placed in a freezer-drier during 2 hours to remove any water from the filter. Then the GF/D filter was removed, placed in a silver-cup and analyzed immediately in an EA-IRMS. The $\delta^{15}N_{NH4+}$ were analysed by a diffusion method based on protocols by Sebilo et al., (2004) and Holmes et al., (1998). LABORATORY: Applied Mineralogy and Environmental group at Barcelona University (UB).

- Samples for **^{3}H, $^{14}C_{DIC}$ and ^{36}Cl** analysis were taken in 1 L glass bottles and after 0.45 µm filtration were sealed with Parafilm® to minimize any contact with air. The tritium (^{3}H) content of the samples was analyzed by liquid scintillation after electrolytic enrichment. The ^{3}H concentrations are given in tritium units (TU) with a quantification limit of ±0.3 TU. LABORATORY: Universitat Autónoma de Barcelona (UAB). For the analysis of ^{14}C, the dissolved inorganic carbon (DIC) was liberated from the samples with phosphoric acid as CO_2, which was captured using online extraction. The CO_2 was transformed quantitatively into graphite by reduction with hydrogen gas in the presence of an iron catalyst. The ^{14}C activities were measured by accelerator mass spectrometry (AMS) using the 2MV ANSTO Tandetron accelerator STAR and expressed as a percentage of modern carbon (pMC) according to convention (Stuiver et al. 1977), with error ranging between ± 0.03 and ±0.4. LABORATORY: The samples for ^{14}C were analyzed at the Australian Nuclear Science and Technology Organisation (ANSTO). For ^{36}Cl determination, Cl^- was precipitated with silver chloride and then purified to minimize sulfur content. The precipitate was pressed into silver bromide masks in copper holders, and the ^{36}Cl isotope content of water samples was analyzed by the 14UD tandem accelerator (Fifield et al. 1987). Analytical error ranged between ± 1.7 and ± 2.2 ($x10^{-15}$). LABORATORY: Australian National University.

ROCK SAMPLING AND ANALYTICAL PROCEDURES

A total of 16 solid samples from Las Cruces replacement deposit have been analysed. The samples have been selected from boreholes and supplied by the CLC mining company.

The major mineral phases of the solid samples were identified by X-ray diffraction (XRD) using a Cu-Kα radiation source (Figures B4-B8). For $\delta^{34}S_{SO4}$ rock analysis, was determined from $BaSO_4$ by an elemental analyser coupled in continuous flow with a Delta C Finnigan Matt mass spectrometer. LABORATORY: Applied Mineralogy and Environmental group at Barcelona University (UB).

Additionally, some samples have been analysed by, electron microprobe (EPMA) using wavelength dispersive X-ray spectrometry (WDS) and energy dispersive spectrometry (EDS) for quantify weight percent of Fe, As, Pb, S and Sb in goethite.

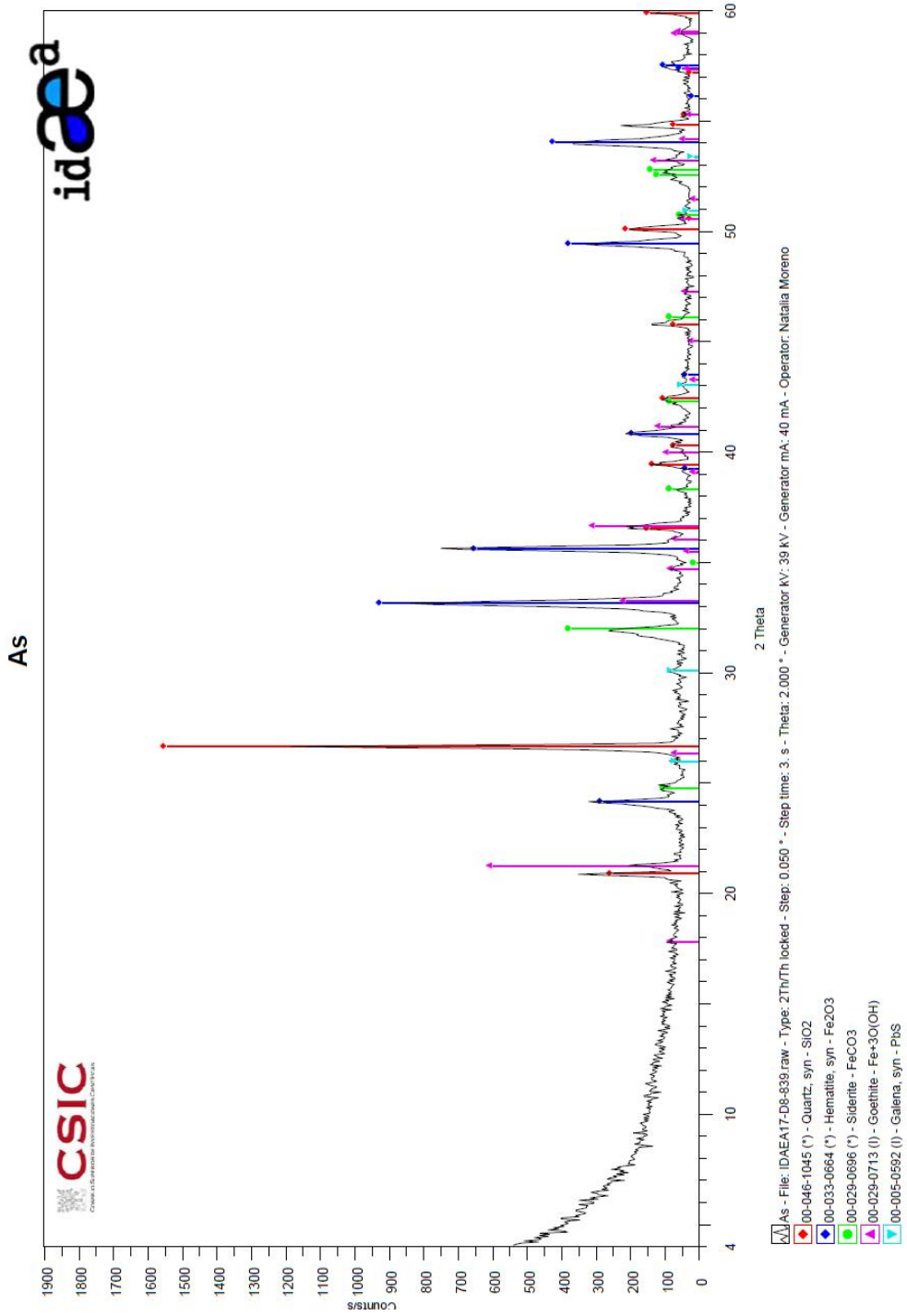

Figure B5. X-ray diffractogram of sample As from Las Cruces gossan

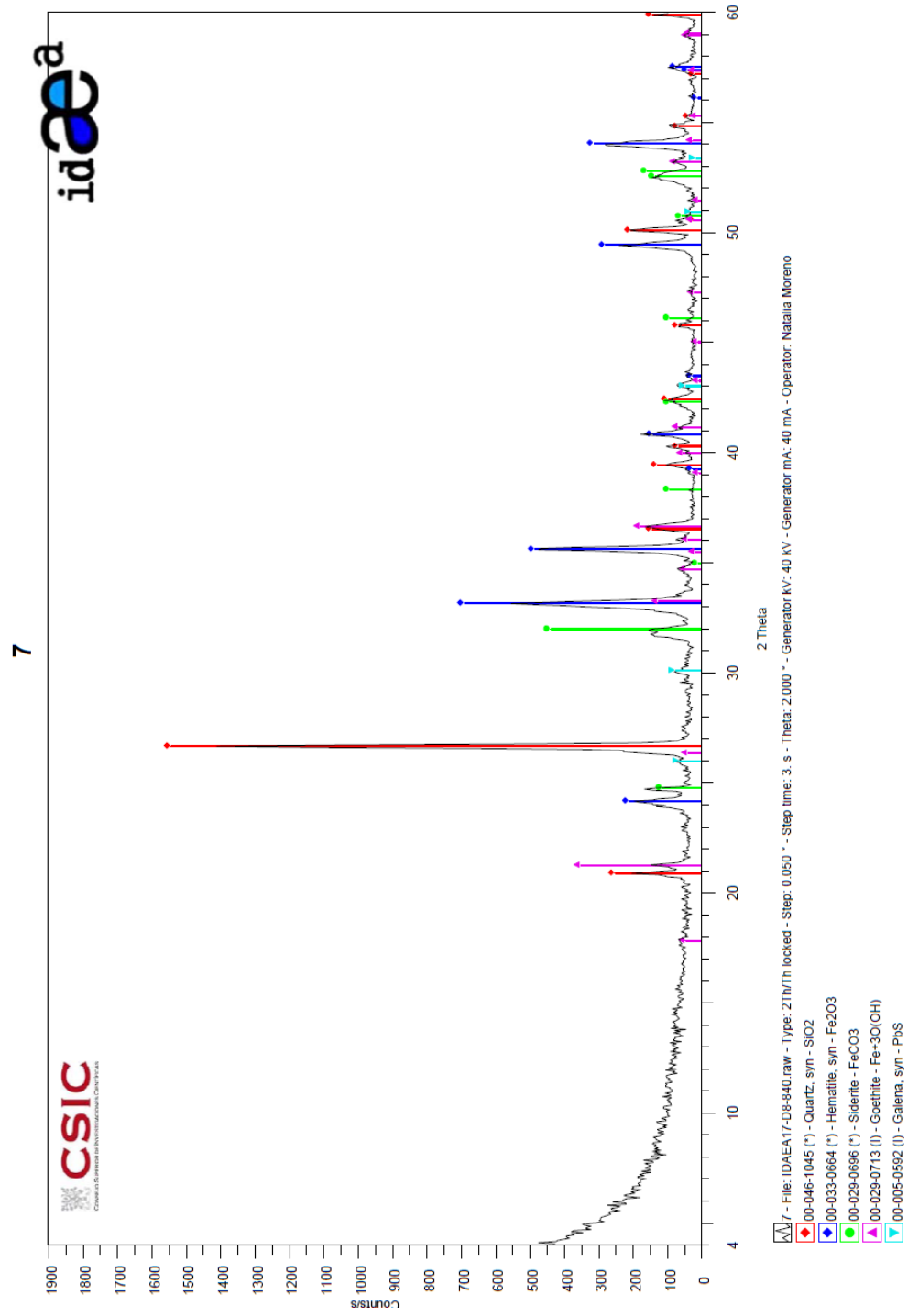

Figure B6. X-ray diffractogram of sample 7 from Las Cruces gossan

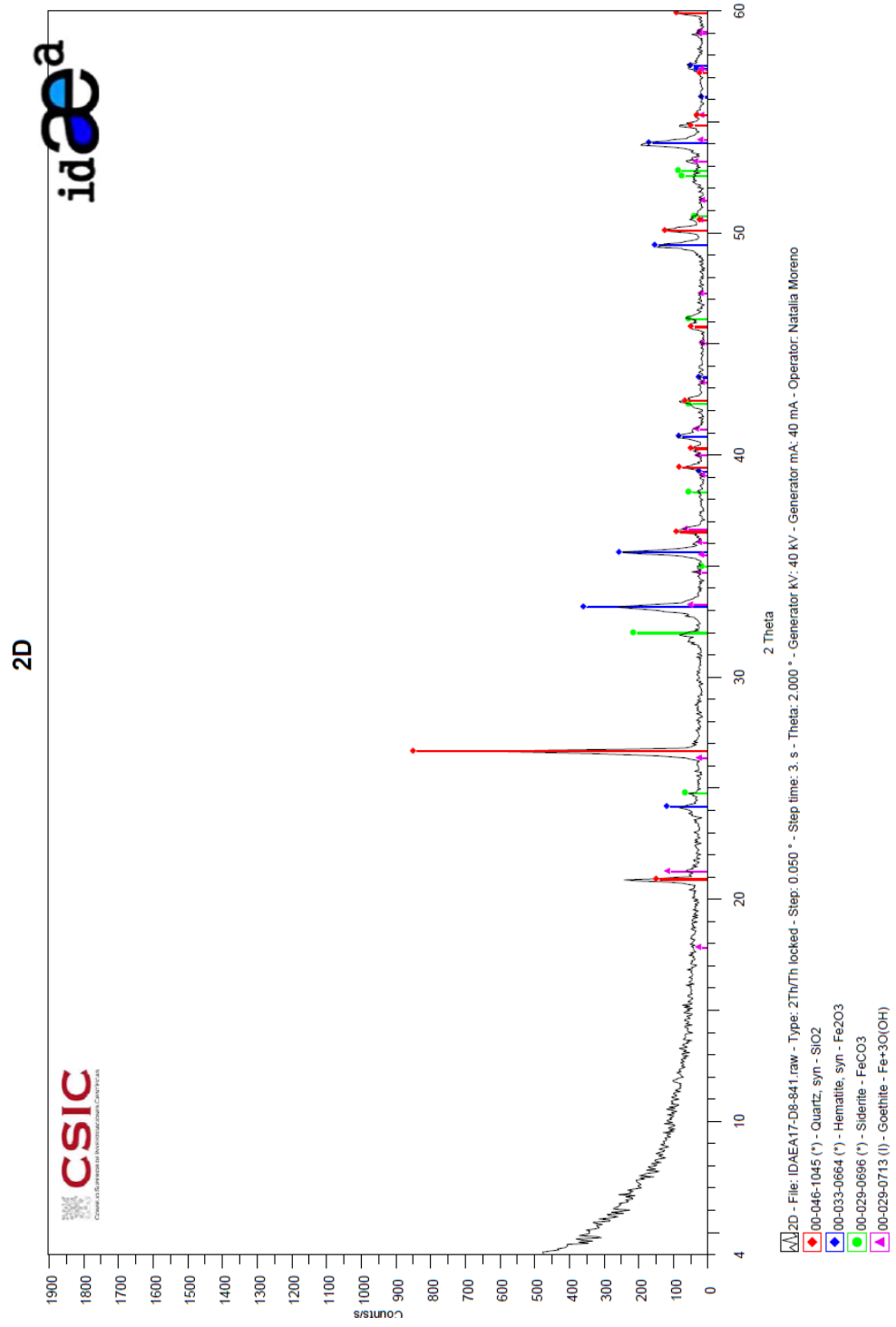

Figure B7. X-ray diffractogram of sample 2D from Las Cruces gossan

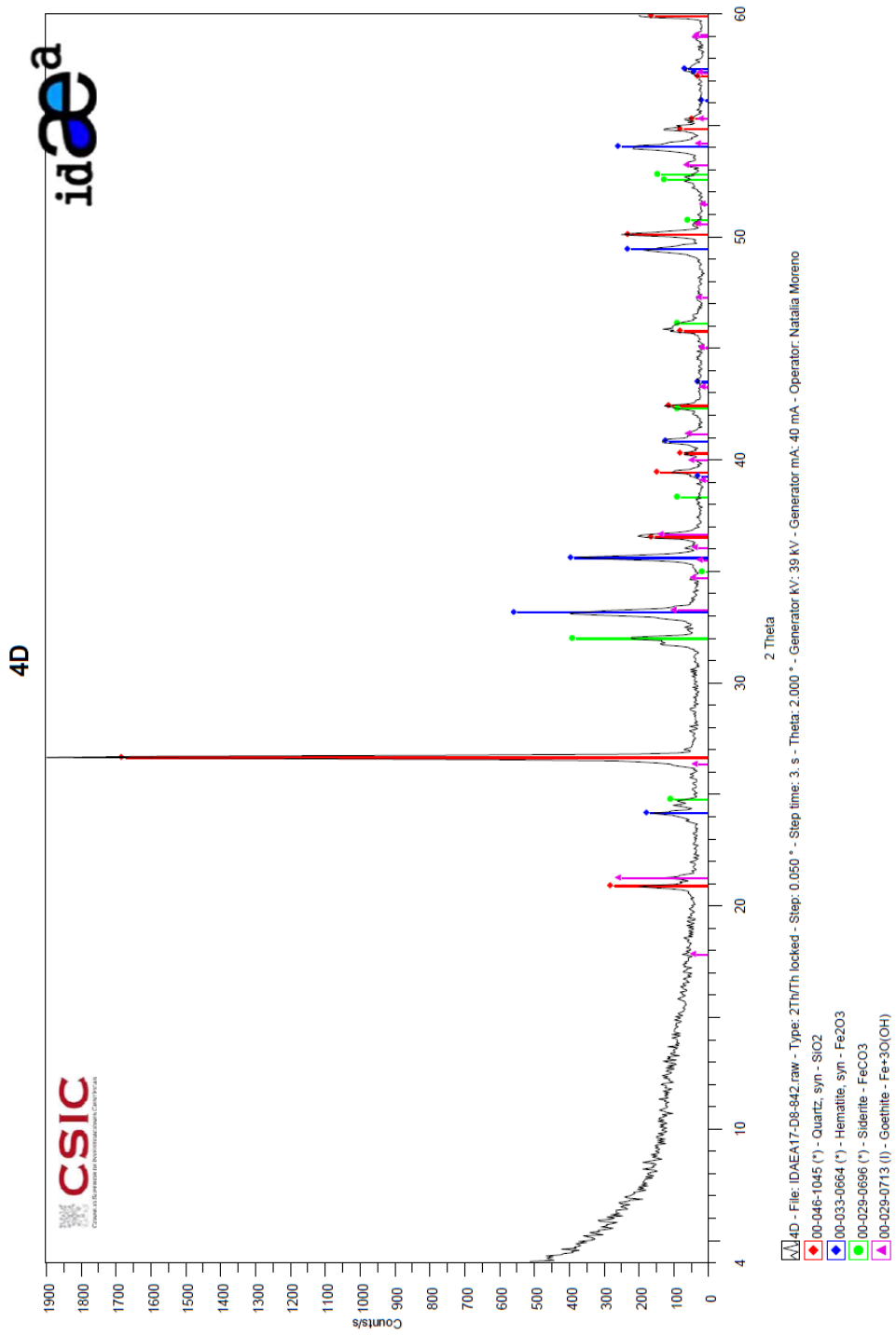

Figure B8. X-ray diffractogram of sample 4D from Las Cruces gossan

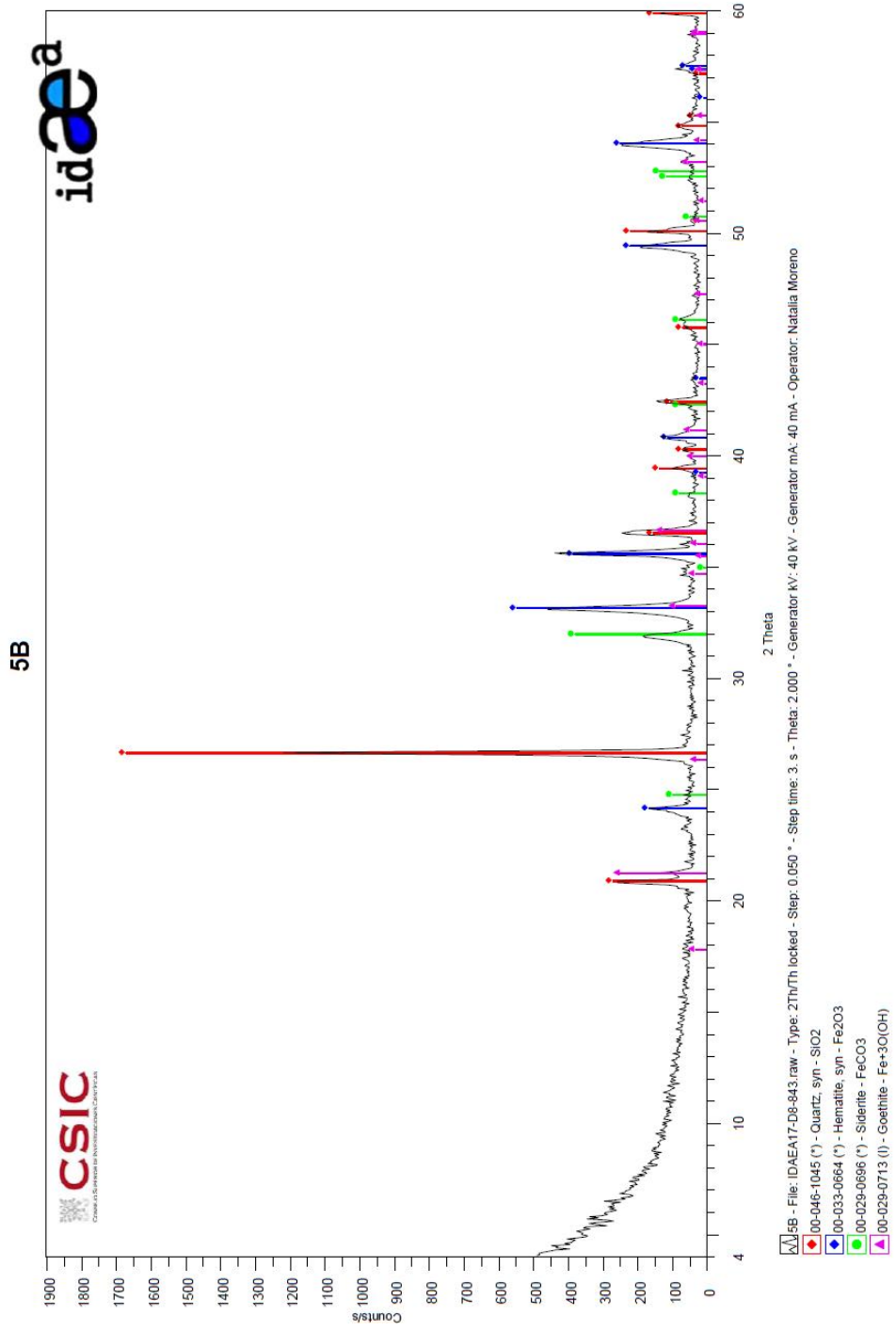

Figure B9. X-ray diffractogram of sample 5B from Las Cruces gossan

APPENDIX A. Sampling and analytical procedures

APPENDIX B. SUPPLEMENTARY TABLES

	ID	pH	Eh (mV)	T(ºC)	SC (uS/cm)
RECHARGE ZONE	44	6.9	159	22.5	957
	42	6.9	306	19.8	922
	40	7.1	163	18.6	903
	43	7.1	234	14.7	999
	41	6.9	165	19.6	1028
	27	7.4	368	20.4	607
INTERMEDIATE ZONE	46	7.2	137	21.2	629
	32	7.1	222	19.8	916
	24	7.3	-25	21.3	491
	1	8.4		28.1	1015
	11	7.5	-200	23.3	578
	29	7.4		25.1	837
	17	7.7	-50	24.3	812
	25	7		21.7	4200
	10	8.2	-297	22.6	388
	19	8		21.7	989
	22	10.3		23.5	943
DEEP ZONE 1	28	8.7	30	27	1846
	4	8.6	169	31.7	1006
	33	8.9		21.8	1441
	13	8.3		26.6	1275
	30	7.4	65	25.6	834
	7	8.4		29.2	1491
	35	9		27.8	1397
	36	8.6	17	28.2	1889
	23	8.4		24.4	2360
	20	8	-130	26	1499
	38	8.4	-24	26.7	1973
	34	8.3		29.3	2326
DEEP ZONE 2	26	7.5		26.5	987
	18	10.1		27.5	2750
	3	8.3	-97	31.8	2510
	16	10.6		25.5	2420
	12	8	-270	32.5	2390
	9	8	-128	32.5	2400
	21	7.9	-190	31.9	2880
	2	7.8		28.7	2080
	8	7.7	-290	35.3	2670
	5	7.8	-240	37.5	5940
	37	7.5		36.5	2714

Table C1. Hydrogeochemical variables of groundwater samples ($mg \cdot L^{-1}$).

	ID	DOC	Cl	NO_3	SO_4	HCO_3	Ca	K	Mg	Na	NH_4
RECHARGE ZONE	44	0.4	39.4	0.1	72.6	442.4	97.8	1.4	14.7	30.8	0.5
	42	0.6	15.5	97.2	16.0	381.3	109.0	0.1	3.8	14.8	0.1
	40	0.3	19.1	48.1	13.1	268.5	102.7	0.1	2.8	14.6	0.1
	43	0.0	35.0	41.6	19.6	297.5	118.3	0.1	9.9	14.8	0.2
	41	0.5	27.7	47.1	19.9	427.1	120.2	0.1	4.3	15.8	0.1
	27	0.7	12.6	16.4	17.3	213.6	68.6	1.9	2.3	16.3	0.1
INTERMEDIATE ZONE	46	0.7	16.4	24.3	19.4	236.4	68.0	2.9	6.0	19.3	0.2
	32	0.4	24.7	44.6	30.9	236.4	98.7	4.7	4.0	17.0	0.2
	24	3.3	38.9	0.1	13.2	292.6	58.4	5.2	7.4	33.7	0.0
	1	4.9	80.3	0.1	0.1	548.7	1.6	3.3	0.5	216.0	2.6
	11	4.6	71.1	0.1	18.6	243.8	49.0	3.5	15.0	49.5	0.8
	29	0.2	44.4	0.1	14.4	308.1	33.7	3.9	12.5	77.6	1.0
	17	4.5	128.6	0.1	10.9	317.0	32.0	5.4	8.2	122.7	1.1
	25	4.7	915.6	13.4	75.4	201.5	177.0	4.1	50.6	279.3	0.0
	10	4.6	43.9	0.1	0.1	158.5	29.0	2.4	11.9	34.3	0.3
	19	4.4	155.0	9.2	38.0	317.0	144.7	5.1	16.5	43.3	0.1
	22	7.6	148.4	0.1	0.1	182.9	0.9	3.4	0.0	163.1	1.7
DEEP ZONE 1	28	0.7	198.6	0.1	5.8	328.6	2.1	3.9	0.1	247.3	3.4
	4	4.9	110.6	0.1	0.1	475.5	1.7	3.2	0.4	208.2	2.7
	33	0.3	91.4	0.1	10.4	570.9	1.0	3.4	0.1	255.7	2.8
	13	7.8	212.2	0.1	7.2	390.2	2.2	3.7	0.6	246.8	2.4
	30	0.4	36.0	0.1	14.7	308.1	35.9	3.9	12.5	71.3	1.1
	7	4.2	305.8	0.1	0.1	317.0	4.0	4.5	0.9	277.7	3.2
	35	0.8	97.1	0.1	9.0	401.2	1.0	3.3	0.1	221.1	2.7
	36	0.3	238.0	0.1	6.9	305.1	2.6	4.0	0.1	273.1	2.8
	23	7.1	522.6	0.1	0.1	304.8	7.6	7.0	1.7	422.4	4.2
	20	4.8	276.4	0.1	5.8	426.7	13.3	4.4	4.1	271.3	1.9
	38	0.3	233.1	0.1	0.1	442.4	2.4	4.4	0.1	310.8	2.9
	34	1.3	459.9	0.1	2.1	457.6	3.0	6.3	0.1	475.9	4.2
DEEP ZONE 2	26	15.9	151.4	0.1	0.1	365.8	63.7	3.7	7.1	123.0	5.0
	18	9.8	625.3	8.4	6.3	548.7	1.0	7.2	0.1	525.2	8.9
	3	4.5	589.1	0.1	0.1	402.4	5.1	6.5	2.1	469.1	4.7
	16	7.8	503.3	0.1	0.1	353.6	0.6	5.6	0.0	464.4	12.8
	12	2.9	534.6	0.1	0.1	487.7	5.1	5.6	1.9	442.2	4.6
	9	5.6	574.2	0.1	0.1	414.5	5.5	6.1	2.2	451.7	4.7
	21	5.5	669.3	10.5	10.1	463.3	14.0	9.2	5.4	510.1	4.6
	2	4.8	460.5	0.1	0.1	365.8	5.1	10.1	2.7	378.9	3.3
	8	5.5	624.6	0.1	0.1	524.3	12.8	8.7	5.1	484.1	4.7
	5	4.6	1581.3	16.7	12.5	390.2	95.1	15.0	30.1	1061.8	7.5
	37	0.5	538.4	0.1	62.5	440.8	19.1	7.7	3.7	519.7	6.4

Table C2. Hydrogeochemical variables of groundwater samples ($mg \cdot L^{-1}$).

	ID	I^-	Br^-	Fe_T	Mn_T	B	As_T	F^-	CH_4	HS^-	SI_{FeCO3}
RECHARGE ZONE	44	0.01	0.22	0.400	0.002	0.15	0.0001	0.3			-0.08
	42	0.01	0.14	0.400	0.002	0.03	0.0001	0.2			-0.28
	40	0.01	0.09	0.400	0.000	0.02	0.0001	0.2			-0.42
	43	0.01	0.18	0.400	0.001	0.03	0.0001	0.2			-0.86
	41	0.01	0.14	0.400	0.001	0.03	0.0002	0.2			-0.27
	27	0.01	0.12	0.400	0.001	0.05	0.0002	0.5			-1.23
INTERMEDIATE ZONE	46	0.01	0.11	0.400	0.002	0.02	0.0000	0.3			-1.75
	32	0.01	0.12	0.400	0.003	0.06	0.0005	0.4			-0.48
	24	0.02	0.10	0.006	0.010	0.06	0.0008	0.5			-0.89
	1	0.04	0.10	0.005	0.002	0.91	0.0000	3.7			-1.88
	11	0.02	5.25	0.005	0.014	0.18	0.0009	0.6	0.003		-2.00
	29	0.03	0.23	0.400	0.031	0.23	0.0015	0.8			-1.88
	17	0.04	0.38	0.002	0.035	0.45	0.0016	0.7			-0.41
	25	0.03	0.10	0.006	0.003	0.47	0.0017	3.3			-2.32
	10	0.03	0.46	0.006	0.013	0.10	0.0025	0.5	0.061	0.106	-1.56
	19	0.01	0.10	0.004	0.012	0.13	0.0097	0.3			0.70
	22	0.14	0.35	0.005	0.000	1.49	0.0120	1.7			-6.36
DEEP ZONE 1	28	0.08	0.81	0.400	0.010	0.61	0.0005	1.2			-0.76
	4	0.06	0.10	0.012	0.002	0.76	0.0005	3.3	0.074		-1.82
	33	0.04	0.42	0.400	0.003	0.93	0.0006	4.1			-2.34
	13	0.08	0.56	0.006	0.001	1.01	0.0006	3.3			-1.46
	30	0.03	0.20	0.400	0.049	0.16	0.0011	0.4			-0.03
	7	0.10	0.93	0.006	0.006	0.79	0.0015	1.5	0.023		0.15
	35	0.06	0.45	0.888	0.003	0.77	0.0021	3.0			0.16
	36	0.10	0.86	0.400	0.005	0.63	0.0024	1.4			-0.09
	23	0.20	1.51	0.009	0.036	1.59	0.0025	3.7			-0.30
	20	0.19	0.92	0.002	0.016	1.22	0.0060	1.6			1.14
	38	0.15	0.94	0.400	0.005	1.48	0.0079	5.2			0.95
	34	0.18	1.76	0.400	0.006	1.70	0.0083	3.6			1.25
DEEP ZONE 2	26	0.13	0.10	0.007	0.159	0.75	0.0011	0.6			1.01
	18	0.34	0.40	0.025	0.000	3.15	0.0014	6.8			0.39
	3	0.20	1.14	0.023	0.011	1.64	0.0016	3.6	0.441		1.00
	16	0.49	0.69	0.035	0.000	3.48	0.0024	6.3			-0.48
	12	0.19	0.82	0.020	0.005	2.42	0.0025	6.5	0.437		-0.27
	9	0.17	0.63	0.036	0.007	2.21	0.0039	5.5	0.463		-0.32
	21	0.24	1.99		0.005	2.31	0.0050	5.6		0.095	-0.35
	2	0.13	1.11	0.137	0.009	1.86	0.0052	4.4			-0.32
	8	0.26	1.35	0.016	0.012	2.22	0.0121	5.3	0.285		-0.29
	5	0.67	4.95	0.005	0.112	2.20	0.0138	2.9	1.085	0.113	0.01
	37	0.22	2.17	0.400	0.055	2.24	0.1787	4.5			-0.16

Table C3. Hydrogeochemical variables of groundwater samples ($mg \cdot L^{-1}$).

	ID	$\delta^{15}N_{NH4}$	$\delta^{2}H$	$\delta^{18}O$	$\delta^{13}C$	$\delta^{18}O$	$\delta^{34}S$
RECHARGE ZONE	44		-	-	-11.4	5.8	4.9
	42		-25.6	-4.4	-11.9	3.7	6.3
	40		-27.5	-4.8		5.8	0.9
	43		-26.4	-4.5		5.9	5.5
	41		-26.9	-4.5		5.9	5.8
	27		-25.9	-4.2	-10.7	6.8	0.5
INTERMEDIATE ZONE	46		-27.1	-4.5	-10.0	6.3	-5.6
	32		-27.1	-4.7		6.9	-8.2
	24		-27.4	-4.7	-11.2	18.1	7.2
	1		-29.0	-4.8		9.3	-8.9
	11	-2.3	-28.4	-4.8	-10.1	13.4	-4.8
	29		-27.2	-4.5	-5.6	14.5	-6.9
	17		-27.8	-4.6	-11.1	6.7	-4.0
	25		-26.0	-4.3	-10.1		
	10		-28.8	-4.9	-10.7	9.2	4.9
	19		-28.1	-4.8			
	22		-28.9	-4.7		16.9	10.5
DEEP ZONE 1	28		-27.9	-4.7	-6.2		
	4	-3	-28.9	-5.0	-8.1	18.1	7.2
	33		-27.9	-4.7		16.7	1.3
	13		-29.0	-4.9	-8.8	13.5	-4.4
	30		-27.1	-4.5	-3.8		
	7	-3.9	-29.0	-5.0		17.3	4.9
	35		-27.9	-4.7	-7.6	16.3	9.4
	36		-28.2	-4.8	-7.4		
	23		-28.6	-4.8		7.7	-4.3
	20	-1.5	-29.1	-4.8	-10.8		
	38		-28.9	-4.8			
	34		-28.4	-4.9			
DEEP ZONE 2	26		-20.4	-3.8			
	18		-30.3	-5.1			
	3	-0.8	-29.3	-4.9	-9.3		
	16		-	-			
	12		-30.3	-5.1	-7.6		
	9	-0.9	-29.9	-5.0	-8.9	11.4	4.4
	21		-29.6	-4.9	-10.8		
	2		-29.0	-4.9			
	8	0.5	-28.9	-5.0	-10.7		
	5	0.7	-28.9	-4.9		10.9	20.4
	37		-29.0	-4.9	-9.8	-29.0	-4.9

Table C4. Isotopic variables of groundwater samples (‰).

Pearson	SC	DOC	Cl	NO_3	SO_4	HCO_3	Ca	K	Mg	Na	NH_4	I	Br	Fe	B	As	Mn	F	$\delta^{18}O$	δ^2H
SC	**1**	0.17	0.97	-0.14	0.1	0.28	-0.01	0.75	0.4	0.9	0.61	0.79	0.49	-0.23	0.66	0.23	0.26	0.37	-0.34	-0.35
DOC		**1**	0.3	-0.34	-0.32	0.07	-0.2	0.31	0.02	0.28	0.47	0.39	0.07	-0.74	0.43	-0.12	0.44	0.10	-0.42	-0.31
Cl			**1**	-0.2	0.03	0.23	-0.04	0.82	0.41	0.92	0.62	0.83	0.54	-0.39	0.69	0.21	0.31	0.36	-0.47	-0.46
NO_3				**1**	0.19	-0.17	0.62	-0.41	0.07	-0.33	-0.35	-0.23	-0.18	0.33	-0.38	-0.11	-0.15	-0.15	0.44	0.41
SO_4					**1**	-0.18	0.66	-0.15	0.62	-0.2	-0.31	-0.25	-0.03	0.23	-0.31	0.4	-0.02	-0.07	0.30	0.34
HCO_3						**1**	-0.39	0.25	-0.35	0.46	0.46	0.32	0.04	-0.001	0.51	0.14	-0.01	0.40	-0.28	-0.25
Ca							**1**	-0.28	0.69	-0.37	-0.5	-0.29	-0.11	0.11	-0.55	-0.09	0.10	-0.31	0.39	0.47
K								**1**	0.16	0.85	0.61	0.78	0.57	-0.39	0.68	0.26	0.38	0.32	-0.54	-0.53
Mg									**1**	0.06	-0.23	0.04	0.22	-0.2	-0.23	-0.03	0.27	-0.04	0.02	0.10
Na										**1**	0.78	0.9	0.56	-0.3	0.84	0.28	0.28	0.55	-0.51	-0.53
NH_4											**1**	0.86	0.32	-0.27	0.91	0.25	0.26	0.57	-0.43	-0.41
I												**1**	0.53	-0.33	0.84	0.19	0.36	0.38	-0.46	-0.46
Br													**1**	-0.2	0.3	0.25	0.31	0.04	-0.33	-0.33
Fe														**1**	-0.35	0.12	-0.19	-0.07	0.74	0.65
B															**1**	0.27	0.08	0.82	-0.58	-0.62
As																**1**	0.23	0.04	0.03	-0.01
Mn																	**1**	0.01	0.17	0.28
F																		**1**	-0.3	-0.36
$\delta^{18}O$																			**1**	0.97
δ^2H																				**1**

Table C5. Pearson correlation matrix of groundwater data. The correlation factors above 0.7 are marked.

No.	As	Fe	Cu	Pb	S	Sb	Total
1	0.2736	94.05	0	0.9198	0.3319	0	95.5754
2	0.2872	94.42	0	0.8467	0.2658	0	95.8198
3	0.337	93.71	0.0038	1.0758	0.2707	0	95.3973
4	0.2436	90.53	0	1.0248	0.4181	0	92.2166
5	0.4774	93.85	0.0144	1.0342	0.3332	0.1963	95.9055
6	0.3322	94.36	0.0109	0.8443	0.3216	0.1228	95.9919
7	0.4172	93.99	0	1.1	0.3575	0.1722	96.0369
8	0.2966	94.34	0	0.9578	0.3692	0.1336	96.0973
9	0.244	94.43	0	0.7825	0.3076	0.1132	95.8774
10	0.3178	94.53	0.0078	0.8151	0.3371	0.1653	96.1731
11	0.3714	93.75	0.0034	0.9699	0.3267	0.2094	95.6309
12	0.2993	94.68	0.001	0.704	0.3006	0.0962	96.0812
13	0.3596	93.01	0.0074	0.8845	0.2869	0.3464	94.8949
14	0.237	94.44	0	0.7335	0.2854	0.1043	95.8003
15	0.2572	94.43	0.0006	0.8288	0.329	0.1248	95.9705
16	0.2237	94.48	0.0039	0.7259	0.3445	0.0962	95.8743
17	0.3192	94.44	0.0008	0.8867	0.2888	0.1724	96.108
18	0.4105	92.4	0.0037	1.0753	0.4153	0.3537	94.6586
19	0.3386	90.61	0	1.0309	0.3825	0.2509	92.613
20	0.419	87.66	0	0.7263	0.4319	1.54	90.7773
21	0.239	94.79	0.0174	0.7669	0.2968	0.1679	96.2781
22	0.4269	91.63	0.0077	0.9476	0.4102	0.2546	93.6771
23	0.3729	93.61	0	1.0445	0.3536	0.1749	95.556
24	0.5731	93.77	0	1.33	0.4094	0.3284	96.4109
25	0.6393	93.52	0	1.22	0.3499	0.3559	96.0852
26	0.3257	94.48	0	0.9278	0.3484	0.1777	96.2597
27	0.4551	94	0	1.13	0.3652	0.2311	96.1814
28	0.4157	93.38	0.0422	1.09	0.3566	0.262	95.5465
29	0.3528	94.4	0	0.9099	0.288	0.1445	96.0953
30	0.3307	94.31	0.0066	0.8655	0.2994	0.1942	96.0065
31	0.3276	94.49	0.0088	0.8338	0.2771	0.1216	96.0589
32	0.2588	92.16	0	0.9688	0.3878	0.2043	93.9798
33	0.3044	92.76	0.0027	1.0604	0.3804	0.1878	94.6958

No.	As	Fe	Cu	Pb	S	Sb	Total
34	0.2592	93.17	0.0083	0.9217	0.3715	0.1307	94.8615
35	0.1934	93.37	0.0143	0.7895	0.4046	0.0807	94.8526
36	0.0981	92.55	0.04	0.7609	0.4584	0.1391	94.0466
37	0.2723	92.4	0.0579	0.8196	0.5854	0.1618	94.2971
38	0.3631	93.86	0.0203	0.8488	0.3285	0.1463	95.5671
39	0.2733	94.07	0.0057	0.8206	0.2748	0.1526	95.5971
40	0.434	93.75	0	0.8366	0.3497	0.1284	95.4988
41	0.506	92.67	0.0089	1.13	0.4554	0.2584	95.0287
42	0.4094	91.69	0.0022	1.15	0.5069	0.3663	94.1249
43	0.484	91.53	0.0051	1.16	0.4851	0.3953	94.0596
44	0.4769	90.33	0.0136	1.0442	0.548	0.5255	92.9382
45	0.7124	93.95	0.0265	0.87	0.3364	0.2751	96.1705
46	0.6406	93.84	0.0025	0.8774	0.3488	0.2923	96.0017
47	0.853	93.28	0	0.9503	0.3261	0.4837	95.8932
48	0.6968	94.13	0	0.8617	0.3461	0.3456	96.3802
49	0.7858	93.52	0	1.26	0.4003	0.4989	96.465
50	0.3715	91.78	0	1.0334	0.4095	0.2175	93.812
51	0.3988	90.63	0.0044	0.9866	0.4587	0.2206	92.6992
52	0.4566	91.52	0	0.9254	0.4573	0.3006	93.6599
53	0.4276	90.59	0.0115	1.0615	0.4169	0.3628	92.8703

Table C6. Results of Electron Microprobe Analysis (EPMA) of goethite (wt %)

	TIC	Cl	NH4	Na	B	Ca	I	Br	SC
1	281	39	0.83	69	0.18	50	0.03	0.25	788
2	351	213	3.18	306	0.98	1	0.10	0.93	1959
3	253	39	0.83	52	0.16	45	0.02	0.20	816
4	329	199	3.36	247	0.61	2	0.08	0.81	1846
5	419	571	5.99	587	2.36	11	0.31	2.58	2824
6	308	44	1.03	78	0.23	34	0.03	0.23	837
7	308	36	1.12	71	0.16	36	0.03	0.20	834
8	442	233	2.85	311	1.48	2	0.15	0.94	1973
9	442	433	5.22	471	2.22	2	0.20	1.65	2100
10	401	97	2.72	221	0.77	1	0.06	0.45	1397
11	305	238	2.80	273	0.63	3	0.10	0.86	1889
12	400	1349	9.63	979	2.20	70	0.64	5.41	5817
13	441	538	6.40	520	2.24	19	0.22	2.17	2714
14	458	472	5.25	512	2.15	4	0.21	1.76	2499
15	419	569	4.89	564	2.19	10	0.31	2.10	2858
16	520	428	5.14	506	2.40	4	0.21	1.93	2468
17	214	13	0.09	16	0.05	69	0.01	0.12	607
18	351	907	4.16	697	1.52	64	1.45	4.38	4000
19	236	25	0.17	17	0.06	99	0.01	0.12	916
20	442	39	0.48	31	0.15	98	0.01	0.22	957
21	320	83	1.20	103	0.44	47	0.08	0.41	1103
22	381	16	0.07	15	0.03	109	0.01	0.14	922
23	297	35	0.15	15	0.03	118	0.01	0.18	999
24	236	16	0.15	19	0.02	68	0.01	0.11	629
25	571	91	2.83	256	0.93	1	0.04	0.42	1441
26	458	460	4.23	476	1.70	3	0.18	1.76	2326
27	427	28	0.12	16	0.03	120	0.01	0.14	1028
28	268	19	0.08	15	0.02	103	0.01	0.09	903

Table C7. Hydrogeochemical variables of groundwater samples used for regional mixing calculation

DATA	Open pit area (m^2)	Contact Water (CW) area (m^2)	No Contact Water (NCW) area (m^2)	Precipitation (P) (m)	Runoff (m)	Runoff CW (m^3)	Drain NCW (m^3)	Runoff NCW (m^3)	Runoff NCW - Drain NCW (m^3)	Runoff open pit (m^3)
Sep_14	1014636	353582	661053	0.084	0.029	10176	0	19025	19025	29201
Oct_14	1014636	353582	661053	0.062	0.036	12799	2434	23928	21494	34293
Nov_14	1014636	353582	661053	0.124	0.079	27898	11563	52158	40595	68492
Dec_14	1014636	353582	661053	0.051	0.028	10009	11347	18713	7366	17375
Jan_15	1014636	353582	661053	0.065	0.031	11075	9900	20706	10806	21882
Feb_15	1014636	353582	661053	0.004	0.000	0.00	138	0	0	0
Mar_15	1014636	353582	661053	0.034	0.007	2642	24	4940	4916	7559
Apr_15	1014636	353582	661053	0.057	0.022	7905	2193	14779	12586	20490
May_15	1014636	353582	661053	0.003	0.000	0.00	0	0	0	0
Jun_15	1014636	353582	661053	0.002	0.000	0.00	0	0	0	0
Jul_15	1014636	353582	661053	0	0.000	0.00	0	0	0	0
Aug_15	1014636	353582	661053	0.008	0	0.00	0	0	0	0
Sep_15	1014636	353582	661054	0.008	0	0.00	0	0	0	0
Oct_15	1126000	442600	683400	0.079	0.019	8393	1041	12959	11918	20310
Nov_15	1126000	442600	683400	0.049	0.027	11859	10238	18311	8073	19932
Dec_15	1126000	442600	683400	0.027	0.002	832	1	1284	1283	2115
Jan_16	1126000	442600	683400	0.034	0.003	1496	2720	2310	2310	3806
Feb_16	1126000	442600	683400	0.021	0.001	340	239	524	285	625
Mar_16	1126000	442600	683400	0.022	0.016	342	825	528	528	870
Apr_16	1126000	442600	683400	0.074	0.076	6962	2529	10750	8221	15183
May_16	1126000	442600	683400	0.120	0	33472	21579	51682	30103	63575
Jun_16	1126000	442600	683400	0	0	0.00	0	0	0	0
Jul_16	1126000	442600	683400	0.001	0	0.00	0	0	0	0
Aug_16	1126000	442600	683400	0.001	0	0.00	0	0	0	0

Table C8. Monthly water balance of the open pit.

APPENDIX C. RUNOFF ESTIMATION BY WATER BALANCE

Obtaining independent information that allows us to evaluate the end Runoff requires a balance of water in the open pit. A conceptual approach to the water balance is presented in Figure D1 and D2. The hydrological functioning of the open pit mine area can be summarized as follows. The runoff in the whole area can be divided into two components: (1) No Contact Water area (NCW), i.e., the water runs through materials that do not include any mineralization, and (2) Contact Water area (CW), i.e., the water that comes into contact with mineralization. In each of these areas, the water balance can be established.

Balance in the NCW area:

A. Runoff intercepted by the drainage system led to a pumping raft (Vol NCW) and drained outside the system (Drain NCW)

B. Evapotranspiration of water retained on the surface and in the first centimeters of the ground (Evp. NCW)

C. Water recharging or effective infiltration to the saturated area of the ground (I NCW). Given the impermeability of the marls, this fraction is presumed to be negligible.

D. Runoff not intercepted by the rainwater drain system and reaching the open pit bottom (Runoff NCW). In this case, this water will be mixed with other existing contributions: Paleozoic and Cenozoic.

Balance in the CW area:

A. Evapotranspiration of water retained on the surface of the land (Evp. CW)

B. Runoff water to the open pit bottom (Runoff CW). In this case, this water will be mixed with other existing contributions: Paleozoic and Cenozoic.

C. Water that recharges the saturated area of the ground (I NCW). Since the outcropping mineral may be somewhat more permeable than the marl, it is assumed that a certain proportion may infiltrate the soil (I CW). To simplify the calculations, it is considered that this fraction can be grouped within the runoff end-member.

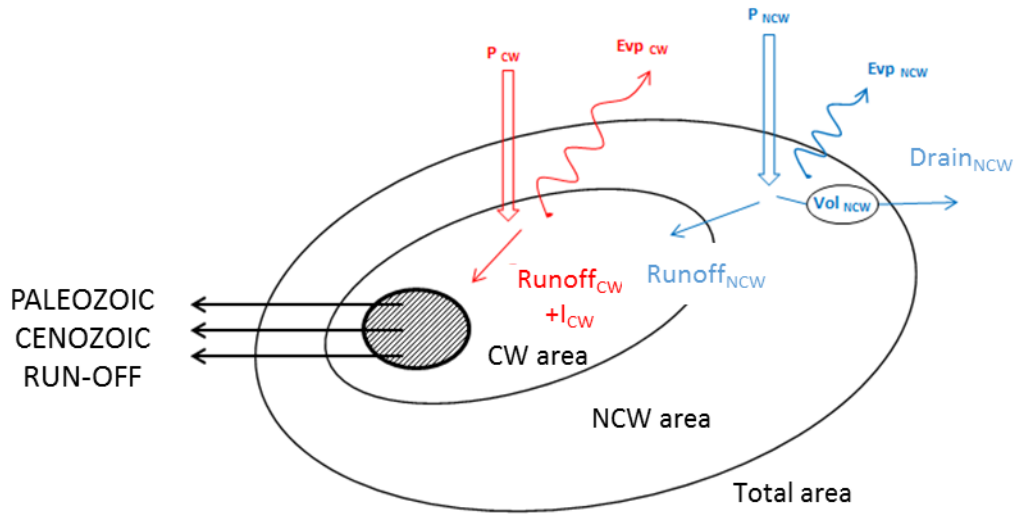

Figure D1. Sketch of the water balance of water in the open pit.

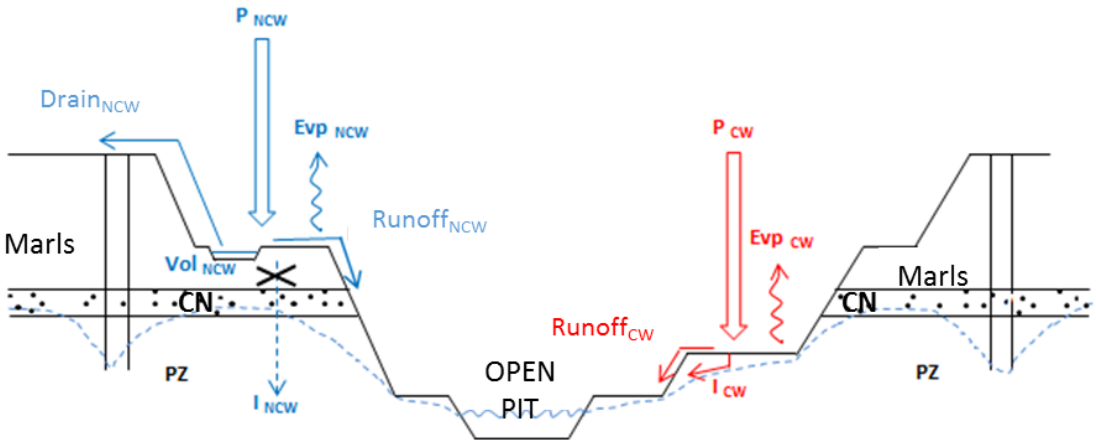

Figure D2. Section of the water balance in the open pit.

Next, the total of Runoff water that reaches the open pit bottom is governed by the following equation:

$$\text{RUNOFF to open-pit} = \text{RUNOFF}_{CW} + \text{RUNOFF}_{NCW}$$

Where,

$$\text{RUN-OFF}_{CW} = P_{CW} - \text{EVP}_{CW}$$

$$RUNOFF_{NCW} = P_{NCW} - EVP_{NCW} - DRAIN_{NCW} - VOL_{NCW}$$

The curve number method has been used to calculate the Runoff. This method was elaborated by the U.S. Soil Conservation Service and is based on the direct estimation of the surface runoff of an isolated rainfall from the characteristics of the soil, its use, vegetation cover and proximity of previous rains. Thus, the relationship between precipitation and runoff can be represented by a curve with two distinct parts: 1) a precipitation threshold below which all rain is trapped in the soil, and there is no runoff, and 2) points beyond this threshold where the runoff increases with precipitation. In our case, we have chosen a curve number of 93 corresponding to the bare ground very low permeability and firm roads. These values are corrected by slopes greater than 3% and corrected with a value that depends on the degree of previous soil moisture.

The daily runoff Q is obtained from:

$$Q = \frac{(P - 0.2 * S)^2}{(P + 0.8 * S)}$$

where P is the daily precipitation in mm, and S is the sum of the infiltration plus the water retained in the soil and evaporated (in mm) and can be calculated from the curve number N:

$$S = 254(\frac{100}{N} - 1)$$

The surfaces of the CW and NCW areas are known. To calculate the Runoff CW, we multiply the corresponding Q by the surface of the zone CW. To calculate the Runoff NCW, we multiply the corresponding Q by the area of the NCW zone and subtract the drained volume (Drain NCW). Finally, to calculate the total of Runoff in the open pit, we add the 2 contributions Runoff CW and Runoff NCW.